BY

BARRY A. BENEDICT, HILLEL RUBIN,
AND STEPHEN A. MEANS

PUBLICATION NO. 71

FLORIDA WATER RESOURCES RESEARCH CENTER
RESEARCH PROJECT TECHNICAL COMPLETION REPORT

ACKNOWLEDGEMENTS

This project was sponsored by the Florida Water Resources Research Center with funds provided by the United States Department of the Interior, Office of Water Research and Technology. Additional funds were provided by the Engineering and Industrial Experiment Station, University of Florida. The assistance of Dr. James Heaney and Mary Robinson of the Water Resources Center is appreciated.

The computer facilities of the Northeast Regional Data Center of the State University System of Florida were used for this work.

The material presented in this report is substantially the same as presented by Mr. Means in partial fulfillment of the requirements for the Master of Engineering degree under the title "Numerical Simulation of Aquifer Mineralization in Northeastern Florida."

TABLE OF CONTENTS

LIST OF TABLES

LIST OF FIGURES

LIST OF SYMBOLS

a	dispersivity
B	thickness of freshwater zone
B_o	thickness of freshwater zone at the edge of the transition zone
B_l	thickness of semiconfining formation
C	solute concentration
C_o	characteristic solute concentration
C_f	solute concentration of freshwater
C_s	solute concentration of mineral water
D	coefficient of dispersion
$\tilde{D}$	dispersion tensor
F	distribution function of specific discharges
$\vec{k}$	unit vertical vector
K	hydraulic conductivity of the aquifer
K_f	hydraulic conductivity of a porous medium containing freshwater
K_l	hydraulic conductivity of the semiconfining formation
K_s	hydraulic conductivity of a porous medium containing saltwater
L	distribution function of solute concentration
m	time index used in finite difference equations
n	porosity
N	pumpage or recharge per unit area
p	pressure

$\vec{q}$ specific discharge vector

s drawdown of the piezometric head

S coefficient of storage

t time

u specific discharge in the transition zone in the x direction

U characteristic specific discharge in the x direction

v specific discharge in the transition zone in the y direction

V characteristic specific discharge in the y direction

x horizontal coordinate

y horizontal coordinate

z elevation

z_b elevation of the bottom of the transition zone

z_t elevation of the top of the transition zone

Greek Letters

α coefficient relating concentration with specific weight

γ specific weight

γ_o specific weight of reference

γ_f specific weight of freshwater

γ_s specific weight of mineral water

δ thickness of the transition zone

η dimensionless coordinate defined in equation (4.11)

ξ buoyancy coefficient defined in equation (4.14)

ϕ piezometric head

ϕ_f piezometric head at freshwater zone

ϕ_{fo} original piezometric head at freshwater zone

ϕ_{ft} piezometric head at the top of the transition zone

ϕ_s piezometric head at mineral water zone

ϕ_{so} original piezometric head at mineral water zone

ϕ_{sb} piezometric head at the bottom of the transition zone

ABSTRACT

Efforts have been directed toward finding ways of reducing computer resources and expertise required for modeling movement of contaminants through the groundwater system. An approach has been developed which simplifies the basic equations. To test the method, it has been applied to the stratified flow problem associated with the upward seepage of saline water into freshwater aquifers overlying semiconfining formations. This seepage in response to pumpage is particularly of concern in northeastern Florida, which obtains the majority of its potable water from the freshwater zone of the Floridan aquifer. This region is being subjected to increasing rates of pumpage.

Traditional attempts to simulate the mineralization process in a stratified aquifer arose by applying a sharp interface assumption or by a complete solution of the equations of motion and solute transport through the aquifer. The sharp interface approach suffers from a lack of coherence with the physical phenomena while the complete solution approach involves sets of highly nonlinear differential equations, the solution of which is subject to serious problems of stability and convergence.

This study attempts to simplify the basic model by the application of the Dupuit approximation in conjunction with the boundary layer theory to a flow field divided into three zones as follows: (a) the freshwater zone, (b) the saltwater zone, and (c) the transition zone. The equations of continuity, motion, and solute transport are solved simultaneously subject to the conditions found in the simplified flow field. The result is the development of three partial differential

CHAPTER 1

INTRODUCTION

1.1 Ojectives and Possible Approaches

The primary project objective is the development of simplified, yet physically correct, mathematical models to describe groundwater systems, reducing needed computer resources. Two basic approaches can be taken to achieve this goal: (1) use analytical solutions to pertinent equations, or (2) simplify the basic equations in such a way as to enable development of numerical models using reduced computer resources. A number of published analytical solutions exist, including those by Wilson and Miller [1978], Sagar [1982], Hunt [1978], and Prakash [1982]. In addition, several solutions based on perturbation techniques have been presented [see section 3.4]. In addition, numerous solutions to the diffusion equation can readily be adapted to groundwater transport problems. A review of these is given by Benedict [1981].

The above analytical models are perceived to have much utility, but the major focus of this study was to be on density-stratified fluids. Handling such effects in analytical solutions can be partially accounted for by using modified dispersion coefficients, but this cannot account for density influences on the flow field, changing density influences through the flow field, and non-unidirectional flows. In addition, use of perturbation techniques for three-dimensional flows would become very complicated. For these reasons, and due to the great interest in the saltwater intrusion problem in Florida, this problem was selected for the main thrust of the work.

1.2 General Scope of the Study

The Floridan Aquifer is the primary source of potable water for the northeastern Florida area. The aquifer is extremely productive and supplies freshwater for domestic, municipal, industrial, and agricultural purposes. In most areas semiconfining formations containing saline water underlie the freshwater aquifer.

The inland areas of northeastern Florida are predominantly rural and highly agriculturalized. The demand for irrigation water is intense during the growing season and heavily taxes the freshwater supply found within the Floridan Aquifer. Where the rates of pumpage of this aquifer are high, the saline water found in underlying formations is subject to upward migration. This process leads to the formation of stratified flow conditions within the aquifer and is termed mineralization. The mineralization process is typical to the highly agriculturalized areas of northeastern Florida and is known to cause a gradual increase in the chloride content of freshwater derived from wells penetrating the artesian aquifer. The understanding of the physical phenomena associated with the mineralization process is essential to sound groundwater management programs.

1.3 Methodology

The quantitative analysis of an aquifer system subject to stratified flow conditions involves the solution of highly nonlinear partial differential equations. This study seeks to simplify these nonlinear equations, and thus the basic model, by the application of appropriate quantitative tools while still maintaining a three-dimensional simulation. This model will specifically relate to mineralization phenomena in the Floridan Aquifer in inland areas of northeastern Florida.

Contemporary groundwater flow problems are generally solved by a variety of analytical and numerical techniques. For aquifers subject to steady state conditions and simple boundary conditions, analytical solution techniques have been proven to work well. On the other hand, numerical solution techniques are usually superior when analyzing aquifers subject to transient flow conditions, heterogeneous soil conditions, and complicated boundary conditions.

Because of the complicated nature of the transient stratified flow conditions in the aquifer system, a numerical solution technique is chosen for simulation purposes. The nonlinear nature of the basic model presents problems with stability and convergence in a numerical scheme. With an appropriate selection of simplifying steps, a highly stable and convergent numerical scheme describing the transient effects of stratified flow conditions within an aquifer is possible. The numerical results, being coherent with the physical phenomena, could then be used as a tool for the design and implementation of groundwater programs associated with groundwater management in the area.

The remaining chapters will describe an application of this modeling system to a particular set of conditions peculiar to the salt water intrusion problem in northeastern Florida. The area will be described and the model features and typical results described in detail. It is important to realize that contaminants other than salt can also be modeled using the same integral formulation, thereby enabling analysis of hazardous waste movement. Extension to other geometries and pumping patterns is also possible, although it is not included in the following work.

CHAPTER 2

THE FLORIDAN AQUIFER IN NORTHEASTERN FLORIDA

2.1 Introduction

Florida is underlain by extensive limestone deposits which form some of the most productive aquifers in the United States. Known as the Floridan Aquifer, this system is the major geologic unit underlying northeastern Florida. Confined by the Hawthorn Formation in most areas of northeastern Florida, the Floridan Aquifer is artesian and supplies the majority of potable water to this area. Domestic, municipal, and irrigational needs constitute the majority of demand for potable water.

Freshwater is supplied to the Floridan Aquifer primarily in the form of infiltrated precipitation. Recharge occurs where the upper portion of the aquifer outcrops in the middle areas of Georgia and through local sites such as sinkholes and other breaches in the Hawthorn Formation. This recharge helps maintain the freshwater balance in the aquifer system.

Underlying the freshwater zone of the Floridan Aquifer in northeastern Florida are deposits saturated with mineralized water of varying quality and origin. This condition creates the potential for well contamination due to the upward migration of the mineralized water.

Of special interest to this study is the area located in northeastern Florida comprised of Flagler, Putnam, and St. Johns counties (Figure 2.1). Known as the Tri-County area, this area is extremely agriculturalized. A lack of precipitation during the growing season forces

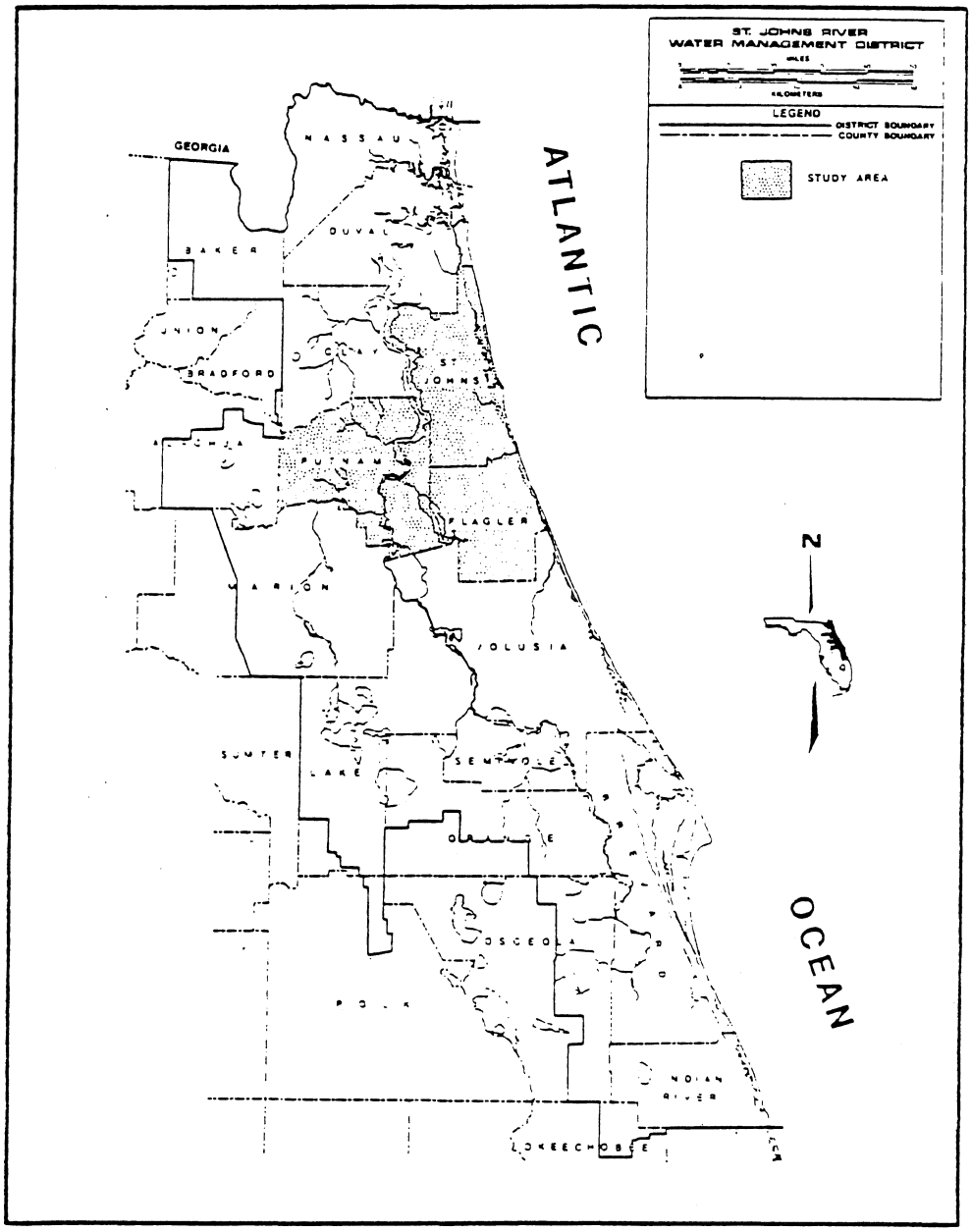

Figure 2.1 - Delineation of the study area. Figure from Munch et al. [1979].

the agriculturalists to obtain their irrigation water directly from the Floridan Aquifer. Excessive pumpage of this aquifer since the turn of the century has caused a general decline in its piezometric surface in the vicinity of the agriculturalized areas. This decline was accompanied by a noticeable increase in the salt content of the freshwater pumped from certain wells, and prompted the Florida State Legislature to appropriate funds for an investigation. The investigation began in 1955 as part of the statewide cooperative program between the United States Geological Survey and the Florida Geological Survey.

Major investigative studies into well contamination in the Tri-County area are few but in most cases well documented. The November, 1955 investigation resulted in an extremely thorough and informative report by Bermes et al. [1963]. Two subsequent well studies were conducted in the area but went unpublished. It should be noted that even though these investigations recognized the mineralization problem, no remedial programs were specified. A report by Munch et al. [1979] contains the most recent developments and data concerning well contamination in the area. Prepared in cooperation with the St. Johns Water Management District, this report outlines recommendations for safe well use in the area.

2.2 Geology

An inspection of a geologic column from the Tri-County area reveals several distinct rock units. In ascending order these units are as follows: the Lake City Limestone, the Avon Park Limestone, the Ocala Group, the Hawthorn Formation, and a surficial unit. The geologic column is represented in Figure 2.2. Bermes et al. [1963], Chen [1965], and Munch et al. [1979] provide thorough descriptions of these units.

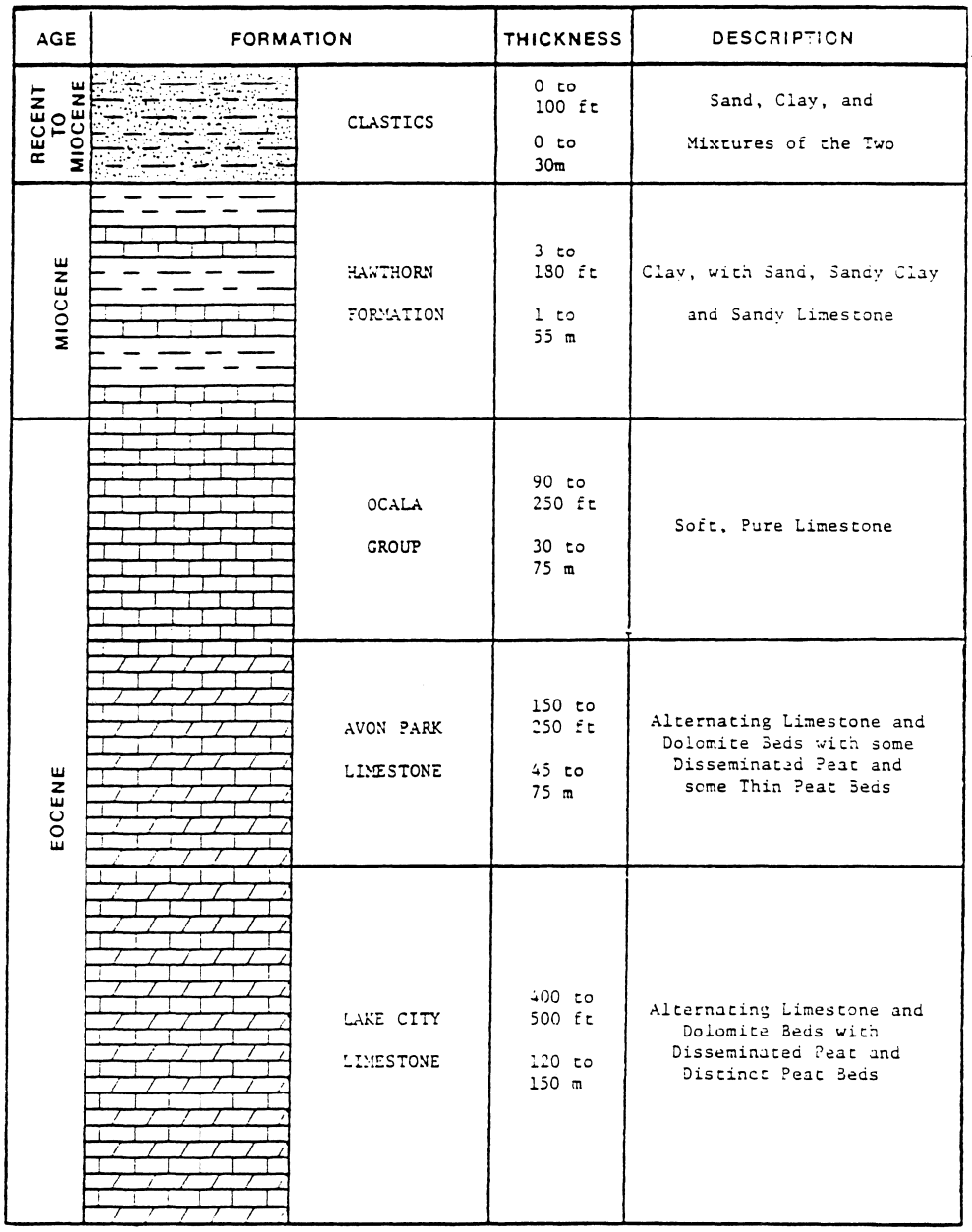

AGE	FORMATION	THICKNESS	DESCRIPTION
RECENT TO MIOCENE	CLASTICS	0 to 100 ft 0 to 30m	Sand, Clay, and Mixtures of the Two
MIOCENE	HAWTHORN FORMATION	3 to 180 ft 1 to 55 m	Clay, with Sand, Sandy Clay and Sandy Limestone
EOCENE	OCALA GROUP	90 to 250 ft 30 to 75 m	Soft, Pure Limestone
EOCENE	AVON PARK LIMESTONE	150 to 250 ft 45 to 75 m	Alternating Limestone and Dolomite Beds with some Disseminated Peat and some Thin Peat Beds
EOCENE	LAKE CITY LIMESTONE	400 to 500 ft 120 to 150 m	Alternating Limestone and Dolomite Beds with Disseminated Peat and Distinct Peat Beds

Figure 2.2 - Geologic column showing rock units in the Tri-County area. Figure from Munch et al. [1979].

The Lake City Limestone and the Avon Park Limestone units are both of Middle Eocene Age and are comprised of alternating beds of limestone and dolomite. Peat beds are found scattered throughout these two units. Johnson [1979] characterized the top of the Avon Park Limestone as the "Avon Park low porosity zone" which consists of hard, low permeability dolomite. This distinguishing feature of the Avon Park Limestone can be seen as a semi-impervious barrier to vertical groundwater flow.

The Ocala Group of late Eocene Age consists predominantly of pure soft limestone and shows a lower average resistivity than does the Avon Park Limestone [Munch et al., 1979]. The Ocala Group contains principally freshwater and supplies large quantities of potable water to the Tri-County area.

The Hawthorn Formation of Miocene Age consists of clays and sands with some interbedded limestones and dolomites and serves as a confining formation for the underlying limestone units. The base of the formation consists predominately of hard dolomite and in most cases is impermeable. A distinguishing feature of the formation is its high phosphate content relative to the Ocala Group. This feature provides for very accurate logging of the contact between these two units.

The Hawthorn Formation underlies the entire Tri-County area except for portions of southeastern Putnam County and most of southern Flagler County. The formation is breached locally by sinkholes, faults, and general erosional processes.

The surficial unit of recent to Miocene Age consists of interbedded lenses of marine sediments, fine to medium sands, shell, and green calcareous silty clay. Thin beds of limestone can be found in certain areas. Small volumes of artesian and nonartesian waters are found in this unit.

2.3 The Availability of Potable Groundwater

Large quantities of potable groundwater are available from the permeable formations underlying northeastern Florida. The hydrologic regime of these formations is commonly divided into two units termed the nonartesian (surficial) aquifer and the artesian (Floridan) aquifer (Figure 2.3). Although the majority of potable water is obtained from the artesian aquifer, small quantities of water are pumped from the nonartesian aquifer for a domestic use. Seasonal irrigation provides the heaviest demand for freshwater derived from the artesian aquifer.

Recharge and withdrawal rates from both aquifers along with the respective aquifer characteristics determine the availability of potable groundwater in the Tri-County area. Recharge rates to the two aquifers have a direct influence on the safe yield from wells in the area. Therefore, a thorough knowledge of the physiography and climatic conditions of the area is essential to a groundwater survey.

The climate of the Tri-County area is classified as humid subtropic with a mean annual rainfall of 135 cm (54 in.). Normally over 50 percent of the total annual rainfall occurs during the months of June through September, with the driest months being November through May. Because the dry season coincides with the area's growing season, large quantities of irrigation water are needed to perpetuate the crops.

The topography of the Tri-County area is generally flat with the majority of land area located in the Eastern Valley. The area is bounded to the west by the Palatka Hill and the Crescent City Ridge and to the east by the Atlantic Coastal Ridge. Figure 2.4 illustrates the physiography of the area. Recharge to the surficial aquifer occurs over the entire area. Recharge to the Floridan Aquifer occurs primarily in the western portions of the area (Figure 2.3).

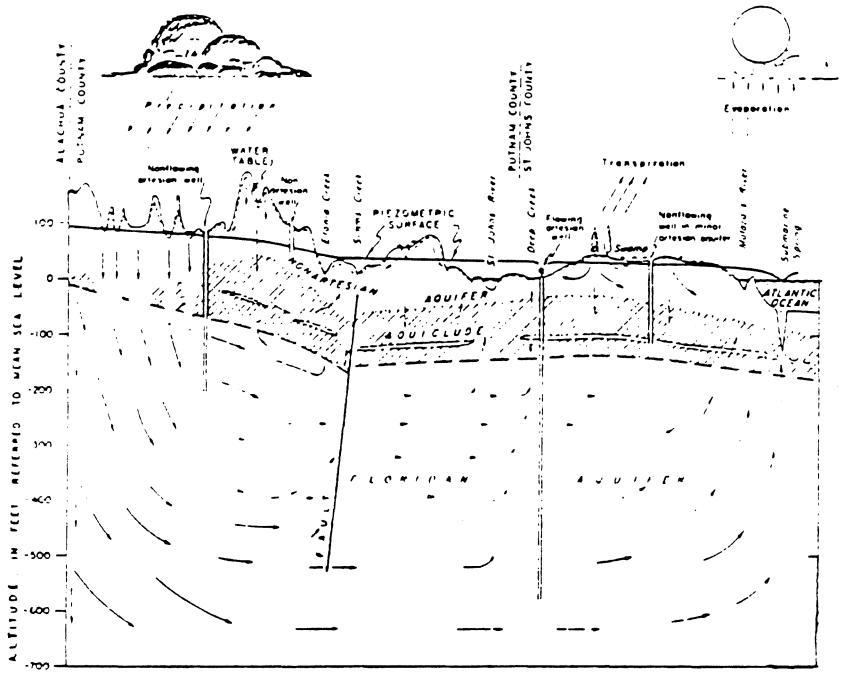

Figure 2.3 - Diagram showing the generalized hydrologic conditions in Northeastern Florida. Figure from Bermes et al. [1963].

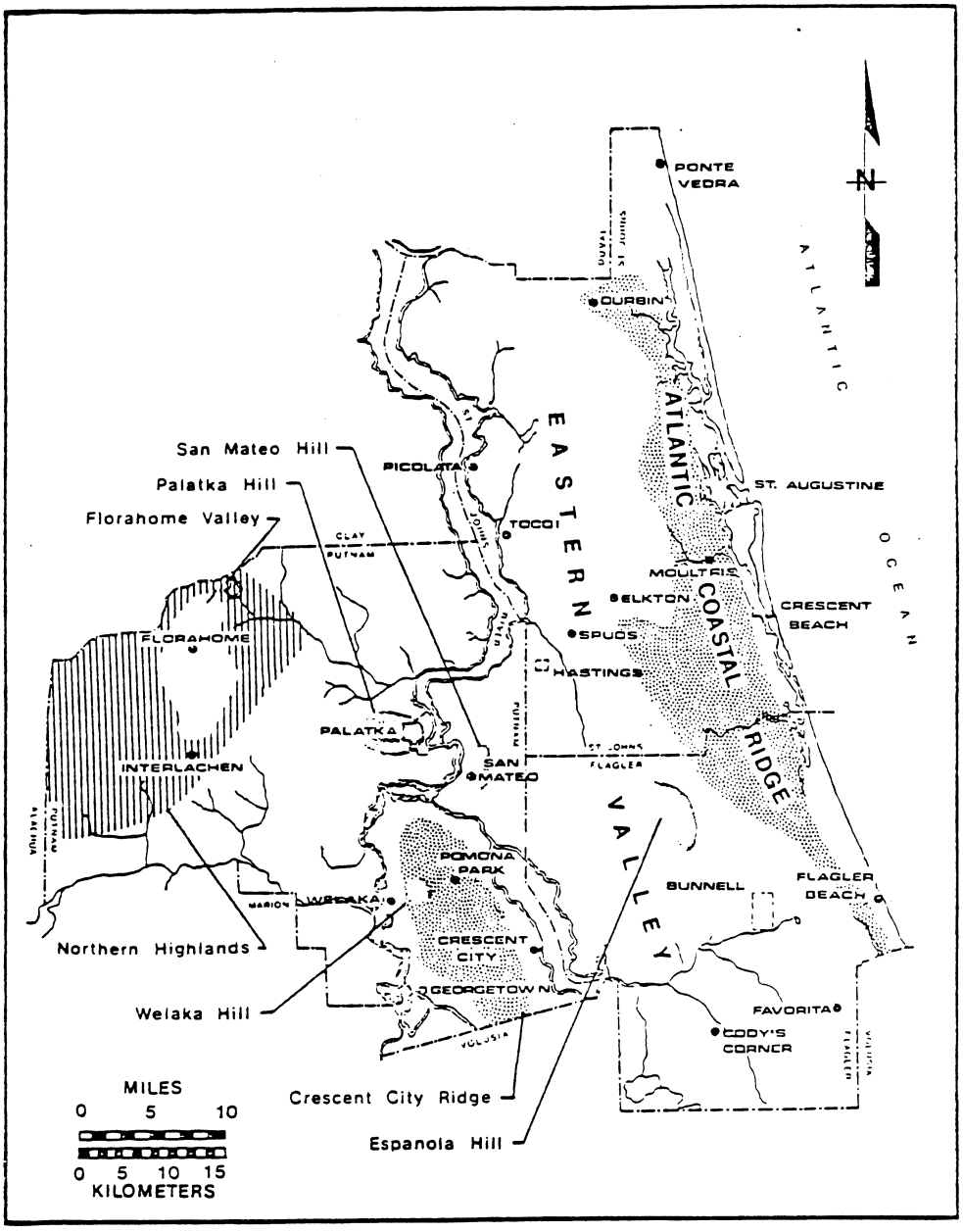

Figure 2.4 - Physiographic features of the Tri-County area. Figure from Munch et al. [1979].

Although the surficial aquifer supplies only a small amount of potable water to the Tri-County area, this aquifer is nevertheless an important source of groundwater. The aquifer grades from deposits of high average permeability at the surface to very low average permeable deposits as the Hawthorn Formation is encountered. The aquifer underlies the entire area attaining its maximum thickness of about 46 m (154 ft) in inland areas and gradually thinning as the Atlantic Ocean is approached. The piezometric head in the aquifer is generally sufficient to bring the top of the water table to within 1 to 3 meters of the ground surface.

In the inland areas, withdrawals from the nonartesian aquifer are generally limited to domestic use. This is due to the small amounts of water and to the high degree of inhomogeneity found within the aquifer. Municipal well fields tapping the nonartesian aquifer can be found in the immediate coastal areas where the underlying artesian aquifers contain saline water.

The artesian aquifer underlying the Tri-County area consists of a principal aquiclude, secondary aquifers, and the Floridan Aquifer. The principal aquiclude is the Hawthorn Formation, which serves to restrict vertical groundwater movement to and from the artesian aquifers. The secondary aquifers consist of lenses of sand, shell, and limestone and occur within the Hawthorn Formation. These aquifers are recharged by the overlying nonartesian aquifer and the underlying Floridan Aquifer. They are important sources of potable groundwater in some coastal areas where the underlying Floridan Aquifer contains saline water.

The Floridan Aquifer is the principal freshwater zone for irrigational, municipal, and industrial uses. Irrigation demands constitute the majority of withdrawal from the aquifer. Table 2.1 summarizes irrigation

Table 2.1 - Historical groundwater withdrawals for irrigated crops in the Tri-County area.

COUNTIES	IRRIGATED ACRES	GROUND WATER WITHDRAWAL (MGD)
	1956	
Putnam	No Report	5
Flagler	4,000	6
St. Johns	16,000	26
	1965	
Putnam	13,000	11.6
Flagler	6,500	3.5
St. Johns	22,000	13.9
	1970	
Putnam	11,200	7.6
Flagler	8,230	9.0
St. Johns	19,000	22.1
	1975	
Putnam	11,380	15.8
Flagler	4,500	6.7
St. Johns	20,120	28.57

Table from Munch et al. [1979]

withdrawals over the past 26 years for the area. Withdrawals for irrigation purposes have generally increased over the past 26 years while the land area under irrigation has remained relatively constant.

Figures 2.5 and 2.6 illustrate a piezometric map of the area and the locations of intensive agriculture in the area, respectively. The impact of irrigation withdrawal upon the piezometric map of the Floridan Aquifer is seen when these two figures are compared. The piezometric sinks roughly coincide with the heavily agriculturalized areas.

Recharge to the aquifer principally occurs in the western and southeastern portions of Putnam County where the aquiclude is breached by sinkholes, in Flagler County where the aquiclude is either thin or absent, and to a smaller extent by downward leakage through the aquiclude. Groundwater is discharged in spring areas, wells, and to some of the overlying secondary aquifers.

At the turn of the century, artesian pressure in the Floridan Aquifer was sufficient to produce free-flowing wells. By the 1950's, artesian water levels dropped, and free-flowing wells could no longer supply enough water for irrigation [Munch et al., 1979]. In response to this condition, several well studies were prepared to determine aquifer characteristics and the potential impact on the Floridan Aquifer due to heavy seasonal withdrawals [Bermes et al., 1963; Bentley, 1977; Munch et al., 1978]. Bentley's study in 1977 consisted of two types of aquifer tests performed on eighteen well sites (Figure 2.7). The results of the individual well test are given in Table 2.2. Based on the aquifer tests, Bentley [1977] concluded that on a regional scale the hydraulic characteristics throughout the Tri-County area were relatively homogeneous with local variations to be expected.

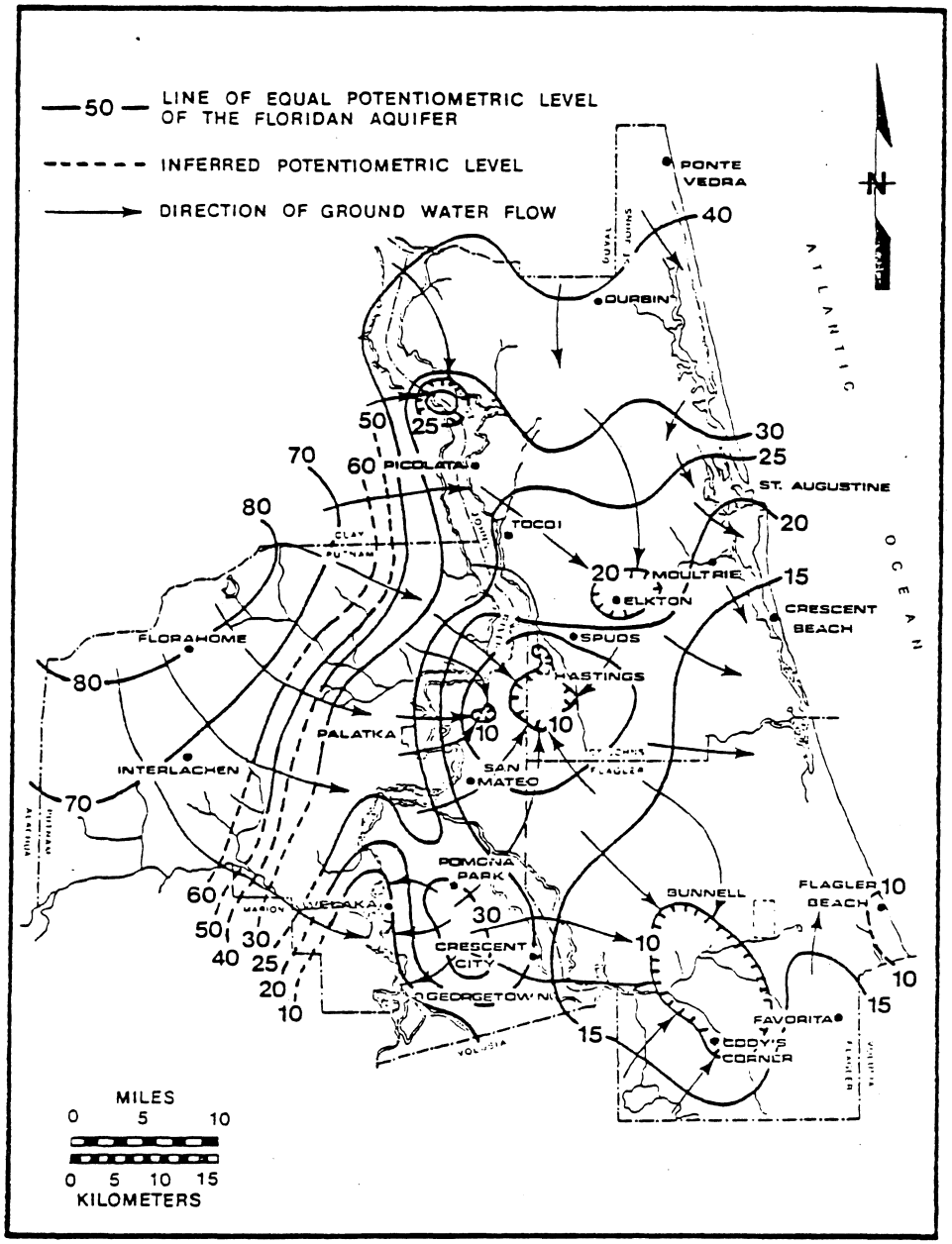

Figure 2.5 - Piezometric level and generalized direction of groundwater movement in the Tri-County area, March, 1975. Figure from Munch et al. [1979].

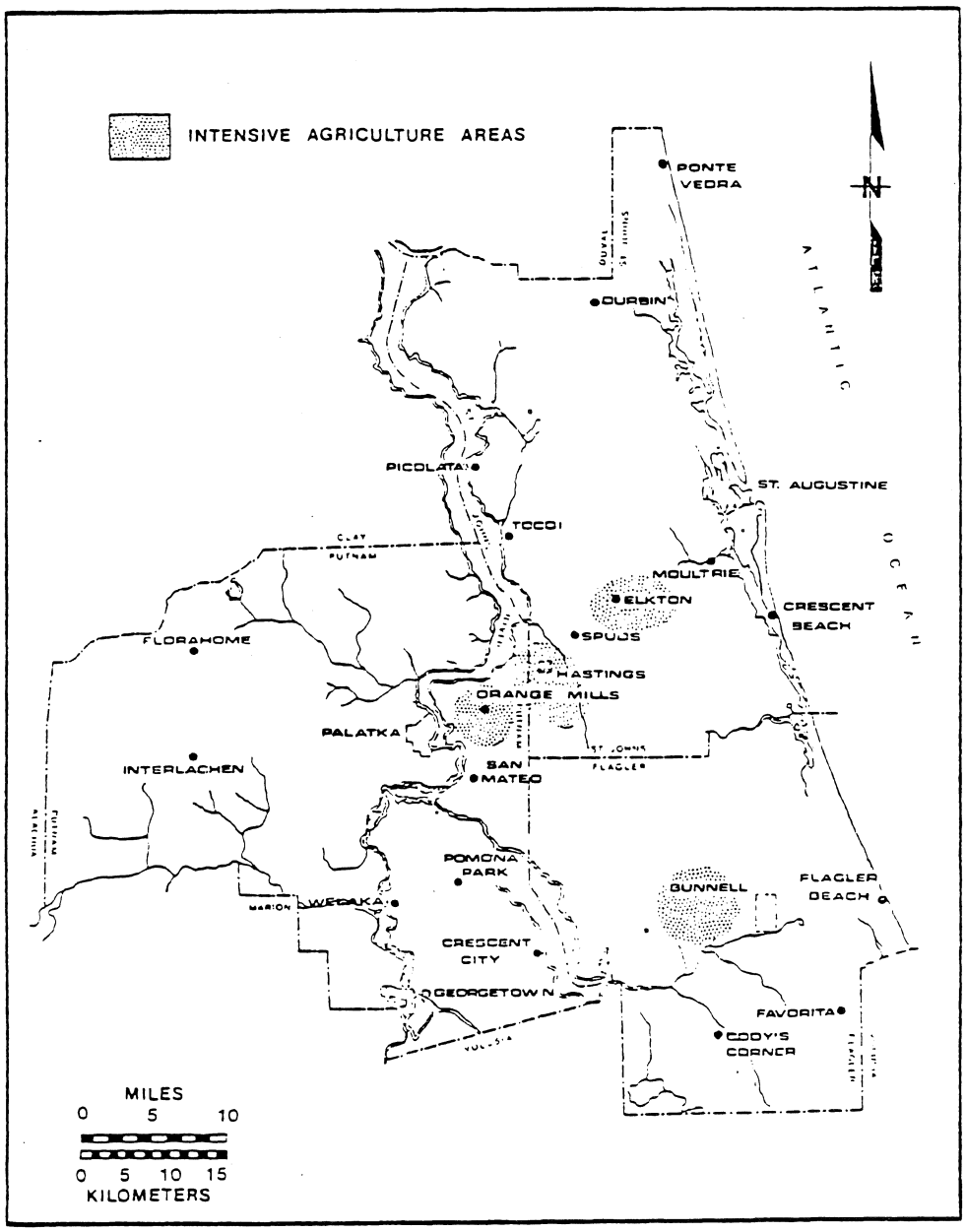

Figure 2.6 - Location of the areas of intensive agriculture within the Tri-County area. Figure from Munch et al. [1979].

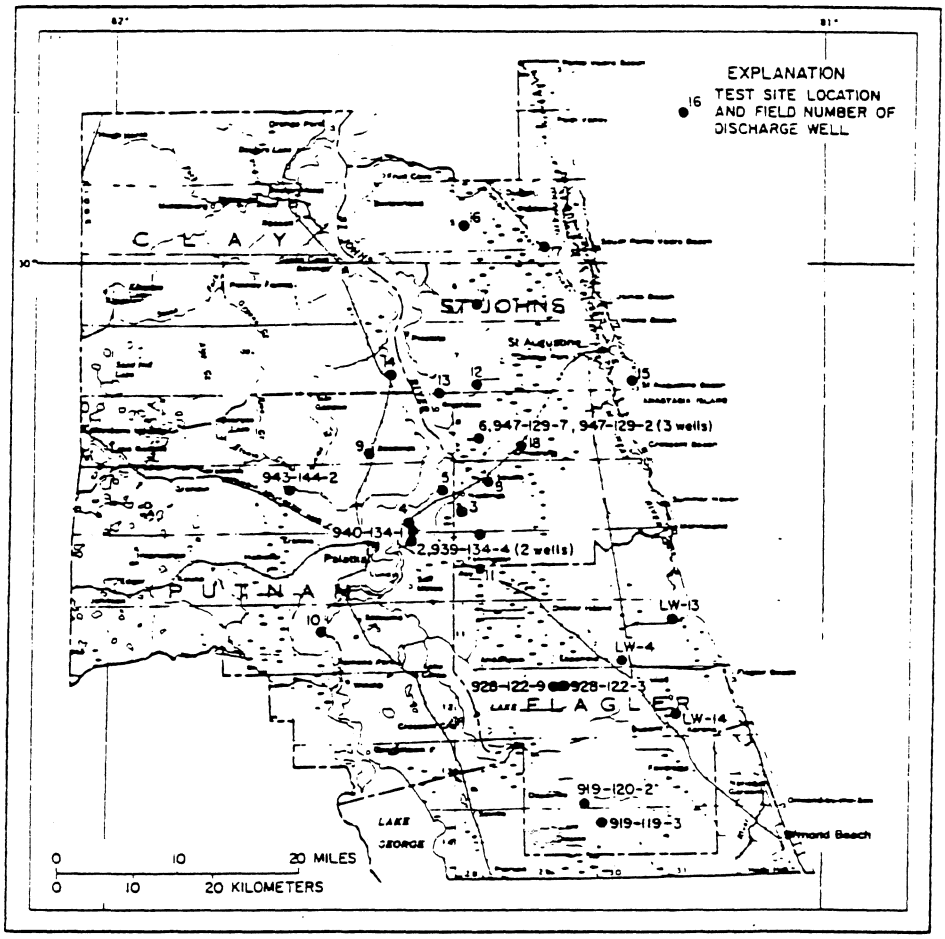

Figure 2.7 - Location of aquifer test sites in the Tri-County area. Figure from Bentley [1977].

Table 2.2 - Aquifer test data.

Location	Well Number	USGS ID Number	Well depth (ft)	Thickness of aquifer (ft)	Observed hydrologic characteristics: Transmissivity, ft^2/d	Storage coefficient,	Leakance d^{-1}
3 mi southeast of Hastings	1	2939580812842.01	200	40	88,000	0.0006	0.019
	1A	2939500812842.01	450	250			
1.2 mi east of East Palatka	2	2939300813436.01	300	180	46,000	.001	.016
	2A	2939330813428.01	547	434			
	2B	2939320813458.01	-	-			
2 mi south of Hastings	3	2940490812944.01	550	430	56,000	.0006	.0051
	3A	2940490812952.01	610	480			
	3B	2940530812927.01	568	420			
1.5 mi northeast of East Palatka	4	2940330813502.01	250	130	24,000	.0008	.010
	4A	2940320813455.01	-	-			
	4B	2940450813515.01	222	90			
2 mi west of Hastings	5	2942570813247.01	300	150	55,000 & 60,000	.001	.021
	5A	2942550813240.01	300	150			
3 mi northwest of Armstrong	6	2947480812906.01	302	130	25,000	.0001	.0011
	6A	2947520812905.01	325	150			
	6B	2947480812924.01	325	150			
7 mi northeast of Picolata	7	2957250812910.01	525	325	54,000	.0002	.0050
	7A	2957300812930.01	525	325			
Spuds	8	2943430812833.01	280	100	29,000	.0001	.00096
	8A	2943430812840.01	280	50			
0.5 mi south of Bostwick	9	2945400813833.01	260	70	17,000	-	-

Table 2.2 - continued.

Location	Well Number	USGS ID Number	Well depth (ft)	Thickness of aquifer (ft)	Observed hydrologic characteristics: Transmissivity, (ft^2/d)	Storage coefficient,	Leakance d^{-1}
10 mi south of Palatka	10	2932340814241.01	295	240	41,000	-	-
Roy	11	2937160812936.01	405	250	26,000	-	-
4 mi northeast Riverdale	12	2951060812909.01	400	200	(data not used in analysis)		
1.5 mi north of Riverdale	13	2950280813309.01	300	70	8,700	-	-
10 mi south of Greencove Springs	14	2951440813717.01	340	80	7,800	-	-
St. Augustine Beach	15	2951320811648.01	248	55	13,000	-	-
4 mi southwest of Durbin	16	3003540813012.01	362	40	6,800	-	-
9 mi north of St. Augustine	17	3000480812333.01	258	10	1,600	-	-
1.5 mi northeast Armstrong	18	2946120812534.01	306	150	15,000	-	-

Table adapted from Bentley [1977, Table 2]

equations describing in three dimensions the distribution of the drawdowns in the flow field, the growth of the saltwater mound, and the development of the transition zone. These equations are formulated into a numerical model by utilizing an iterative alternating direction implicit (ADI) method and the appropriate linear finite difference representation.

The results of the execution of the numerical model indicate that a highly stable, convergent numerical scheme is developed in this study. The model is capable of describing the three-dimensional effects associated with the transient nature of stratified flow in an aquifer.

While the specific example treated salt movement, other contaminants, including hazardous wastes, could easily be modeled in the same way in a stratified flow. In addition, if the contaminant did not bring about stratified conditions or occur in a saline-stratified region, the same basic procedure can be utilized by removing contaminant influence on the flow field in the equation of motion.

2.4 Mineralization

The Floridan Aquifer in northeastern Florida contains zones of saline water which underlie the freshwater artesian aquifer. The origin of the saline water was probably due to the infiltration of sea water during the Pleistocene Epoch when the sea stood above its present elevation. As the sea level subsequently receded, recharge to the mineralized aquifer flushed out the saline water in the upper portions of the aquifer. This flushing action is a continuous process and will occur as long as the inland piezometric heads are above sea level.

Currently, the Floridan Aquifer in the area consists of a freshwater aquifer and a saline water aquifer (Figure 2.8). The freshwater aquifer extends from the bottom of the Hawthorn Formation, through the Ocala Group, and ends at or near the "low porosity zone" marking the top of the Avon Park Limestone. The saline water aquifer underlies the freshwater aquifer. Because fresh and saline waters are miscible fluids, there exists a small zone of transition between the fresh and saline aquifers.

Contaimination of the freshwater aquifer occurs from downward leakage through the Hawthorn Formation and from the upward migration of saline water from deep semiconfining formations. Large differences between the values of the piezometric heads of the freshwater aquifer and the overlying phreatic aquifer suggest minimal leakage through the Hawthorn Formation. This would imply that the majority of leakage occurs from deep semi-confining formations. In this study the contamination of the freshwater aquifer from underlying saline water is termed "mineralization". The mineralization process is shown schematically in Figure 2.9.

The mineralization of the freshwater aquifer in the Tri-County area stems from heavy seasonal pumpage in the highly agriculturalized areas

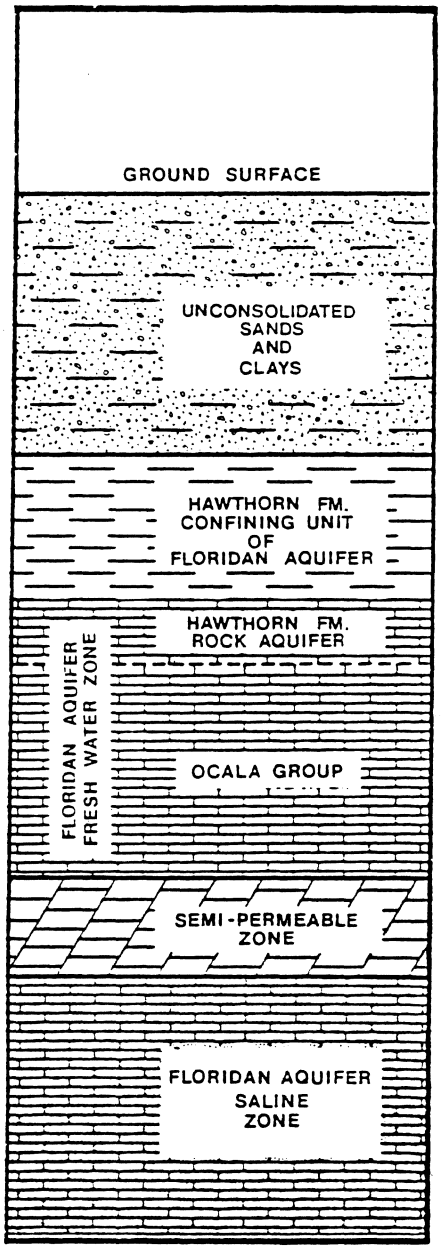

Figure 2.8 - Location of the freshwater zone and the saline water zone within the Floridan Aquifer. Figure adapated from Munch et al. [1979, Figure 32].

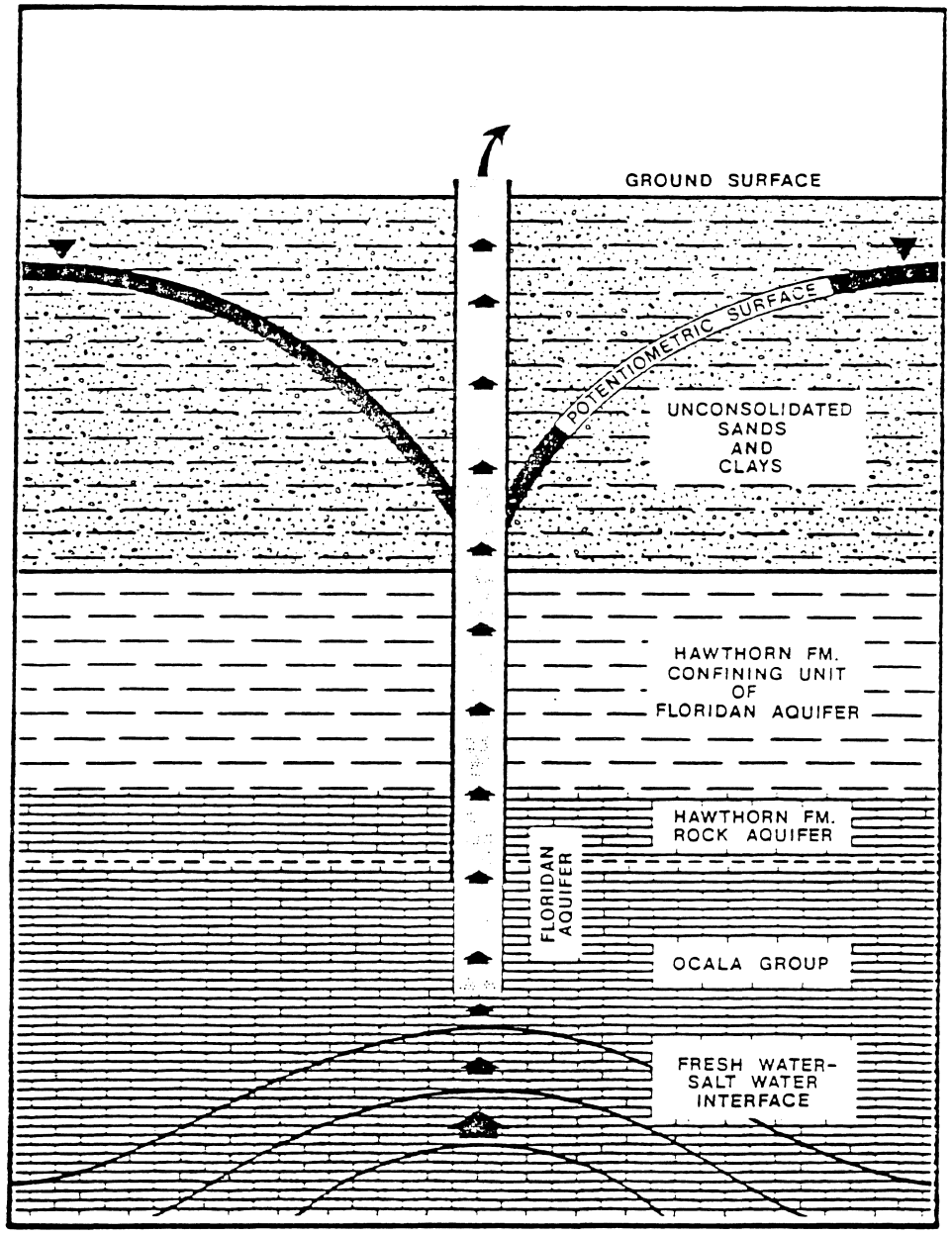

Figure 2.9 - Schematic diagram of saltwater coning as related to the Tri-County area. Figure from Munch et al. [1979].

(Figure 2.6). Irrigation of crops begins in late September and continues through May. At the beginning of the growing season the piezometric surface of the freshwater aquifer is sufficiently high to produce many free-flowing wells. Intense groundwater withdrawals during the season in the agriculturalized areas produce cones of depressions that may exceed 6 m (20 ft) below the land surface, and water quality deteriorates rapidly. Partial to total recovery of the original piezometric surface occurs due to natural recharge during the summer months when little to no pumpage occurs. The recovery process is illustrated in Figures 2.10 and 2.12. These piezometric maps are accompanied by their respective isochlor maps in Figures 2.11 and 2.13. Note the correspondence between the agriculturalized areas, the piezometric sinks, and the areas of higher chloride content. This correspondence again suggests that the mineralization process occurs due to upward leakage of saline water into the freshwater aquifer in response to heavy pumpage.

Two major mineralization studies [Bermes et al., 1963; Munch et al., 1979] have been performed in the Tri-County area. The most recent study, completed in 1979, thoroughly reviews the mineralization process and reflects the current policy in the area. In general, this study has found that in the area: (1) a gradual decline in the piezometric surface of the Floridan Aquifer has occurred due to increasing groundwater withdrawals during this century and (2) the areas and amounts of saltwater contamination have increased from 1956 to 1975.

2.5 Current Assessment

Current assessments concerning the problems of groundwater mineralization in the Tri-County area are presented in the study [Munch et al., 1979] prepared by the St. Johns Water Management District. A portion of

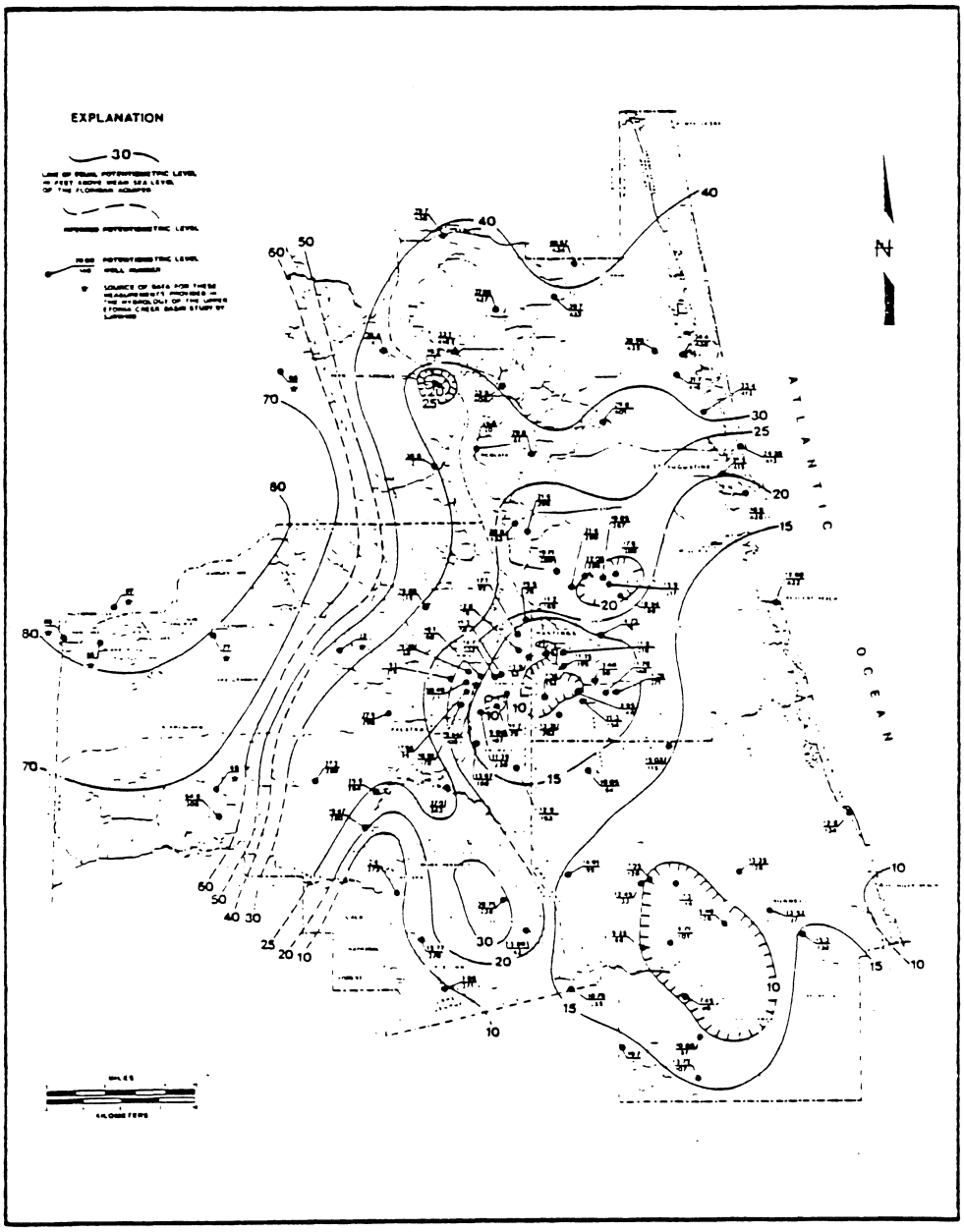

Figure 2.10 - Piezometric map of the Floridan Aquifer, March, 1975. Figure from Munch et al. [1979].

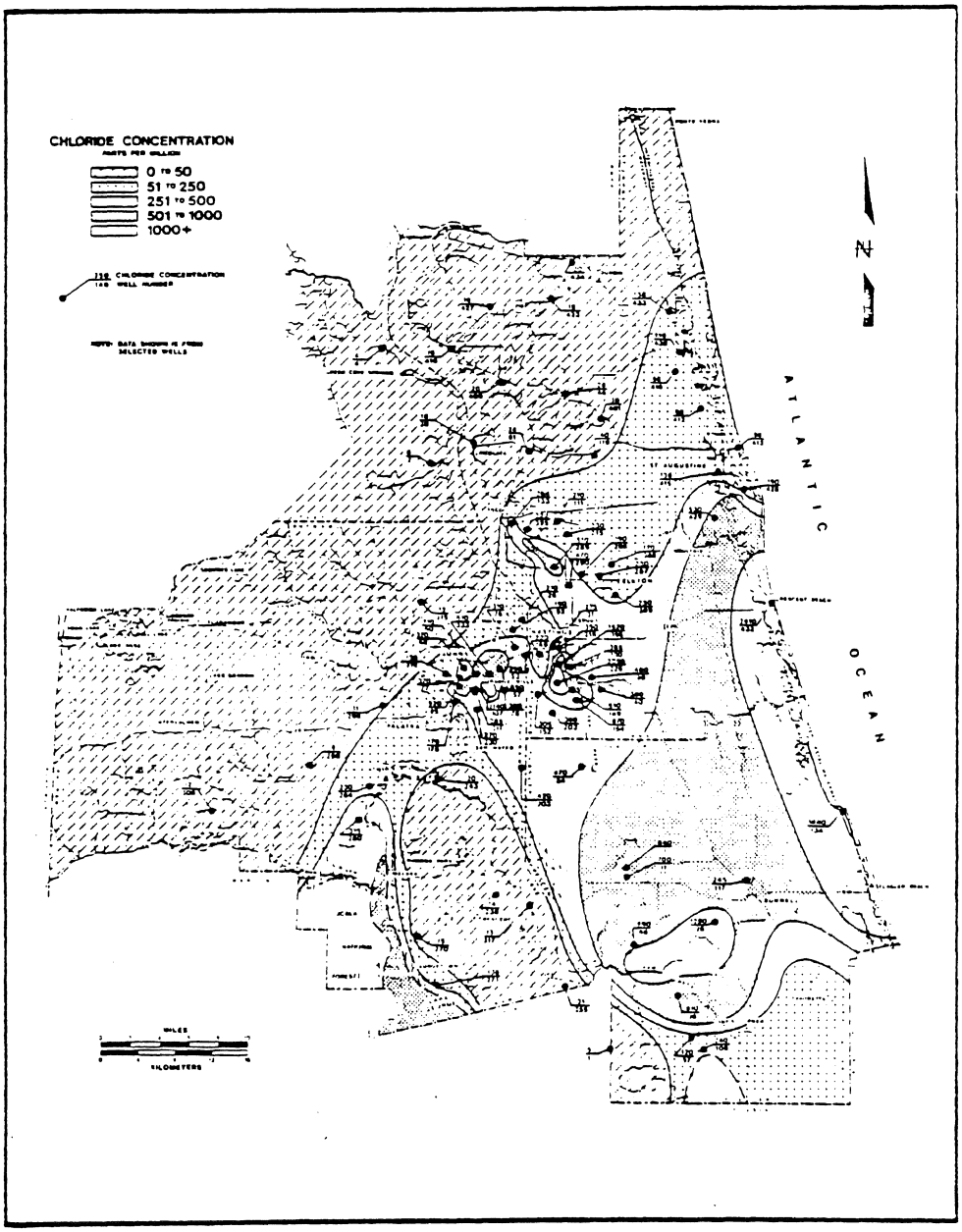

Figure 2.11 - Isochlor map of the Floridan Aquifer, March, 1975. Figure from Munch et al. [1979].

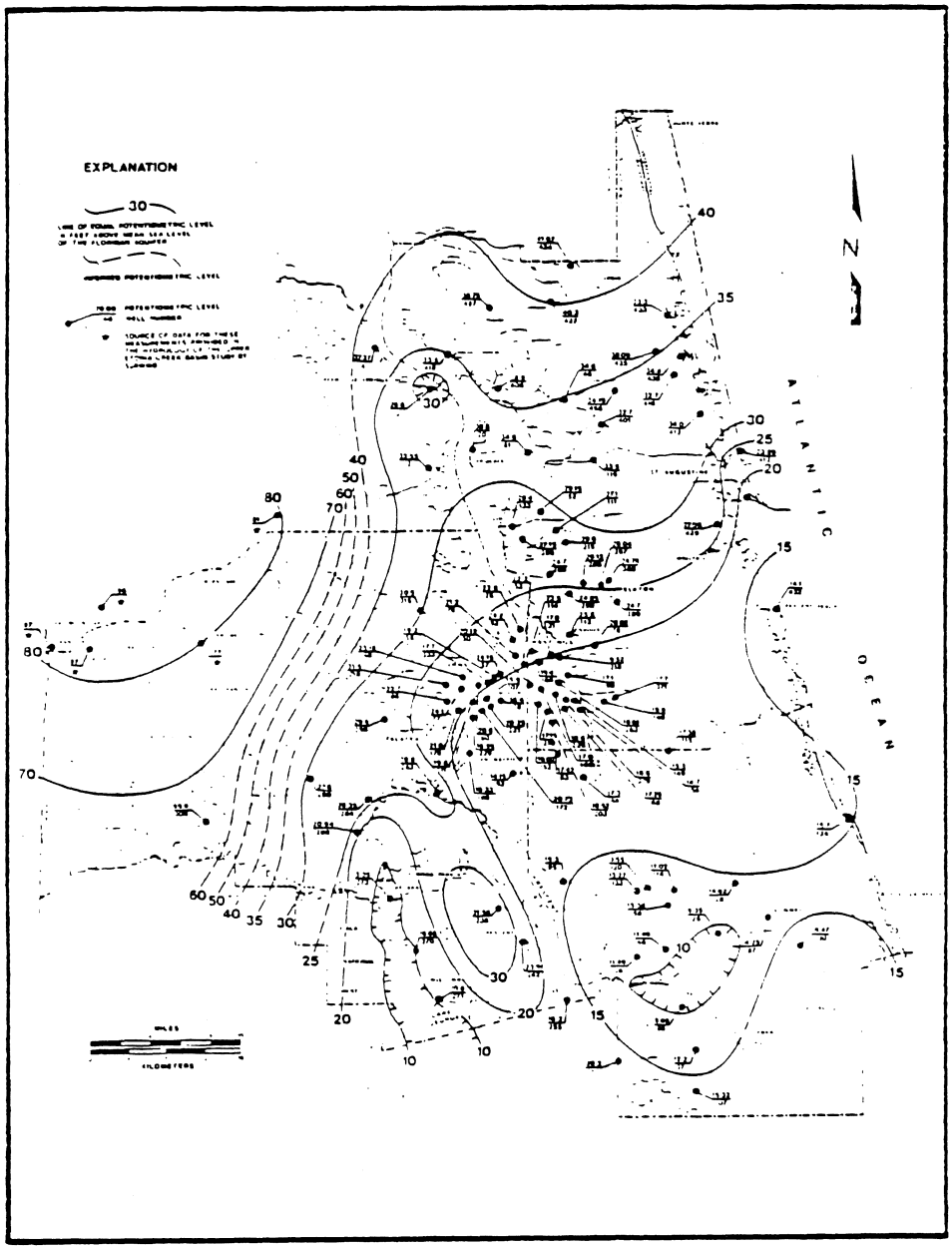

Figure 2.12 - Piezometric map of the Floridan Aquifer, September, 1975.
Figure from Munch et al. [1979].

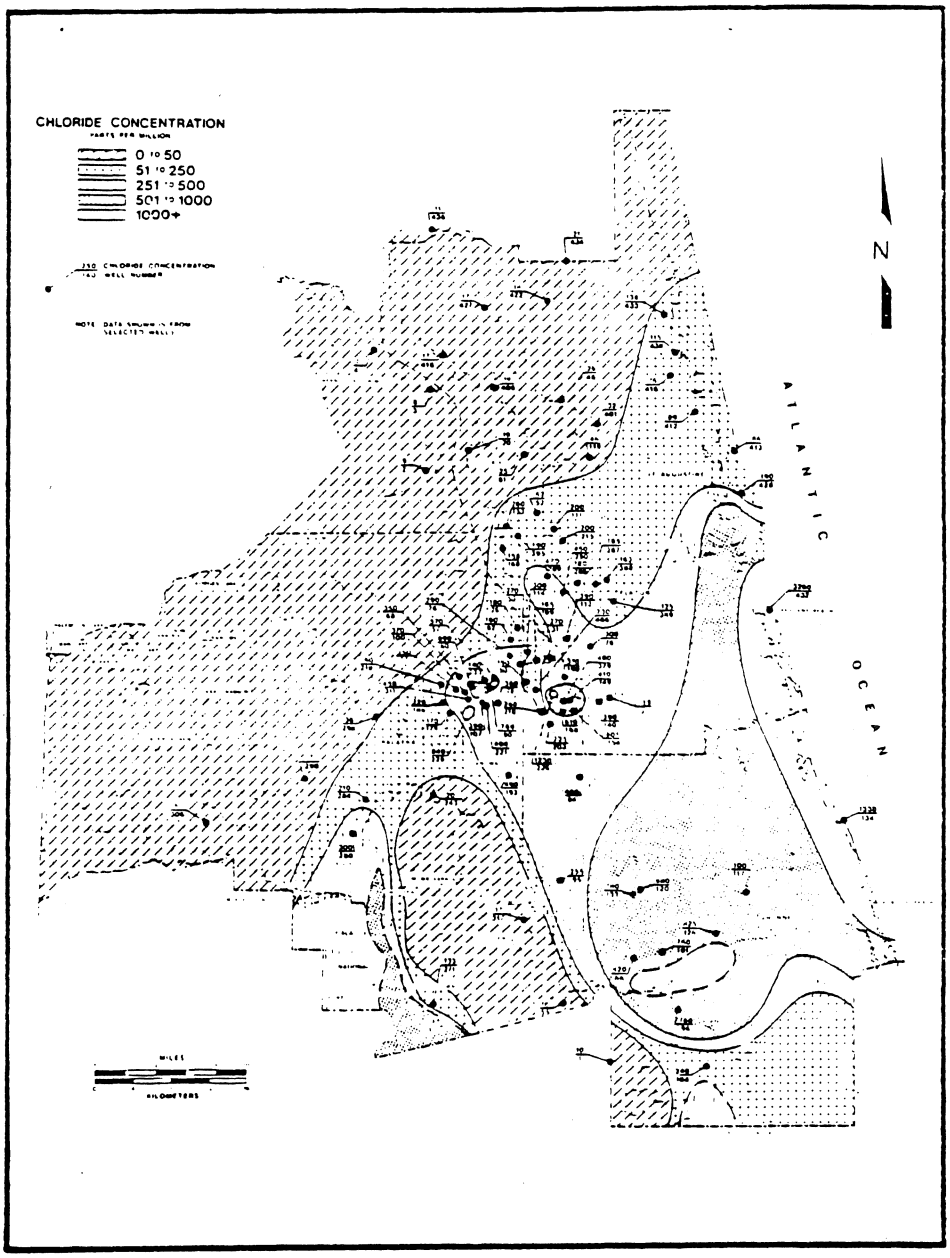

Figure 2.13 - Isochlor map of the Floridan Aquifer, September, 1975. Figure from Munch et al. [1979].

this study attempts to correlate chloride concentration with pumpage rate, well depth, aquifer penetration, and piezometric level by a regression analysis and polynomial expansion. The compiled data illustrate that in response to pumpage, piezometric levels decrease and chloride concentrations increase. The reverse situation prevails during the non-growing season when pumpage is small and recovery occurs. A statistical analysis indicated that 50 percent of the wells in the study area may produce water with a chloride content less than or equal to 210 ppm, and that 10 percent of the wells may exceed 778 ppm chloride during any time of the year. At times some of the deeper wells can act as direct conduits for the transport of saline water into the freshwater aquifer.

During periods of intense pumpage, local cones of depression are formed in the areas of Orange Hills, Hastings, Elkton, and Bunnell (Figure 2.5). Recharge to the aquifer from leakage is insufficient to stabilize the local cones of depression. The lowest piezometric levels and the highest chloride concentrations were apparent in the local cones of depression during the month of March. The greatest variation in water levels and water quality occurred during the months of March through September when recovery of the aquifer occurs.

The combination of well construction, well spacing, and overdraft lead to the upconing of saline water beneath pumping wells. The study attempted to calculate safe yields from various theoretical formulas which might stabilize the local cones of depression during periods of low piezometric levels. Pumpage rates ranged from 817 m^3/d (150 gpm) within the central portions of the local cones of depression to as much as 1910 m^3/d (350 gpm) in areas where the freshwater aquifer thickness exceeds 61 m (200 ft). According to a statistical analysis, it was

determined that at least 120 wells in the area could benefit from rehabilatative construction procedures.

Recommendations available to the agriculturalists and the various governing agencies are presented at the end of the study.

2.6 Summary

The geologic structure of the Tri-County area consists of rock units ranging in age from Middle Eocene to recent. These units in ascending order are the Lake City Limestone, the Avon Park Limestone, the Ocala Group, the Hawthorn Formation, and a surficial unit. The Lake City Limestone, the Avon Park Limestone, and the Ocala Group consist predominately of porous limestone and dolomite. The Hawthorn Formation consists primarily of sands, clays, and marls and is considered a confining unit.

The hydrologic regime of the area consists of a nonartesian (surficial) aquifer, a principal (Hawthorn Formation) aquiclude, and an artesian (Floridan) aquifer. The nonartesian aquifer supplies small amounts of potable water to the area mainly for domestic use. In the Floridan Aquifer the Ocala Group contains predominately freshwater while the underlying units contain saline water. This aquifer supplies the majority of irrigational, municipal, and industrial waters to the area. Irrigational needs constitute the majority of withdrawals from the aquifer.

Because of excessive pumpage for irrigational purposes, the chloride content of the freshwater zone of the Floridan Aquifer has increased steadily since the turn of the century. It is suggested that this condition is caused by the upward migration of saline water from deep semiconfining formations. The mineralization problem is most severe in the vicinity of the highly agriculturalized areas.

Two major mineralization studies have been conducted in the Tri-County area [Bermes et al., 1963; Munch et al., 1979]. Munch's study in 1979 supplies a thorough overview of the mineralization problem and presents recommendations for the control and prevention of well contamination.

CHAPTER 3

STUDIES LEADING TO THE QUANTITATIVE ANALYSIS OF AQUIFER MINERALIZATION

3.1 Introduction

The intense development of certain coastal regions of the world in the twentieth century has created a situation where saltwater intrusion has jeopardized the quality of freshwater derived from coastal aquifers. The east and west coasts of Florida pose various problems associated with salinity intrusion into coastal aquifers. In response to the problems presented by saltwater intrusion within coastal aquifers, a great variety of studies have been conducted to better understand and evaluate these problems.

Many aquifers located quite far from coastal areas are also subject to the mineralization phenomenon. This has of late begun to attract much attention. The mineralization phenomenon associated with inland aquifers is very similar to that experienced by coastal aquifers. Many of the techniques utilized for the study of the mineralization phenomenon in coastal aquifers may be applied for the study of inland aquifers. Several studies pertaining to both types of aquifer mineralization are reviewed within.

In the analysis of flow through porous media, the nomenclature concerning the number of dimensions in which the analysis is conducted is often confusing. Therefore for the sake of clarity, a two-dimensional analysis will be defined as representing flow in a plane region while a three-dimensional analysis will be defined as representing flow in a spatial region.

3.2 Early Studies

The first analytical relationship relating fresh and saline waters in a phreatic coastal aquifer was presented by two independent investigators [Ghyben, 1888; Herzberg, 1901]. The Ghyben-Herzberg relationship states that the depth below sea level at which saltwater can be found in a coastal aquifer is about forty times that of the corresponding height of freshwater above sea level. Although this is an approximate relationship for a phreatic aquifer subject to horizontal flow, it can be used to obtain a rough estimate of the location of the freshwater-saltwater interface within the aquifer.

Despite the efforts of Ghyben [1888] and Herzberg [1901], investigators working for the oil industry were the first to complete detailed analytical mineralization studies [Muskat and Wychoff, 1935; Arthur, 1944]. These studies describe the upconing of saline water into overlying oil deposits. Their applications were limited due to the simplified geometry utilized in the development of the analysis. Nevertheless these first studies provided valuable insight into the physical phenomena associated with the mineralization process.

Subsequent mineralization studies stemmed primarily from the groundwater quality problems associated with the intensive development of the world's coastal regions. These studies attempted to simulate the flow conditions within an aquifer subject to mineralization by a variety of physical, analog, and mathematical models.

Before the emergence of high speed digital computers in the late 1950's, physical and analog models were popular in mineralization studies. The Hele-Shaw model was especially well suited for this purpose. Although physical and analog models are useful for the understanding of the

physical phenomena associated with aquifer mineralization, a new model must be constructed for each unique application incurring great time and expense. With the advent of digital computers came a switch from physical and analog models to sophisticated analytical and numerical models. These latter models are the basis for our contemporary knowledge of the mineralization phenomenon.

3.3 Current Approaches

Two basic approaches can be adopted when applying an analytical or numerical model to an aquifer mineralization problem. The first approach assumes the immiscibility of the fresh and saline waters whereby an assumed sharp interface is found at their mutual boundaries [Bear and Dagan, 1964; Hantush, 1968; Shamir and Dagan, 1971; Haubold, 1975]. The second approach simultaneously solves the equations of motion and solute transport to describe the transient position of a dispersive saltwater front migrating into the freshwater aquifer.

With the sharp interface approach, potential flow theory can be applied to both sides of the sharp interface between the fresh and salt waters. But because fresh and saline waters are miscible fluids, this approach suffers from a lack of coherence with the physical phenomena. However, the assumption of a sharp interface sometimes supplies a good approximation to the transient position of the transition zone between freshwater and saltwater zones.

The inclusion of the solute transport equation in the second approach implies the existence of a zone of transition or a dispersive front either of which migrates through the porous media. The solute (salt) is dispersed within the flow field due to diffusion and mechanical dispersion processes and thereby affects the dynamics of the flow. The

mineral distribution in the flow field introduces nonlinear terms into the equations that should be used in the analysis. For numerical schemes these nonlinear terms cause problems with convergence and stability. Various approaches attempt to linearize the equations to facilitate analytical solutions.

The analysis of either a transition zone or a dispersive front may be performed in a variety of ways. If the solute is a neutrally buoyant material, then various perturbation methods can work extremely well and generate simplified models that can lead to analytical solutions. If the solute is not a neutrally buoyant tracer then various combinations of perturbation approaches can also be used in order to simplify the mathematical model. Some of these methods are discussed in detail in subsequent sections.

3.4 Analytical Techniques

The analysis of stratified flow in porous media by analytical techniques usually involves the application of certain perturbation methods. When applied to a steady flow field, perturbation methods can reduce the solute transport equation to an equation of the heat conduction type. Solutions to the heat conduction equation are well documented in various texts.

Dagan [1971] analyzed the migration of neutrally buoyant tracers. He considered both longitudinal and lateral hydrodynamic dispersion in the porous medium. The analysis derives an inner boundary layer solution for a transition zone in a steady flow field by utilizing the stream function and the velocity potential function as coordinates. In this analysis it is required that the stream function and the velocity potential function be defined for every point in the flow field prior

to the calculation of the solute dispersion. This is true only when a neutrally buoyant material is introduced into the flow field. Only problems with constant hydraulic conductivity and a constant coefficient of dispersion can be solved by this analysis. Eldor and Dagan [1972] later extended their analysis to include radioactive decay and adsorption.

Gelhar and Collins [1971] applied a second perturbation method to analyze dispersive flow in porous media. The study develops an approximate analytical technique for the description of longitudinal dispersion in unidirectional steady flow with variations along a streamline. The governing equation is reduced to a simple diffusion equation, and a general solution is obtained. Results are obtained by evaluating two integrals in the velocity field. Lateral dispersion is not treated in the analysis. Thus, a solution is not found for a boundary layer which develops along a streamline.

Hunt [1978] introduced a perturbation method that can be used for nonuniform, steady and unsteady flow through heterogeneous porous media. The solution, while being very general, is most accurate when the boundary layer is relatively thin and accurate numerical solutions are difficult to obtain due to numerical dispersion. The study suggests that the perturbation solution initially be used until the size of the boundary layer approaches a predetermined limiting value where a numerical solution is then employed to finish the analysis.

The above perturbation methods are based in part upon the assumption of the existence of potential flow at every point in the flow field. In the case of saltwater intrusion problems, this assumption fails due to the density differences between the fresh and salt waters whereby

nonpotential flow conditions exist in the boundary layer. Dagan [1971] addressed a saltwater intrusion problem but assumed that the minerals within the saltwater act as ideal tracers.

Rubin and Pinder [1977] solved the nonpotential flow problem in the boundary layer by the utilization of the integral method of boundary layer approximation [Ozisik, 1980] in conjunction with a perturbation method. The dispersion process is described as a migration of a sharp interface perturbed by small disturbances due to salinity dispersion. Salinity dispersion creates a mixing zone in which boundary layer similarity exists. Although this study gives only steady state solutions, the boundary layer integral method supplied a means by which transient mineralization problems may be analyzed, usually by a numerical scheme.

While perturbation methods yield good two-dimensional analyses, the extension of these methods to three dimensions would be extremely difficult. For example, following Dagan [1971] a solution in three dimensions would necessitate the use of stream function planes and velocity potential function planes.

3.5 Numerical Techniques

Numerical techniques have several advantages over analytical techniques when applied to aquifer mineralization problems. Numerical techniques are able to handle complex geometries and boundary conditions, heterogeneous and anisotropic porous media, and time dependent problems whereas most analytical techniques can not. On the other hand, analytical solutions are often easier to apply and can be used to check the accuracy of the numerical solution.

Both finite element and finite difference schemes are used when analyzing aquifer mineralization problems. Pinder and Cooper [1970]

utilized a finite difference numerical scheme to simulate saltwater intrusion within a coastal aquifer. The method of characteristics is used to solve the solute transport equation and the alternating direction implicit (ADI) method is used to solve the equation of motion for a two-dimensional problem. The method is applicable to heterogeneous, anisotropic porous media with irregular geometry, constant head, and constant flux boundary conditions.

Segol et al. [1975] applied a Galerkin-finite element technique for the two-dimensional simulation of saltwater intrusion within a coastal aquifer. The Galerkin-finite element theory is used to formulate approximations to the nonlinear equations for velocity and pressure. With this information the solute transport equation is solved separately. Iteration between the solute transport equation and the flow equations continues until convergence is reached.

Rubin and Christensen [1982] and Rubin [1982] developed numerical schemes for the two-dimensional simulation of stratified flow in a coastal aquifer and an inland aquifer, respectively. Both studies utilize the integral boundary layer method where the solute transport equation is integrated over the thickness of the boundary layer subject to certain similarity conditions. The resulting equation is then solved simultaneously with the equations of continuity and motion by an implicit-explicit finite difference numerical scheme. The study presented herein extends Rubin's work [1982] to obtain a three-dimensional analysis.

3.6 Summary

The problems associated with the mineralization of coastal aquifers have generated a large number of studies attempting to describe the phenomenon. Few studies have dealt with the mineralization problems

found in inland aquifers. However, some of the analytical and numerical concepts developed for coastal aquifers can be applied to inland aquifers.

Two common approaches can be applied to the flow field for the description of the mineralization phenomenon. The first approach assumes a sharp interface which exists between the fresh and saltwater zones. This approach suffers from a lack of physical coherence. The second approach solves the equations of motion and solute transport simultaneously. Perturbation methods as well as numerical schemes can be used for this purpose. Boundary layer methods can be applied in order to generate analytical as well as numerical approaches for the description of the dispersive freshwater-saltwater interface. Various studies utilize all three methods.

CHAPTER 4

THE APPROXIMATE METHOD OF STRATIFICATION ANALYSIS

4.1 Introduction

Stratified flow in an aquifer stems from the contact between fresh and saline waters in the aquifer. Flow within the aquifer creates a zone of transition separating the fresh and saline waters. The mineral (salt concentration) distribution within the transition zone affects the dynamics of the flow field. On the other hand, the transport of the minerals within the flow field depends on the structure of the flow field. It is clear that complicated flow conditions exist within an aquifer subject to mineralization.

To simulate stratified flow within an aquifer the equations of continuity, motion, and solute transport are solved simultaneously subject to a given set of boundary conditions. This procedure leads to a set of highly nonlinear equations which cause problems associated with stability and convergence in the numerical solution.

This study presents an approach whereby the equations describing stratified flow within an aquifer are simplified. The Dupuit approximation and the integral boundary layer method are used for this purpose. The result is a highly stable, convergent numerical scheme describing the mineralization process in three dimensions.

4.2 Description of the Flow Field

Figure 4.1 shows a schematic description of a flow field typical to an inland aquifer. According to this figure the flow field is divided into three zones as follows: (a) the upper zone of freshwater, (b) the transition zone, and (c) the lower zone of saltwater. By applying the Dupuit approximation to the flow field, certain simplifying assumptions are made. The flow in the freshwater zone is mainly horizontal and potential. The flow in the transition zone is mainly horizontal and is nonpotential due to the mineral distribution within this zone. The flow in the saltwater zone is vertical and potential. For the purposes of this study, this flow field description will be extended in the remaining horizontal dimension to yield a two-dimensional flow field.

4.3 Basic Equations

The basic equations used for the simulation of stratified flow in an aquifer are the equations of continuity, motion, solute transport, and state represented respectively as follows

$$\nabla \cdot \vec{q} + \frac{\partial n}{\partial t} = 0 \tag{4.1}$$

$$\nabla p + \gamma \vec{k} + \frac{\gamma}{K} \vec{q} = 0 \tag{4.2}$$

$$n \frac{\partial C}{\partial t} + \nabla \cdot (\vec{q}C) = \nabla \cdot (\tilde{D} \cdot \nabla C) \tag{4.3}$$

$$\gamma = \gamma_0 (1 + \alpha C) \tag{4.4}$$

where, $\vec{q}$ = specific discharge; n = porosity; t = time; p = pressure; γ = specific weight; $\vec{k}$ = unit vertical vector; K = hydraulic conductivity; C = mineral concentration; $\tilde{D}$ = dispersion tensor; γ_0 = specific weight

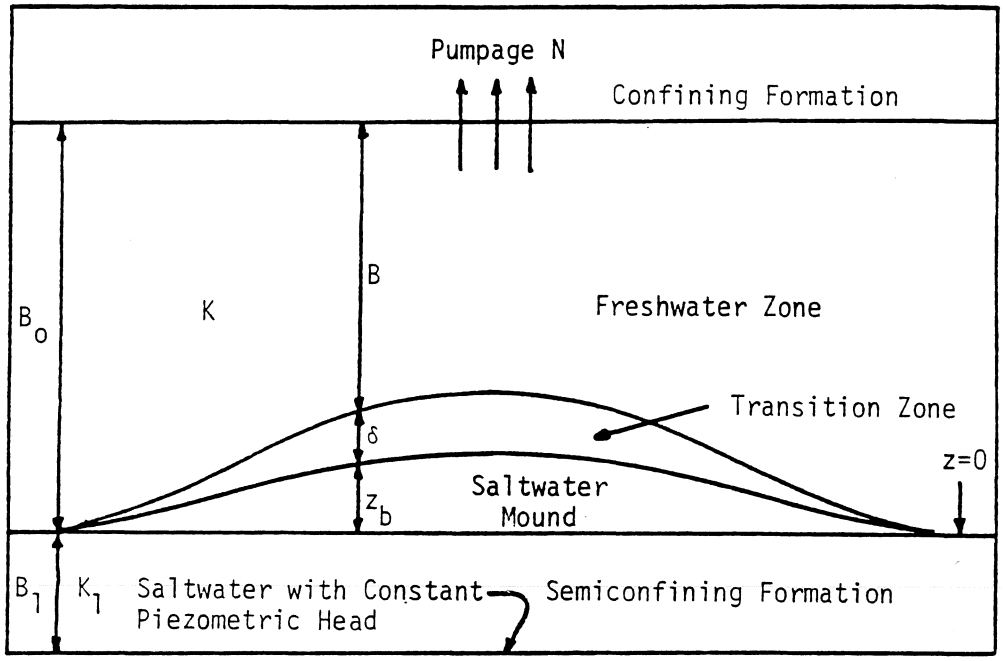

Figure 4.1 - Schematic description of the development of a transition zone in a stratified aquifer.

of reference; α = constant relating changes in mineral concentration with specific weight.

Equations (4.1), (4.2), (4.3), and (4.4) are solved simultaneously utilizing a finite difference numerical scheme as shown in the following sections.

4.4 The Integral Method of Boundary Layer Approximation

The integral method of boundary layer approximation is an analytical tool first introduced by von Kármán. The method is applicable to both linear and nonlinear transient value problems for certain boundary conditions. Basically, the method simplifies the appropriate equations by integrating over a phenomenological distance thereby creating a boundary layer. The distribution of the desired parameters within the boundary layer is given for example by a polynomial profile that satisfies similarity conditions. Thus, the parameter distribution is given as a function of time and position in the medium. In this study, the phenomenological distance is the thickness of the transition zone and the desired parameters are the solute concentration and the specific discharge.

This study applies the integral method of boundary layer approximation for the simplification of the simultaneous solution of the basic equations (4.1), (4.2), (4.3), and (4.4) in the three-dimensional simulation of the stratified flow process. The analysis is based upon the work of Rubin [1982] and represents an extension of his approach for the simulation of the mineralization process in the two-dimensional flow field.

In Figure 4.1 the upper zone includes freshwater whose specific density is constant. Therefore, in this zone equation (4.2) yields

$$\vec{q} = -K_f \nabla\phi_f \tag{4.5}$$

where

$$\phi_f = p/\gamma_f + z \tag{4.6}$$

Here, ϕ_f = piezometric head at the freshwater zone; K_f = hydraulic conductivity of the porous medium containing freshwater; γ_f = specific weight of the freshwater; z = elevation with respect to an arbitrary datum.

The lower zone includes mineral water whose specific density is constant. Therefore, in this zone equation (4.2) yields

$$\vec{q} = - K_s \nabla\phi_s \tag{4.7}$$

where, K_s = hydraulic conductivity of the porous medium containing saltwater.

$$\phi_s = p/\gamma_s + z \tag{4.8}$$

Here, ϕ_s = piezometric head at the mineral water zone; γ_s = specific weight of the mineral water.

We may assume $K_f \approx K_s \approx K$.

Assuming the flow in the transition zone is mainly horizontal, then an integration of equation (4.2) between the bottom and the top of the transition zone yields

$$\frac{\gamma_s}{\gamma_o}(\phi_{sb} - z_b) - \frac{\gamma_f}{\gamma_o}(\phi_{ft} - z_t) = \int_{z_b}^{z_t} \frac{\gamma}{\gamma_o}\, dz \tag{4.9}$$

where, b,t = indices referring to the bottom and the top of the transition zone, respectively.

It is assumed that the transition zone is represented by a boundary layer where the specific discharge and the solute concentration profiles satisfy the following similarity conditions

$$u = UF(\eta) \qquad v = VF(\eta) \qquad C = C_o L(\eta) \tag{4.10}$$

where, u,v = components of the specific discharge in the transition zone in the horizontal x and y directions, respectively; U,V = characteristic specific discharge in the horizontal x and y directions, respectively; C_o = characteristic concentration; F,L = distribution functions; η = dimensionless coordinate of the transition zone defined as follows

$$\eta = (z - z_b)/\delta \qquad \delta = z_t - z_b \tag{4.11}$$

Here, δ = thickness of the transition zone.

Introducing equations (4.4), (4.10), and (4.11) into equation (4.9) yields

$$(1 + \alpha C_s)\, \phi_{sb} - (1 + \alpha C_f)\, \phi_{ft} + \alpha C_f \delta - \alpha (C_s - C_f)\, z_b = \alpha C_o \delta \int_0^1 L d\eta \tag{4.12}$$

Assuming $C_f \simeq 0$ and $C_s = C_o$ yields

$$\phi_{ft} = (1 + \xi)\, \phi_{sb} - \xi\, z_b - \xi \delta \int_0^1 L d\eta \tag{4.13}$$

where

$$\xi = \alpha C_s = (\gamma_s - \gamma_f)/\gamma_f \tag{4.14}$$

Referring to Figure 4.1, it is assumed that beneath the semiconfining layer the piezometric head is not affected by pumpage and has a constant value ϕ_{so}. Initially, the freshwater-saltwater interface is assumed to be a sharp interface and is horizontal. Therfore, continuity of the pressure yields

$$\gamma_f \phi_{fo} = \gamma_s \phi_{so} \tag{4.15}$$

where, o = subscript referring to initial conditions.

The piezometric head at the bottom of the transition zone is given as follows

$$\phi_{sb} = \phi_{so} - n \frac{\partial z_b}{\partial t} \left(\frac{B_1}{K_1} + \frac{z_b}{K}\right) \tag{4.16}$$

where, B_1 = thickness of the semiconfining layer; K, K_1 = hydraulic conductivities of the aquifer and the semiconfining formation, respectively.

Combining equations (4.13) and (4.16) yields

$$\phi_{ft} = \phi_{fo} - n (1 + \xi) \frac{\partial z_b}{\partial t} \left(\frac{B_1}{K_1} + \frac{z_b}{K}\right) - \xi z_b$$

$$- \xi\delta \int_0^1 L d\eta \tag{4.17}$$

Reference to the drawdown, s, instead of the freshwater piezometric head, and an application of equations (4.1) and (4.2) yield for a two-dimensional flow field

$$\frac{\partial}{\partial x}\left[K\left(B + \delta\int_0^1 F d\eta\right)\frac{\partial s}{\partial x}\right] + \frac{\partial}{\partial y}\left[K\left(B + \delta\int_0^1 F d\eta\right)\frac{\partial s}{\partial y}\right]$$

$$- n\frac{\partial z_b}{\partial t} + N = S\frac{\partial s}{\partial t} \qquad (4.18)$$

where, S = coefficient of storage; N = rate of pumpage per unit area.

Rearranging (4.17) yields

$$\frac{\partial z_b}{\partial t} = \frac{K K_1}{n(B_1 K + z_b K_1)(1 + \xi)}\left(\dot{s} - \xi z_b\right.$$

$$\left. - \xi\delta\int_0^1 L d\eta\right) \qquad (4.19)$$

The equation describing the growth of the transition zone is developed with reference to Figure 4.2. In this figure a portion of the transition zone is considered as a control volume. The application of the equation of solute transport to this control volume and an integration over the thickness of the transition zone yields

$$\frac{\partial}{\partial t}\left(\int_{z_b}^{z_b+\delta} nC dz\right)dx + \frac{\partial}{\partial x}\left(\int_{z_b}^{z_b+\delta} uC dz\right)dx = - D\left.\frac{\partial c}{\partial z}\right|_{z_b} dx \qquad (4.20)$$

where, n = porosity of the porous medium.

Introducing the similarity conditions given in equation (4.10) into (4.20) and rearranging yields

$$\left(\frac{n}{2}\int_0^1 L d\eta\right)\frac{\partial \delta^2}{\partial t} + \left[\frac{U}{2}\frac{\partial \delta^2}{\partial x} + \delta^2\frac{\partial U}{\partial x}\right]\int_0^1 LF d\eta = - DL'(0) \qquad (4.21)$$

where, $L'(0) = (dL/d\eta)_{\eta=0}$.

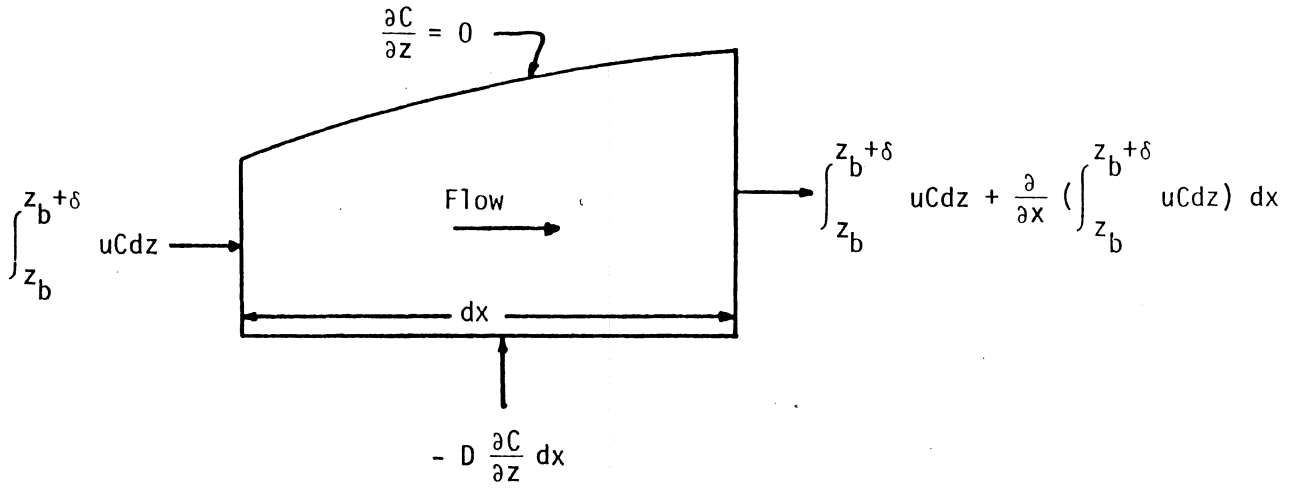

Figure 4.2 - Control volume for the development of equation (4.22).

Equation (4.21) represents the growth of the transition zone for a unidirectional flow. The application of the same approach to a two-dimensional horizontal flow field yields

$$\left(\frac{n}{2}\int_0^1 L\,d\eta\right)\frac{\partial \delta^2}{\partial t} + \left[\delta^2\left(\frac{\partial u}{\partial x} + \frac{\partial v}{\partial y}\right) + \frac{1}{2}\left(U\frac{\partial \delta^2}{\partial x}\right.\right.$$

$$\left.\left. + V\frac{\partial \delta^2}{\partial y}\right]\right]\int_0^1 F L\,d\eta = -DL'(0) \qquad (4.22)$$

This analysis considers that the bottom of the transition zone is represented by z_b and is stationary. However, z_b is a function of time thereby generating one additional term in equation (4.22). However, this term is canceled by the convection term generated by the vertical specific discharge in the saltwater zone.

In general the coefficient of dispersion, D, is proportional to the absolute value of the specific discharge. Therefore, it is assumed that

$$D = a(U^2 + V^2)^{1/2} \qquad (4.23)$$

where, a = constant almost identical to the transverse dispersivity of the aquifer.

According to Figure 4.1, it is evident that

$$B = B_o - z_b - \delta \qquad (4.24)$$

Equation (4.18) is a parabolic second order equation and describes the distribution of the drawdown in the flow field. Equation (4.19) describes the rate of growth of the saltwater mound. Equation (4.22)

is a hyperbolic first order equation describing the development and propagation of the transition zone in the aquifer.

For the simulation of flow conditions in the two-dimensional flow field, an implicit-explicit finite difference scheme for equations (4.18), (4.19), and (4.22) is developed in the next chapter. This numerical scheme results in a three-dimensional simulation of the mineralization process in the aquifer.

4.5 Summary

Stratified flow in an aquifer is associated with quite complicated flow conditions. The mineral transport within the flow field depends upon the structure of the flow field. On the other hand, the mineral distribution affects the dynamics of the flow.

A two-dimensional flow field is described where a freshwater zone, a transition zone, and a saltwater zone are found. By the application of the Dupuit approximation and the integral method of boundary layer approximation to the two-dimensional flow field, the simultaneous solution of the equations of continuity, motion, and solute transport yields three partial differential equations describing a three-dimensional stratified flow process. Originally these equations are highly nonlinear and create problems with stability and convergence within a numerical scheme. By applying the boundary layer approach the complexity of the system is reduced and its susceptibility to numerical problems of convergence and stability is diminished.

CHAPTER 5

NUMERICAL SIMULATION

5.1 Introduction

The governing equations, (4.18), (4.19), and (4.22), developed in the last chapter have the unique ability to completely describe the mineralization phenomenon in an inland aquifer. The objective of this chapter is to formulate a solution for these equations that is coherent with the actual mineralization process. Because the equations are non-linear and expressed in two independent space variables and one independent time variable, a numerical scheme is the only practical means by which a solution may be obtained. Most groundwater flow problems are numerically approached by a variety of finite difference, finite element, and boundary element methods. Satisfactory groundwater flow models have been developed utilizing each of the above methods.

Several finite difference methods offer approaches leading to approximate solutions to partial differential equations. Implicit schemes with their exceptional stability properties are almost always used for the solution of initial value problems in two space variables. A variety of solution techniques are offered in the literature [Mitchell, 1976] and include the alternating direction implicit (ADI) method, the locally one-dimensional (LOD) method, and the successive overrelaxation (SOR) method, among others.

In selecting the appropriate numerical solution technique for unsteady groundwater flow problems, the ease of application and the ability

to utilize the resulting model in various geographical regions is of considerable importance. Finite element and boundary element models are generally specific to one application and are not easily adapted to a distinctly separate region. On the other hand, a finite difference model utilizing an ADI solution method can in most cases analyze a variety of applications, often only with a simple change in parameters. Also, groundwater flow modelers generally accept the ADI method and its variations as the most efficient technique for the simulation of two-dimensional unsteady groundwater flow problems. It is for these reasons that it was decided to adopt the ADI method as a solution technique in this study.

5.2 The Numerical Model

The numerical model developed in this section is based on the linearization of equations (4.18), (4.19), and (4.22) and the application of an iterative ADI method. The equations are linearized by appropriate finite difference representations. The result is a highly stable, convergent numerical scheme capable of completely simulating three-dimensional stratified flow conditions found in an inland aquifer.

The ADI method was first introduced by Peaceman and Rachford [1955] and is especially well suited for the solution of time dependent, linear parabolic systems. The application of the ADI method to a parabolic system involves the solution of tridiagonal sets of equations along lines parallel to the x and y coordinate axes. The appropriate finite difference equations are formulated into two subsets in the horizontal x-y plane. First, the unknowns in the x direction are calculated at the time level (m+1) utilizing known values in the y direction from time level (m). Second, the unknowns in the y direction are calculated at the time level (m+2)

utilizing known values in the x direction from time level (m+1). The method alternates between the two directions for the desired time sequence.

When utilizing an ADI method it is important to realize that a solution can only be found when the tridiagonal matrix contains a set of linear equations. Because equations (4.18) and (4.22) are highly non-linear, extreme care must be taken when formulating their linear finite difference representations. These equations must be linearized correctly for the ADI method to be of any practical use.

The linearization of equations (4.18) and (4.22) is accomplished by referring to certain parameters at different time levels. It is common to use half-time intervals, (m), (m+1/2), (m+1), etc. In this manner non-linear terms may be linearized to accommodate their solution.

The finite difference representation of equations (4.18), (4.19), and (4.22) is now presented. These finite difference equations comprise the numerical model.

An implicit scheme for the calculation of the drawdown in the x direction for time level (m+1) is obtained from equation (4.18) as follows

$$-s_{i-1,j}^{(m+1)} \left[(B + \delta \int_0^1 F d\eta) \frac{K\,\Delta t}{(\Delta x)^2}\right]_{i-1/2,j}^{(m+1/2)} + s_{i,j}^{(m+1)} \{S + [B$$

$$+ \delta \int_0^1 F d\eta) \frac{K\,\Delta t}{(\Delta x)^2}]_{i+1/2,j}^{(m+1/2)} + [(B + \delta \int_0^1 F d\eta) \frac{K\,\Delta t}{(\Delta x)^2}]_{i-1/2,j}^{(m+1/2)} \}$$

$$- s_{i+1,j}^{(m+1)} \left[(B + \delta \int_0^1 F d\eta) \frac{K\,\Delta t}{(\Delta x)^2}\right]_{i+1/2,j}^{(m+1/2)} = S\, s_{i,j}^{(m)}$$

$$- n \left(\frac{\partial z_b}{\partial t}\right)_{i,j}^{(m+1/2)} \Delta t + N_{i,j} \Delta t + (s_{i,j+1}^{(m)} - s_{i,j}^{(m)}) \left[(B + \delta \int_0^1 F d\eta) \frac{K \Delta t}{(\Delta y)^2}\right]_{i,j+1/2}^{(m+1/2)} + (s_{i,j-1}^{(m)} - s_{i,j}^{(m)}) \left[(B + \delta \int_0^1 F d\eta) \frac{K \Delta t}{(\Delta y)^2}\right]_{i,j-1/2}^{(m+1/2)} \tag{5.1}$$

An implicit scheme for the calculation of the squared thickness of the transition zone in the x direction for the time level (m+1) is obtained from equation (4.22) as follows

$$\delta_{i,j}^{2(m+1)} \left[\frac{n}{2} \int_0^1 L d\eta + \frac{\Delta t}{4(\Delta x)^2} K_{i,j} (s_{i+1,j}^{(\bar{m}+1/2)} - s_{i-1,j}^{(m+1/2)}) \int_0^1 FL d\eta\right]$$

$$= \delta_i^{2(m)} \frac{n}{2} \int_0^1 L d\eta - \{\delta_{i,j}^{2(m+1/2)} \frac{\Delta t}{(\Delta x)^2} [K_{i+1/2,j} (s_{i+1,j}^{(m+1/2)}$$

$$- s_{i,j}^{(m+1/2)}) + K_{i-1/2,j} (s_{i-1,j}^{(m+1/2)} - s_{i,j}^{(m+1/2)})]$$

$$- \delta_{i-1,j}^{2(m+1)} \frac{\Delta t}{4(\Delta x)^2} K_{i,j} (s_{i+1,j}^{(m+1/2)} - s_{i-1,j}^{(m+1/2)})\} \int_0^1 FL d\eta$$

$$- \{\delta_{i,j}^{2(m)} \frac{\Delta t}{(\Delta y)^2} [K_{i,j+1/2} (s_{i,j+1}^{(m+1/2)} - s_{i,j}^{(m+1/2)}) + K_{i,j-1/2} (s_{i,j-1}^{(m+1/2)}$$

$$- s_{i,j}^{(m+1/2)})] + \frac{\Delta t}{4(\Delta y)^2} K_{i,j} (s_{i,j+1}^{(m+1/2)} - s_{i,j-1}^{(m+1/2)}) (\delta_{i,j+1}^{2(m)}$$

$$- \delta^{2(m)}_{i,j-1})\} \int_0^1 FL d\eta - \frac{a\ \Delta t}{2} K_{i,j} \left[\left(\frac{s^{(m+1/2)}_{i+1,j} - s^{(m+1/2)}_{i-1,j}}{\Delta x}\right)^2\right.$$

$$\left. + \left(\frac{s^{(m+1/2)}_{i,j+1} - s^{(m+1/2)}_{i,j-1}}{\Delta y}\right)^2\right]^{1/2} L'(0) \qquad (5.2)$$

An implicit scheme for the calculation of the drawdowns in the y direction for time level (m+2) is obtained from equation (4.18) as follows

$$-s^{(m+2)}_{i,j-1} \left[\left(B + \delta \int_0^1 Fd\eta\right) \frac{K\ \Delta t}{(\Delta y)^2}\right]^{(m+1\ 1/2)}_{i,j-1/2} + s^{(m+2)}_{i,j} \{S$$

$$+ \left[\left(B + \delta \int_0^1 Fd\eta\right) \frac{K\ \Delta t}{(\Delta y)^2}\right]^{(m+1\ 1/2)}_{i,j+1/2} + \left[\left(B + \delta \int_0^1 Fd\eta\right) \frac{K\ \Delta t}{(\Delta y)^2}\right]^{(m+1\ 1/2)}_{i,j-1/2} \}$$

$$- s^{(m+2)}_{i,j+1} \left[\left(B + \delta \int_0^1 Fd\eta\right) \frac{K\ \Delta t}{(\Delta y)^2}\right]^{(m+1\ 1/2)}_{i,j-1/2} = S\ s^{(m+1)}_{i,j}$$

$$- n \left(\frac{\partial z_b}{\partial t}\right)^{(m+1\ 1/2)}_{i,j} \Delta t + N_{i,j}\ \Delta t + (s^{(m+1)}_{i+1,j} - s^{(m+1)}_{i,j}) \left[\left(B\right.\right.$$

$$\left.\left. + \delta \int_0^1 Fd\eta\right) \frac{K\ \Delta t}{(\Delta x)^2}\right]^{(m+1\ 1/2)}_{i+1/2,j} + (s^{(m+1)}_{i-1,j} - s^{(m+1)}_{i,j}) \left[\left(B\right.\right.$$

$$\left.\left. + \delta \int_0^1 Fd\eta\right) \frac{K\ \Delta t}{(\Delta x)^2}\right]^{(m+1\ 1/2)}_{i-1/2,j} \qquad (5.3)$$

An implicit scheme for the calculation of the squared thickness of the transition zone in the y direction for the time level (m+2) is obtained from equation (4.22) as follows

$$\delta_{i,j}^{2(m+2)} \left[\frac{n}{2}\int_0^1 L d\eta + \frac{\Delta t}{4(\Delta y)^2} K_{i,j} \left(s_{i,j+1}^{(m+1\ 1/2)} - s_{i,j-1}^{(m+1\ 1/2)}\right) \int_0^1 FL d\eta\right]$$

$$= \delta_{i,j}^{2(m+1)} \frac{n}{2}\int_0^1 L d\eta - \{\delta_{i,j}^{2(m+1\ 1/2)} \frac{\Delta t}{(\Delta y)^2} K_{i,j+1/2} \left(s_{i,j+1}^{(m+1\ 1/2)}\right.$$

$$\left. - s_{i,j}^{(m+1\ 1/2)}\right) + K_{i,j-1/2} \left(s_{i,j-1}^{(m+1\ 1/2)} - s_{i,j}^{(m+1\ 1/2)}\right)]$$

$$- \delta_{i,j-1}^{2(m+2)} \frac{\Delta t}{4(\Delta y)^2} K_{i,j} \left(s_{i,j+1}^{(m+1\ 1/2)} - s_{i,j-1}^{(m+1\ 1/2)}\right)\} \int_0^1 FL d\eta$$

$$- \{\delta_{i,j}^{2(m+1)} \frac{\Delta t}{(\Delta x)^2} [K_{i+1/2,j} \left(s_{i+1,j}^{(m+1\ 1/2)} - s_{i,j}^{(m+1\ 1/2)}\right)$$

$$+ K_{i-1/2,j} \left(s_{i-1,j}^{(m+1\ 1/2)} - s_{i,j}^{(m+1\ 1/2)}\right)] + \frac{\Delta t}{4(\Delta x)^2} K_{i,j} \left(s_{i+1,j}^{(m+1\ 1/2)}\right.$$

$$\left. - s_{i-1,j}^{(m+1\ 1/2)}\right) \left(\delta_{i+1,j}^{2(m+1)} - \delta_{i-1,j}^{2(m+1)}\right)\} \int_0^1 FL d\eta$$

$$= \frac{a\ \Delta t}{2} K_{i,j} \left[\left(\frac{s_{i+1,j}^{(m+1\ 1/2)} - s_{i-1,j}^{(m+1\ 1/2)}}{\Delta x}\right)^2\right.$$

$$\left. + \left(\frac{s_{i,j+1}^{(m+1\ 1/2)} - s_{i,j-1}^{(m+1\ 1/2)}}{\Delta y}\right)^2\right]^{1/2} L'(0) \qquad (5.4)$$

Although an implicit approach was adopted for the development of equation (5.3) and (5.4), it is conceivable to also apply an explicit approach. These two approaches are developed in the Appendix.

Equations (4.19) and (4.24) yield, respectively

$$\left(\frac{\partial z_b}{\partial t}\right)_{i,j}^{(m+1/2)} = \left[\frac{K K_1}{n(B_1 K + z_b K_1)(1+\xi)} (s - \xi z_b - \xi \delta \int_0^1 L d\eta)\right]_{i,j}^{(m+1/2)} \tag{5.5}$$

and

$$B_{i,j}^{(m+1/2)} = B_o - (z_b + \delta)_{i,j}^{(m+1/2)} \tag{5.6}$$

These finite difference equations are solved numerically by the application of an iterative ADI method. The details of the application are presented in the next section.

5.3 Model Execution

The numerical model developed in the previous section is executed with the aid of a high speed digital computer. Following the flow chart given in Figure 5.1, a computer program is written for this purpose. The flow chart illustrates the application of an iterative ADI method in conjunction with a print scheme for the solution of the numerical model.

Before the computer program is written a finite difference grid is constructed which represents an aquifer's flow field. The grid is formulated in a horizontal x-y plane. The grid spacing is chosen as an example to be uniform in both the x and y directions, and for computational convenience Δx equals Δy. A field of pumpage is superimposed

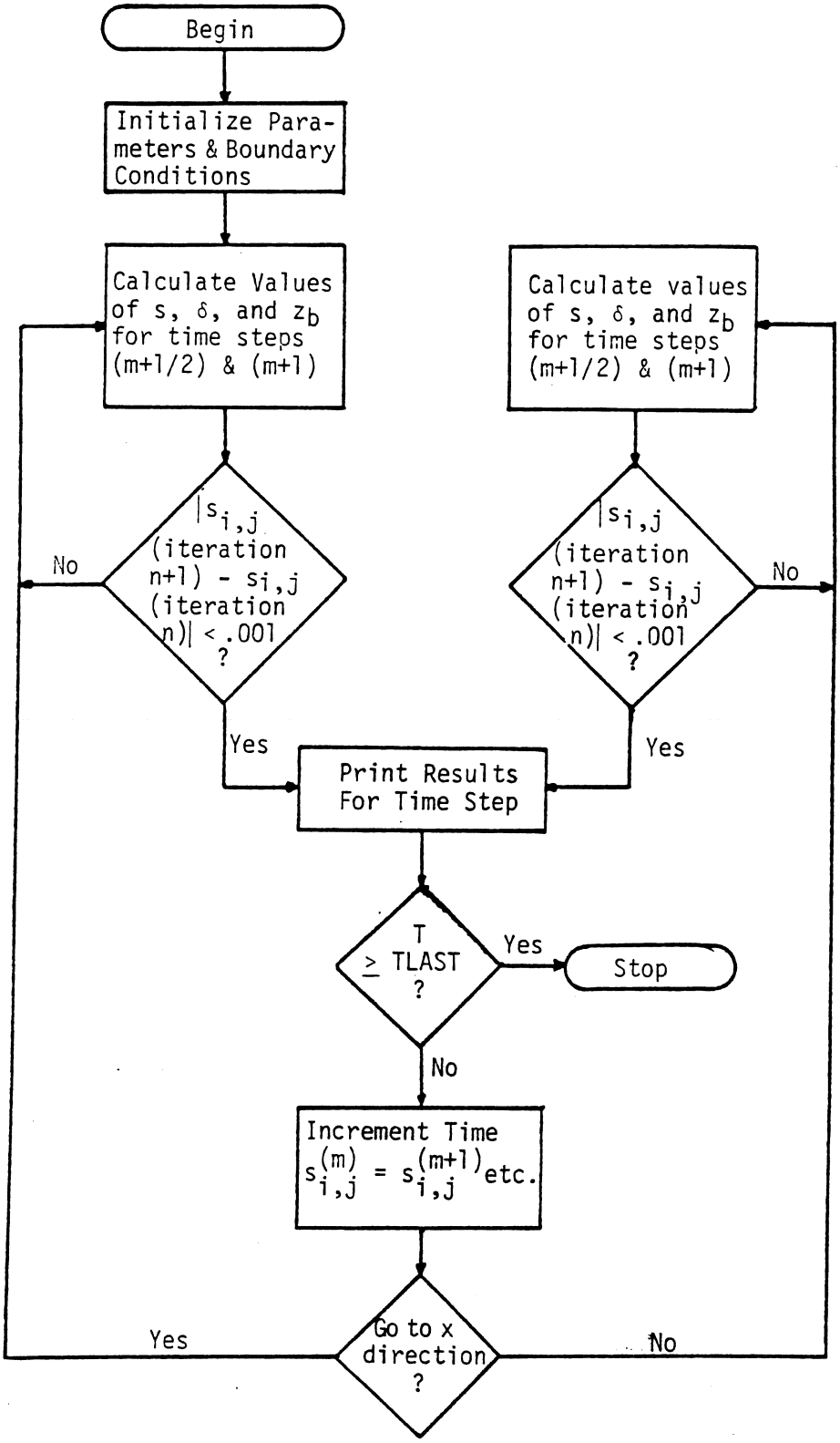

Figure 5.1 - Flow chart.

upon the grid and is located in its center. The size of the pumpage field can be varied according to the application.

Following the flow chart, all parameters are initialized and the boundary conditions stipulated according to the application. From here the iterative procedure begins in the x direction. In the first iteration it is assumed that the parameter values at the time level (m+1/2) are identical to their values at the time level (m). After calculating the parameter values at the time level (m+1) their values are calculated for the intermediate time level (m+1/2). For each row analyzed a tridiagonal matrix of linear equations is generated using equation (5.1). The solution vector is calculated by the application of the Thomas Algorithm. In this manner the drawdown values for the time level (m+1) are calculated for the entire grid. With this information the values of the squared thickness of the transition zone and the height of the saltwater mound are calculated for each node from equations (5.3) and (5.5), respectively. Intermediate parameter values at the time level (m+1/2) are calculated by an arithmetic average between the respective parameters at the time levels (m) and (m+1). This ends the first iteration. The iterative procedure stops when the difference between the drawdown values at each node for two successive iterations is less than some predetermined value. Divergence of the scheme is checked by specifying a maximum number of iterations.

Once convergence is obtained in the x direction the results are printed on a line printer by utilizing subprograms written specifically for this purpose. The computer printout supplies a three-dimensional representation of the distributions within the aquifer of the drawdown, the thickness of the transition zone, and the height of the saltwater mound. Various examples are presented in the next section.

Finally, the time is incremented by a predetermined amount and the parameter values at time level(m+1) are reset to the time level(m).

The procedure for the calculation of the unknown parameter values in the y direction are exactly the same as for the x direction except that equations (5.2) and (5.4) are now used. Thus, the scheme alternates between the x and y directions for the desired time sequence.

The application of the ADI method to the numerical model in conjunction with proper programming yields a highly stable, convergent solution scheme. This was found to be true under a variety of parameter changes. Examples and results are presented in the next section.

The model is executed by utilizing the facilities of the Northeast Regional Data Center of the State University System of Florida, located on the campus of the University of Florida in Gainesville. The model is executed by an IBM 3033N12 utilizing a WATFIV compiler. Memory requirements and execution time are approximately 300 K byte and 1100 CPU seconds, respectively.

5.4 Numerical Results

The numerical results presented in this study are based upon a preliminary simulation and a subsequent series of numerical experiments whereby the values of selected parameters are altered in order to observe the behavior of the numerical model. The parameter values utilized throughout the simulation process are representative of the Floridan Aquifer in northeastern Florida.

The parameter values used in the preliminary simulation are summarized in Table 5.1.

A twenty by twenty km grid is selected with the grid spacing in both principal directions equalling 0.5 km. The rate of pumpage occurs

Table 5.1 - Parameter values for the execution of the preliminary simulation.

Parameter Description		Value
K	hydraulic conductivity of the freshwater zone	40 m/day
K_1	hydraulic conductivity of the semiconfining formation	0.1 m/day
B_o	initial thickness of the freshwater zone	50 m
B_1	thickness of the semiconfining formation	20 m
n	porosity	0.2
S	coefficient of storage	10^{-3}
a	dispersivity	0.5 m
F	distribution function of the specific discharge	$2\eta - \eta^2$
L	distribution function of the solute concentration	$1 - 2\eta + \eta^2$
DT	time step	0.1 day
ξ	buoyancy coefficient defined by equation (4.14)	0.025
N	rate of pumpage per unit area	0.1 m/day

over a 25 Km^2 area centered within the grid (Figure 5.2). Transient conditions are simulated for a period of 10 days at a constant rate of pumpage. Figures 5.3a through 5.5c show three-dimensional maps representing the drawdown, the saltwater mound, and the thickness of the transition zone for the selected times, T, of 2, 6, and 10 days. These maps are photographically reduced versions of the actual computer printout. A comparison of Figure 5.3a and Figure 5.3b demonstrates the two print schemes which are utilized for reporting results. The first print scheme, for example Figure 5.3a, reports ordinate values at each grid point only when these values are between 0.5 and 50 m. These values are rounded to the nearest meter to save space on the computer printout. The second print scheme, for example Figure 5.3b, reports ordinate values between 0.05 and 0.5 m. These values are rounded to the nearest tenth of a meter. Both schemes illustrate the development of the various zones within the aquifer. Figure 5.4 illustrates the rate of growth of the maximal values of the drawdown, the height of the saltwater mound, and the thickness of the transition zone.

Four subsequent experiments were performed to observe the behavior of the numerical model. In each of the four experiments one parameter was altered by an order of magnitude. Table 5.2 summarizes the experimental procedure leading to the numerical results shown in Figures 5.7a through 5.13c. Figure 5.14 illustrates the rate of growth of the maximal values of the drawdown, the height of the saltwater mound, and the thickness of the transition zone for experiment numbers 2 and 3.

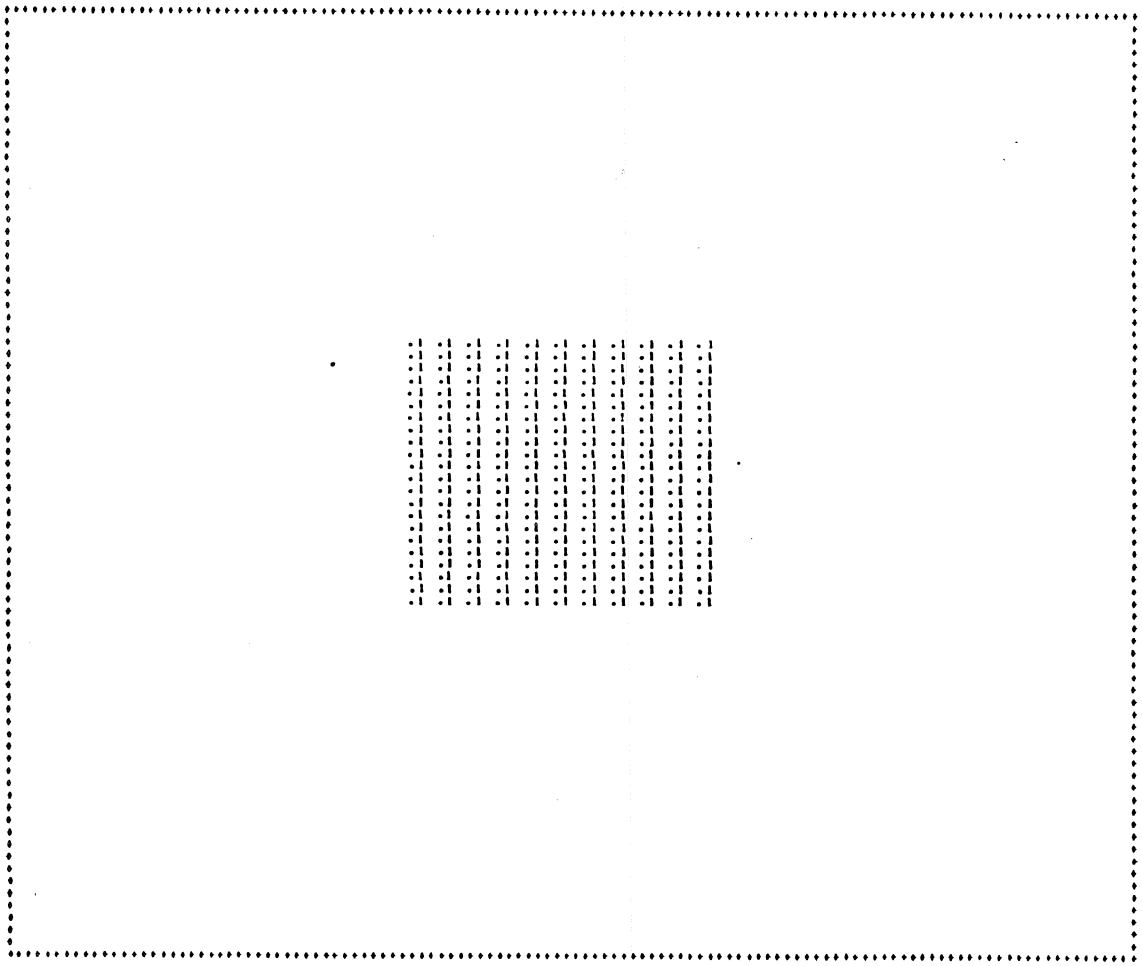

Figure 5.2 - Map of pumpage. Pumpage rate = 0.1 m/day.

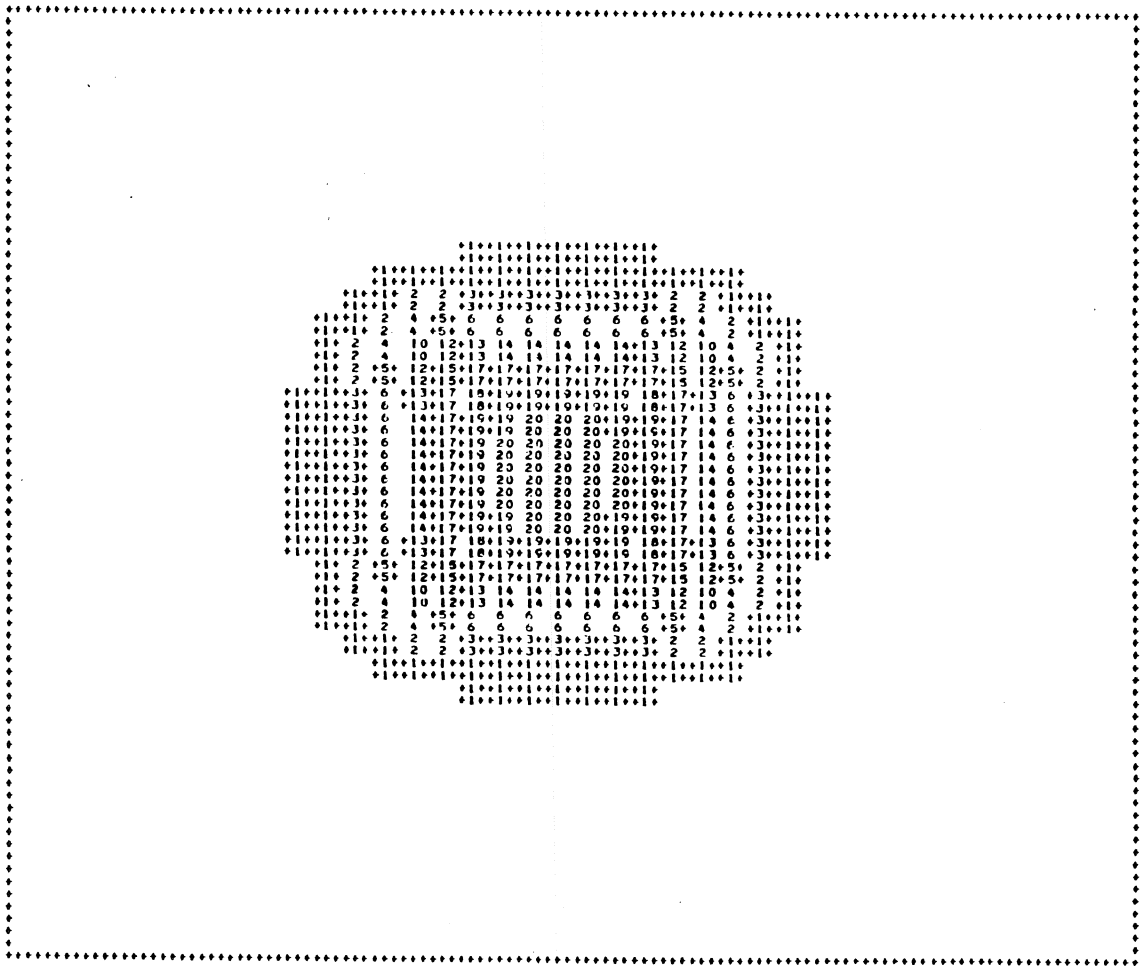

Figure 5.3a - Map of drawdown. T = 2.0 days, maximal ordinate = 20.01 m.

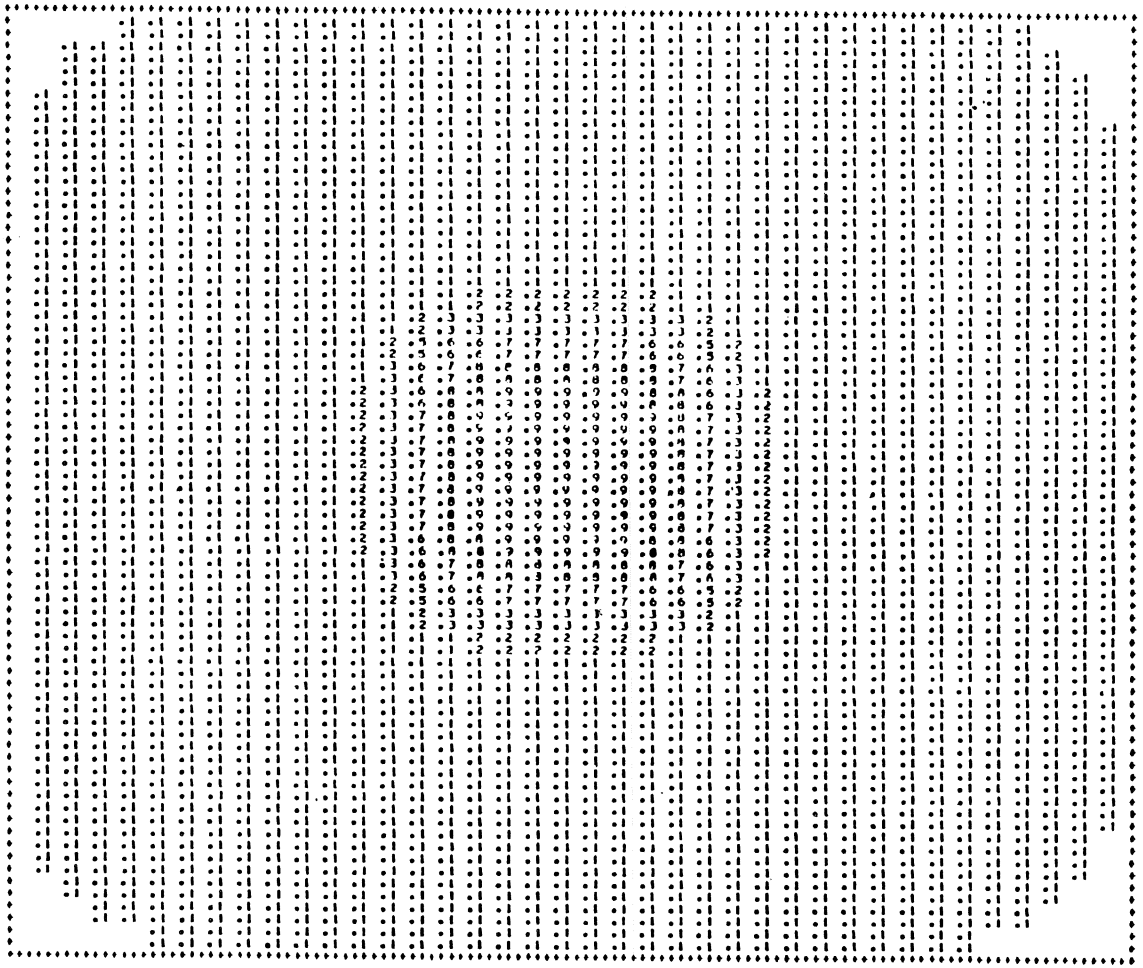

Figure 5.3b - Map of saltwater mound. T = 2.0 days, maximal ordinate = 0.88 m.

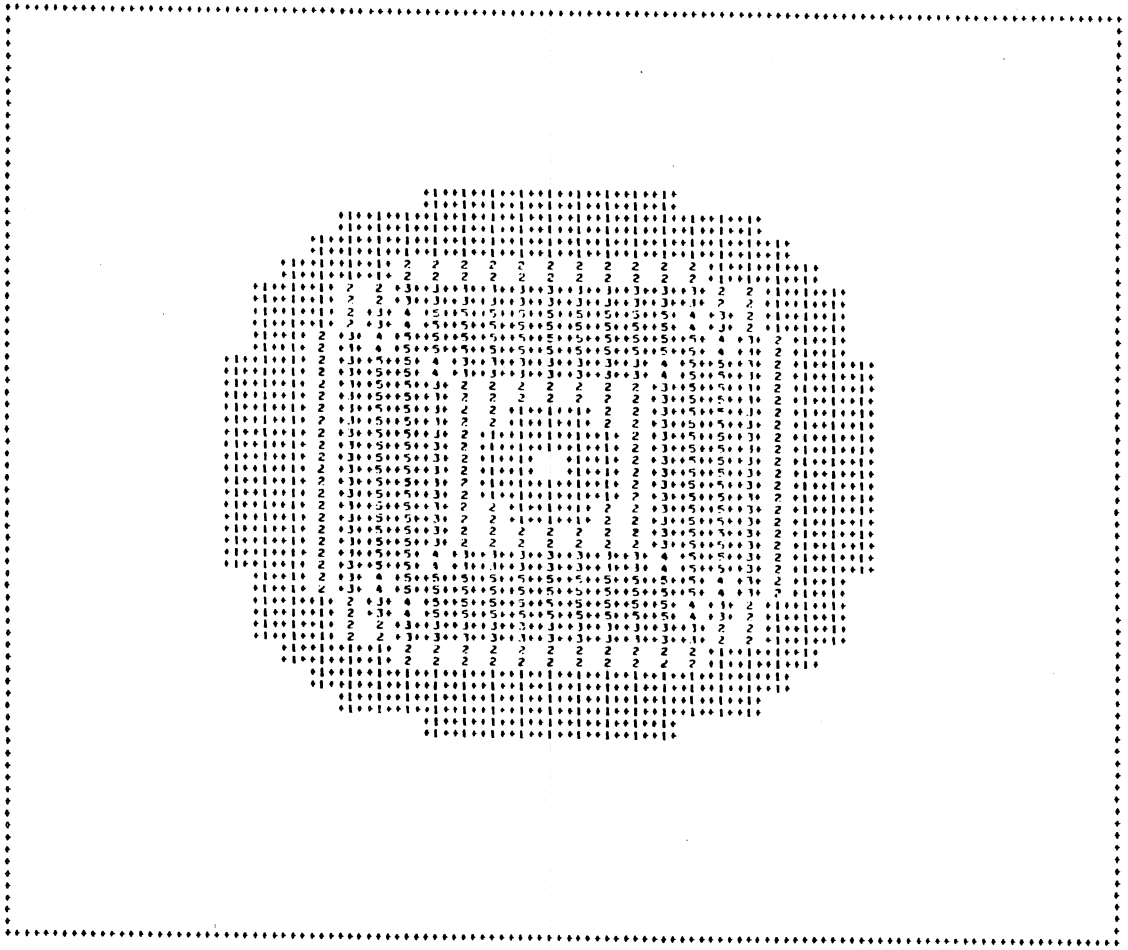

Figure 5.3c. Map of transition zone. T = 2.0 days, maximal ordinate = 5.03 m.

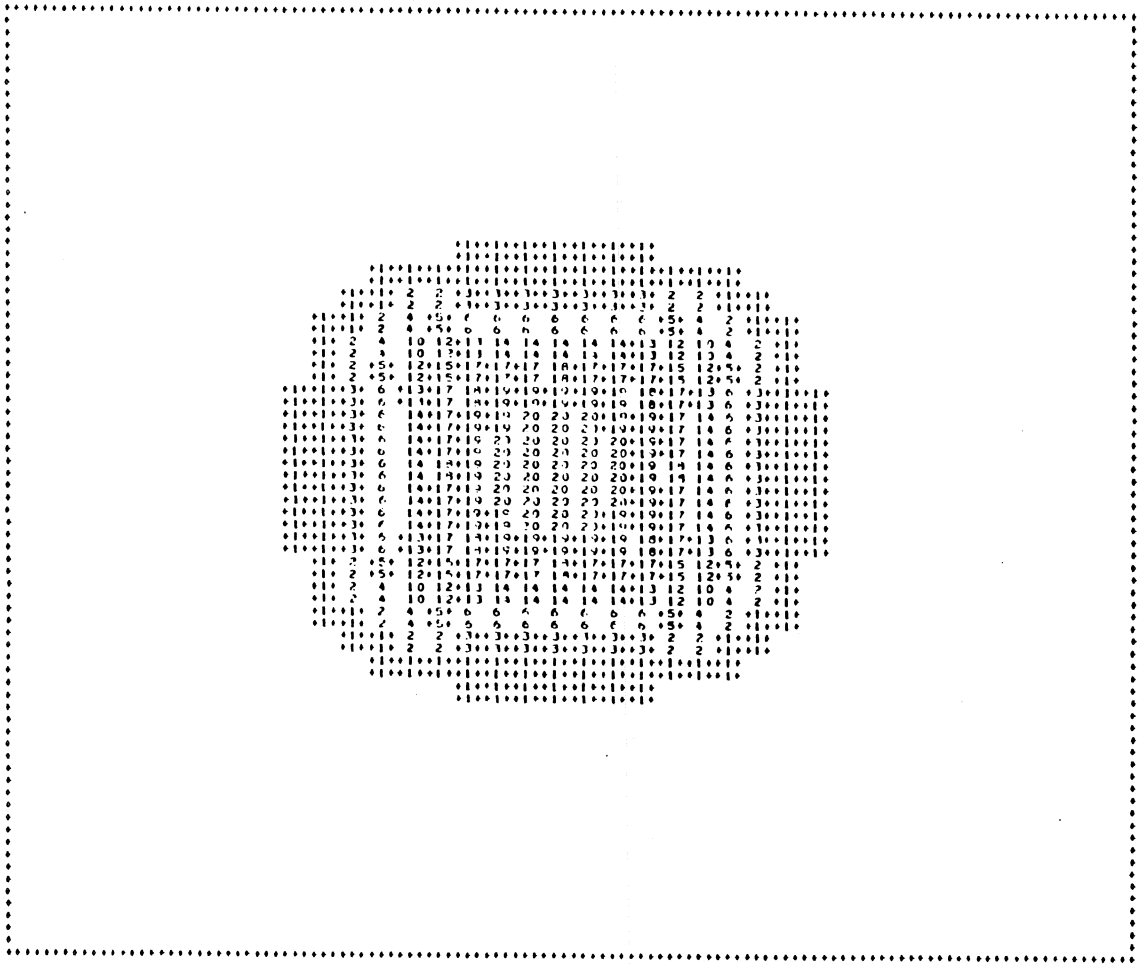

Figure 5.4a - Map of drawdowns. T = 6.0 days, maximal ordinate = 20.12 m.

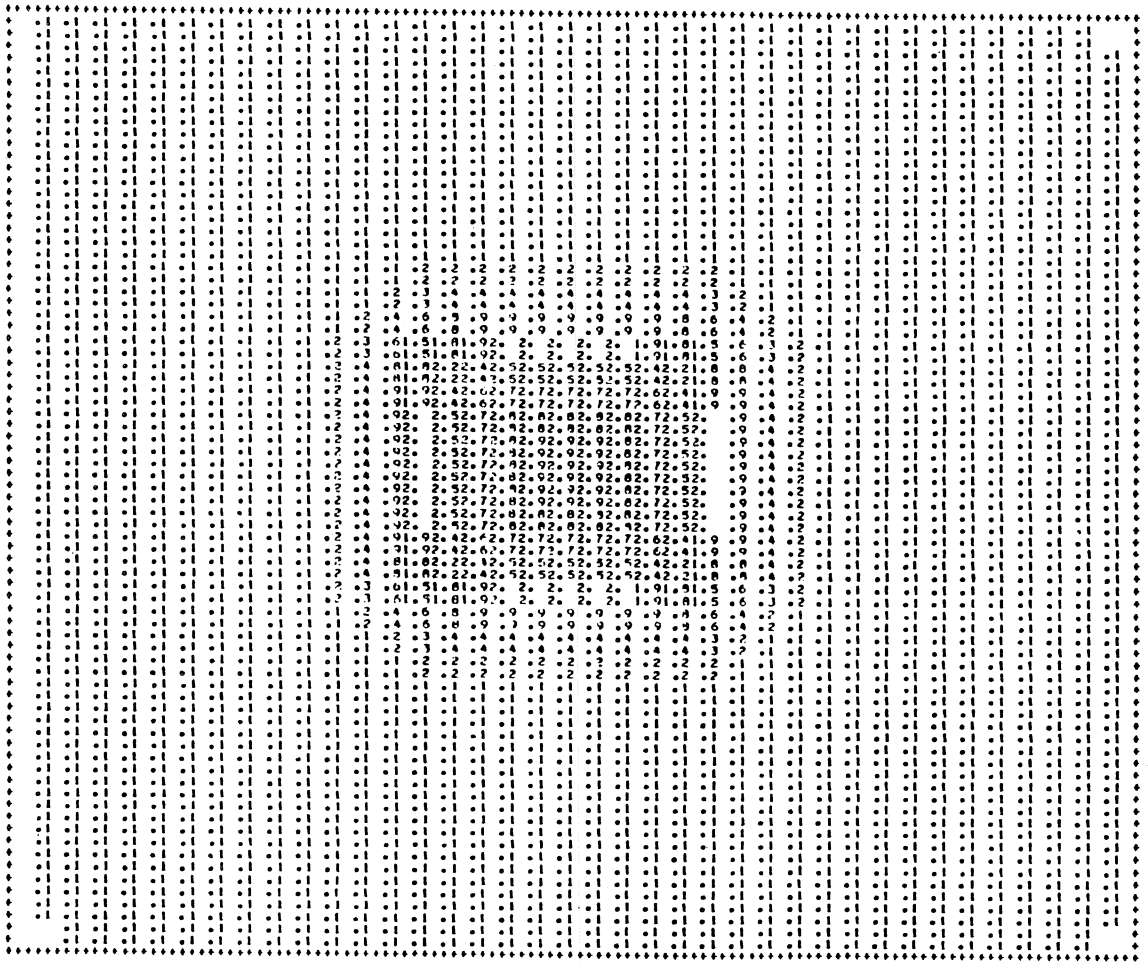

Figure 5.4b - Map of saltwater mound. T = 6.0 days, maximal ordinate = 2.83 m.

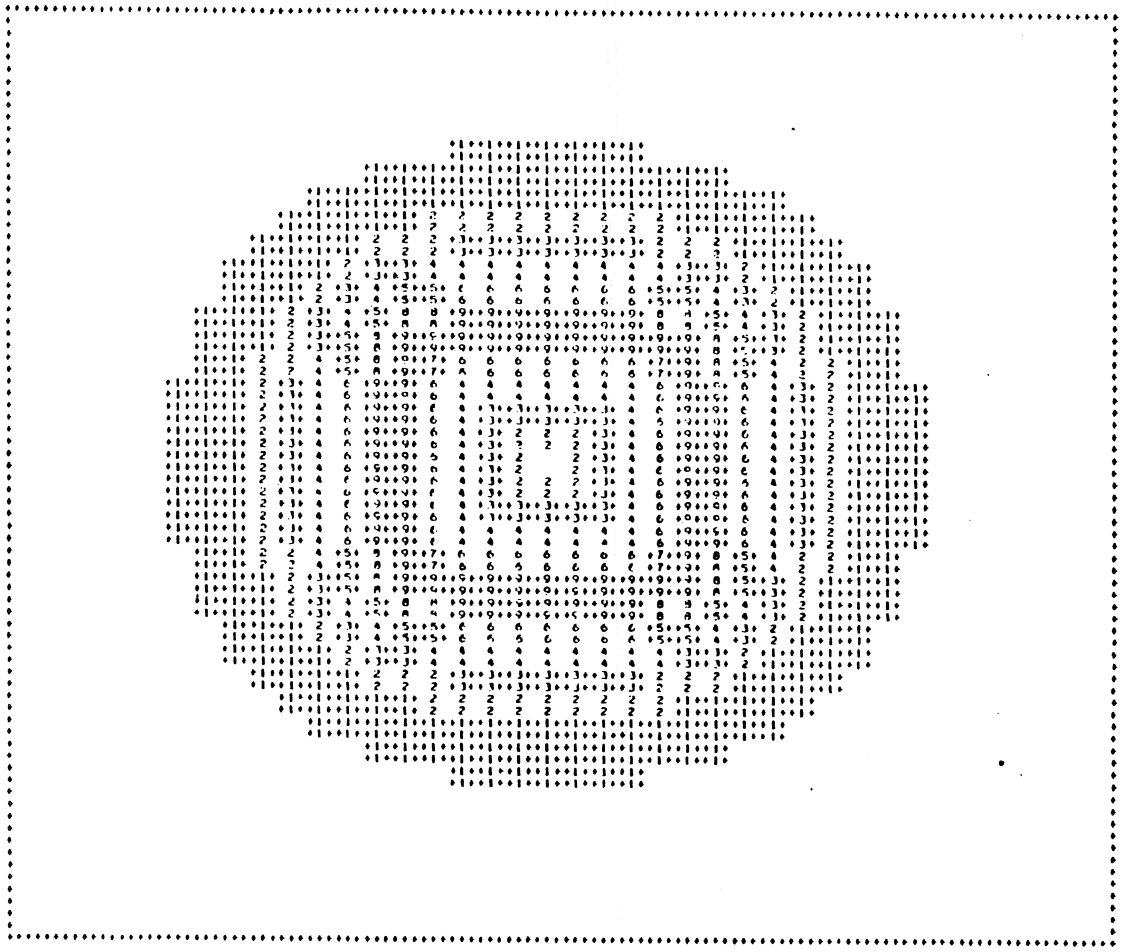

Figure 5.4c - Map of transition zone. T = 6.0 days, maximal ordinate = 9.03 m.

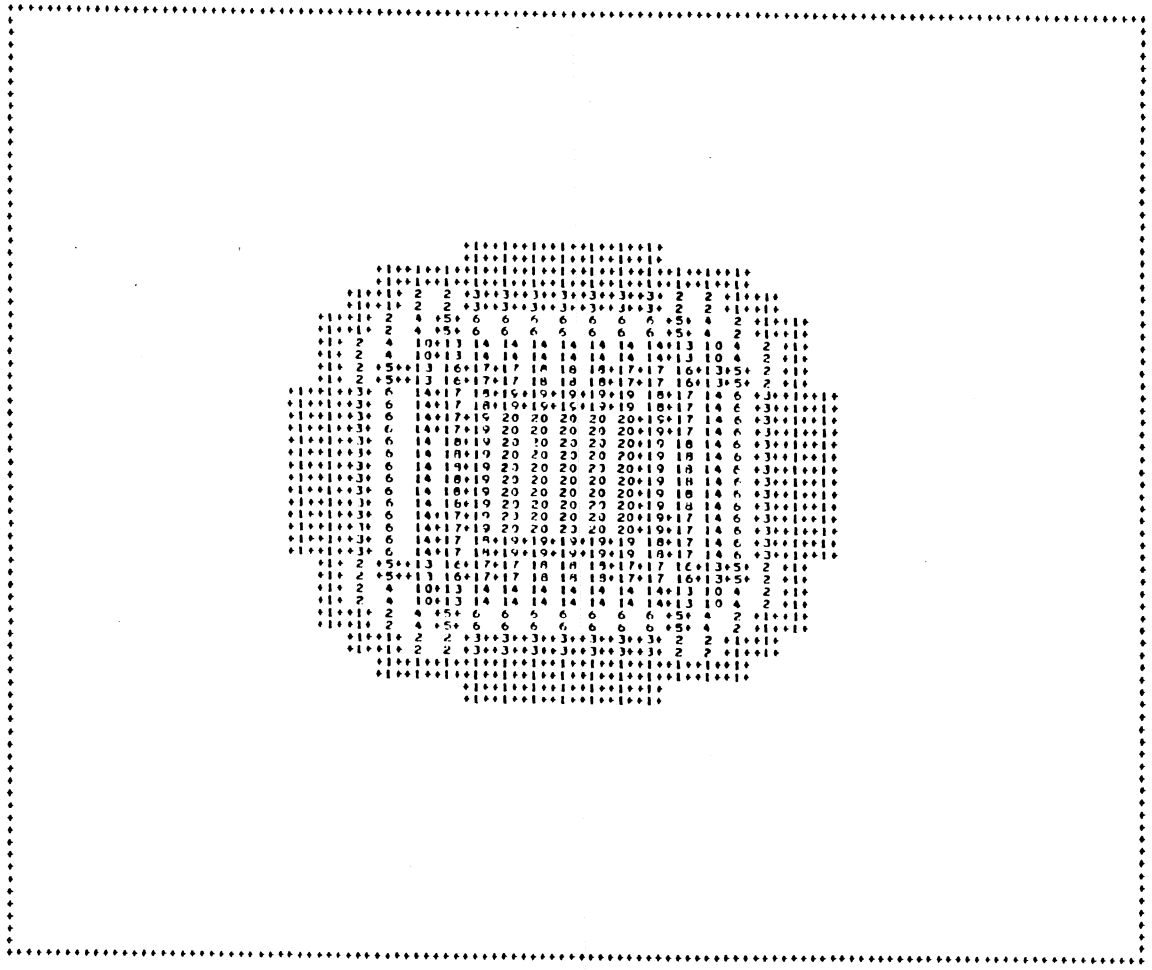

Figure 5.5a - Map of drawdowns. T = 10.0 days, maximal ordinate = 20.22 m.

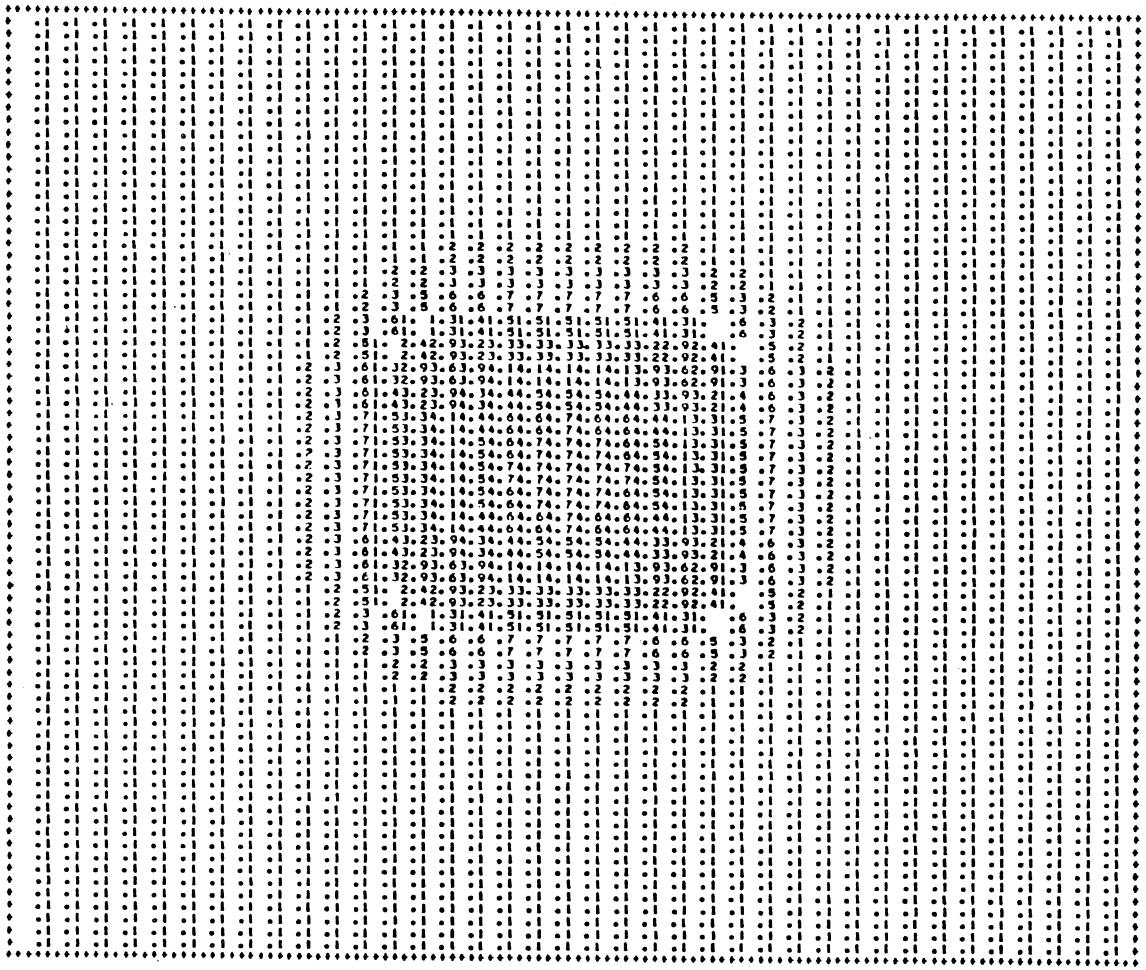

Figure 5.5b - Map of saltwater mound. T = 10.0 days, maximal ordinate = 4.69 m.

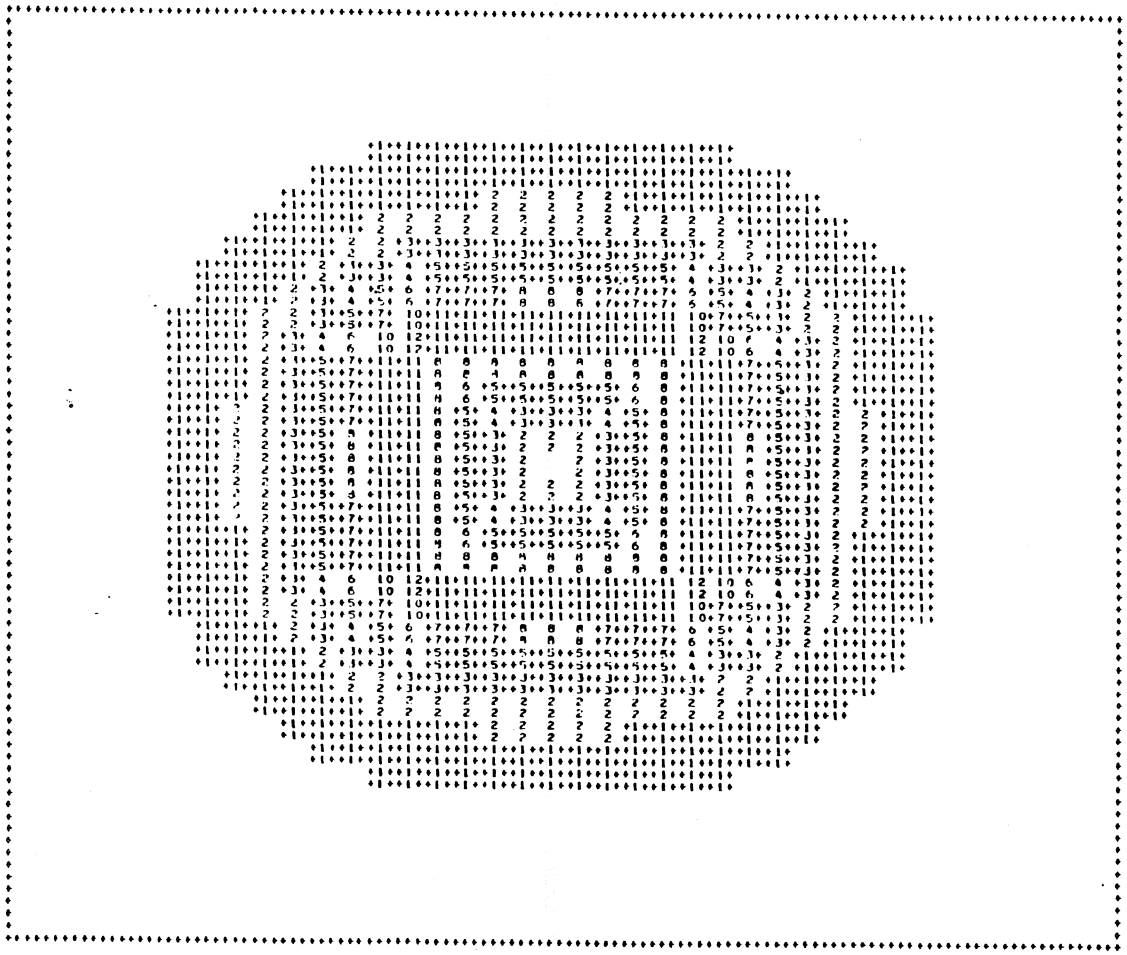

Figure 5.5c - Map of transition zone. T = 10.0 days, maximal ordinate = 11.70 m.

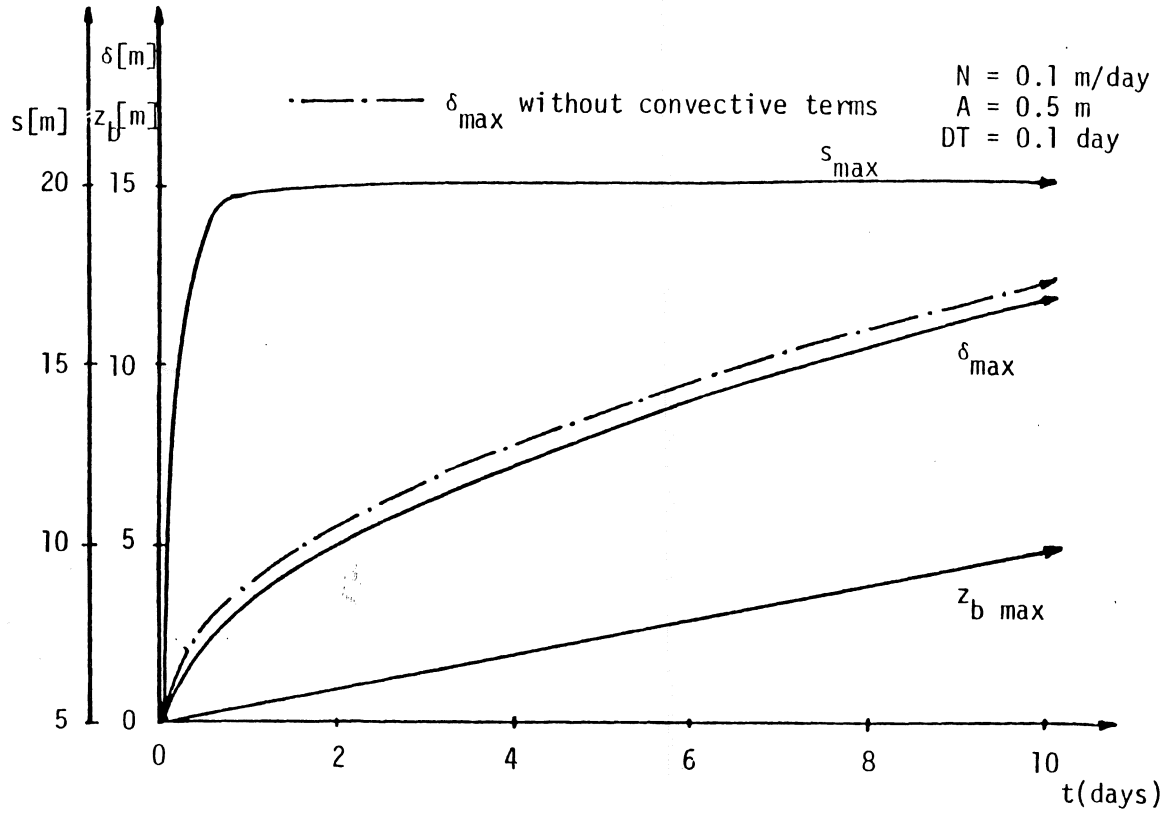

Figure 5.6 - Rate of growth of the maximal value of the drawdown, the height of the saltwater mound, and the thickness of the transition zone.

Table 5.2 - Summary of experiments.

Experiment Number	Altered Parameter	Original Value	Altered Value	Applicable Figures
1	DT	0.1 day	0.2 day	5.7a 5.7b 5.7c
2	a	0.1 m	0.05 m	5.8a through 5.10c
3	N	0.1 m/day	0.01 m/day	5.11a through 5.13c
4	K_1	0.5 m/day	0.05 m/day	None

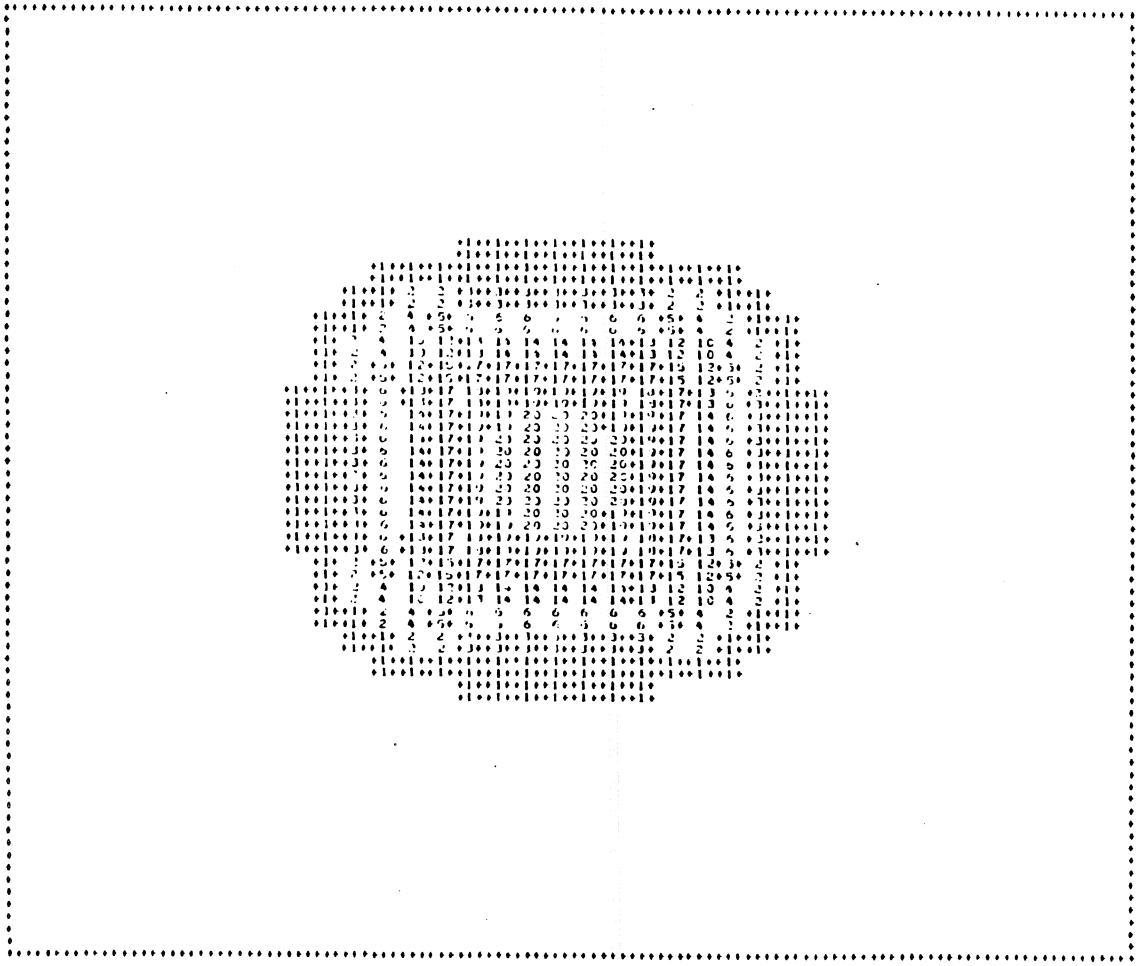

Figure 5.7a - Map of drawdowns. DT = 0.2 days, T = 2.0 days, maximal ordinate = 20.01 m.

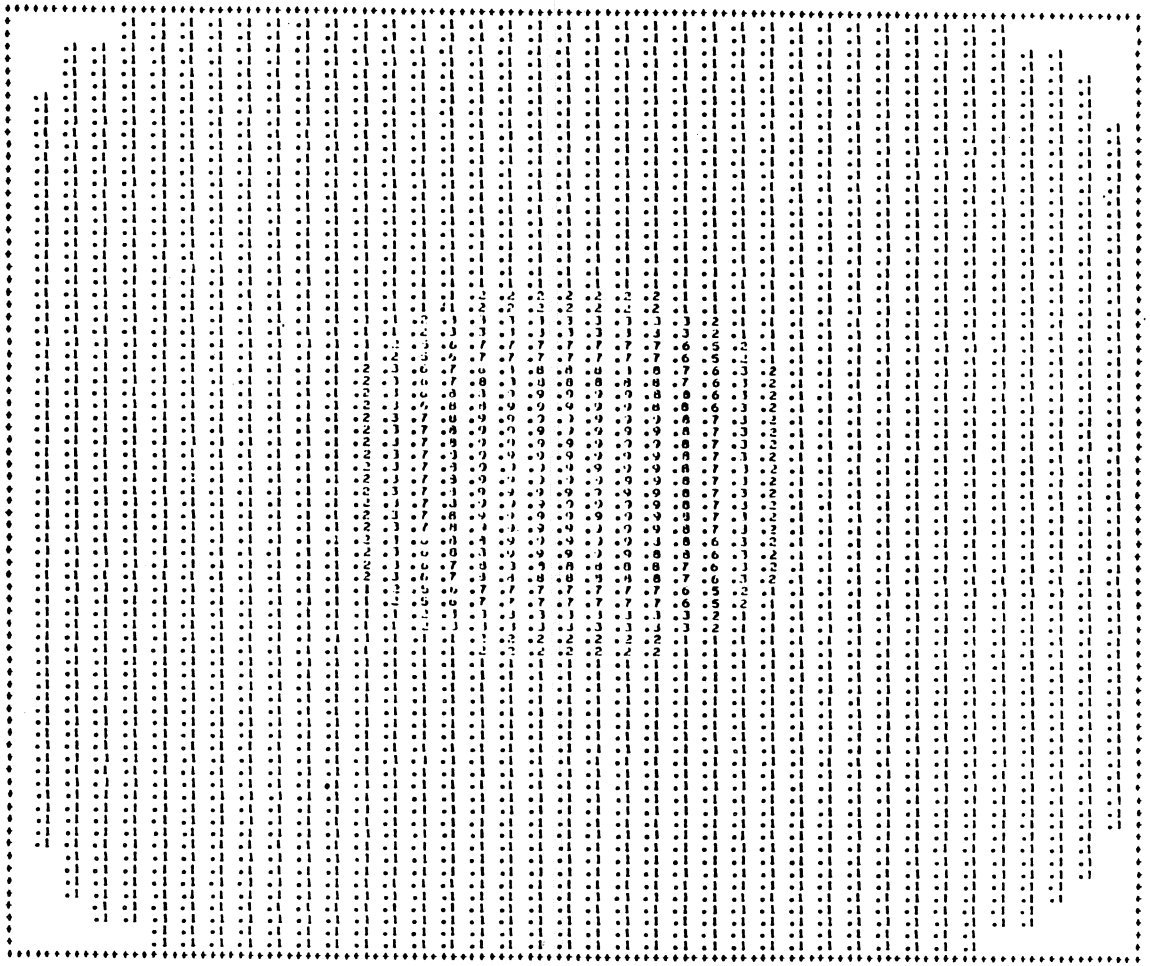

Figure 5.7b - Map of saltwater mound. DT = 0.02 days, T = 2.0 days, maximal ordinate = 0.88 m.

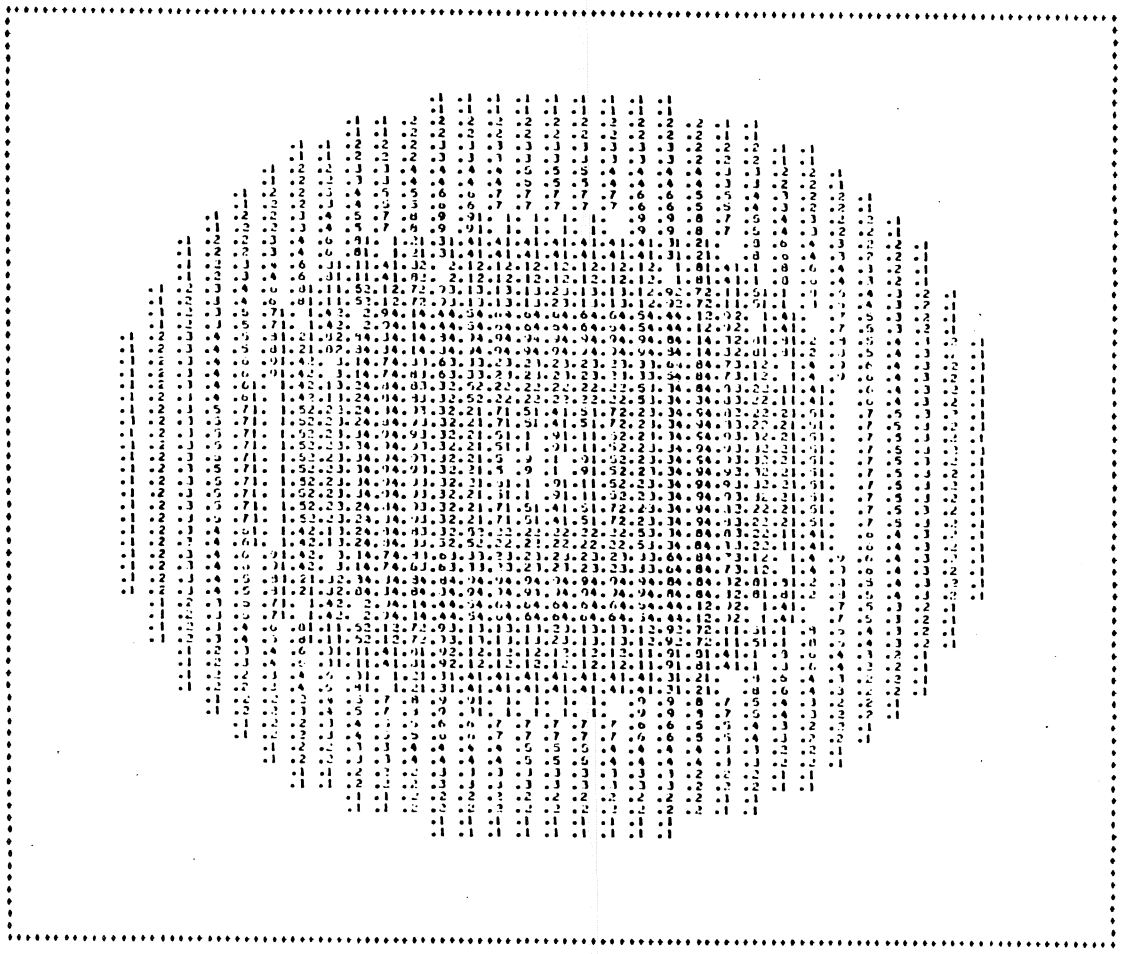

Figure 5.7c - Map of transition zone. DT = 0.2 days, T = 2.0 days, maximal ordinate = 4.96 m.

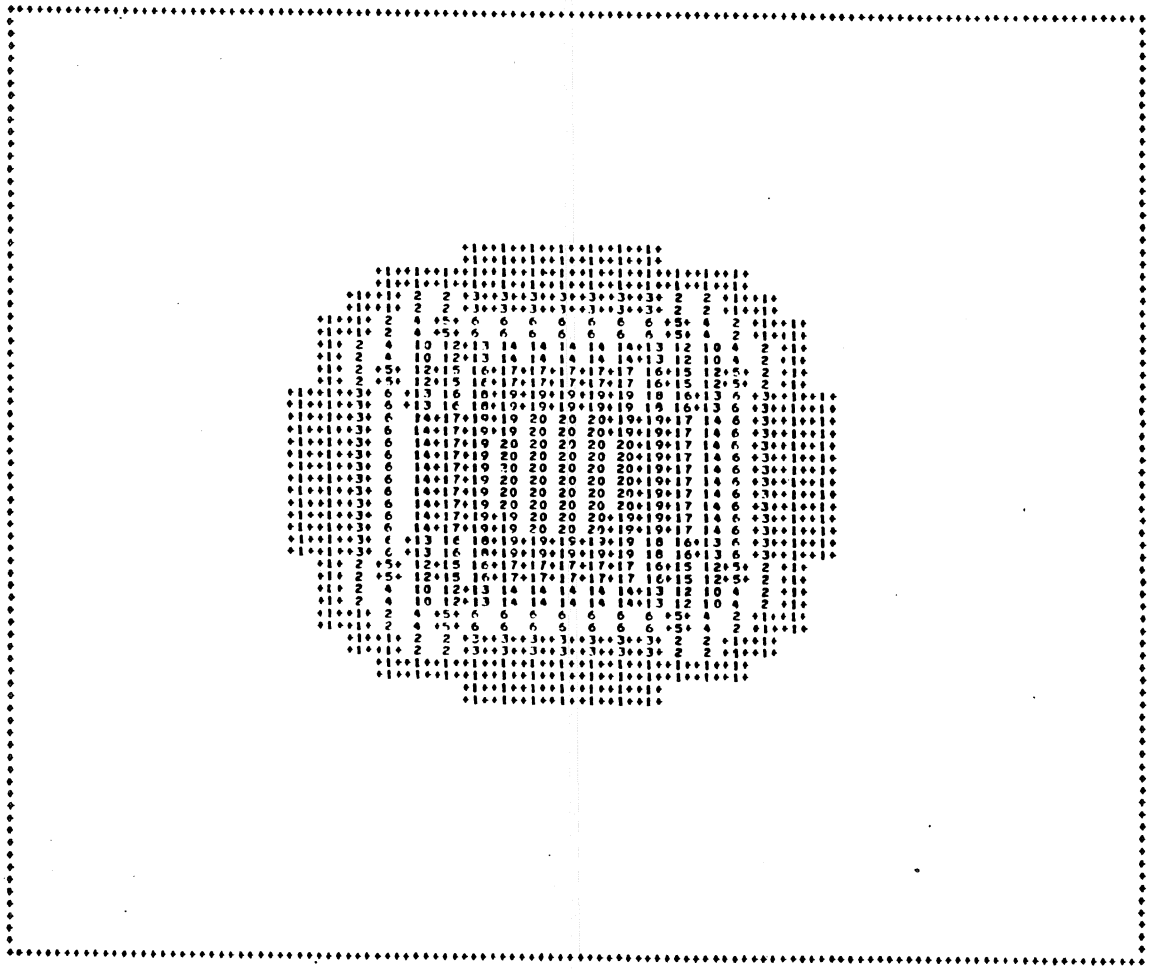

Figure 5.8a - Map of drawdowns. a = 0.05 m, T = 2.0 days, maximal ordinate = 19.99 m.

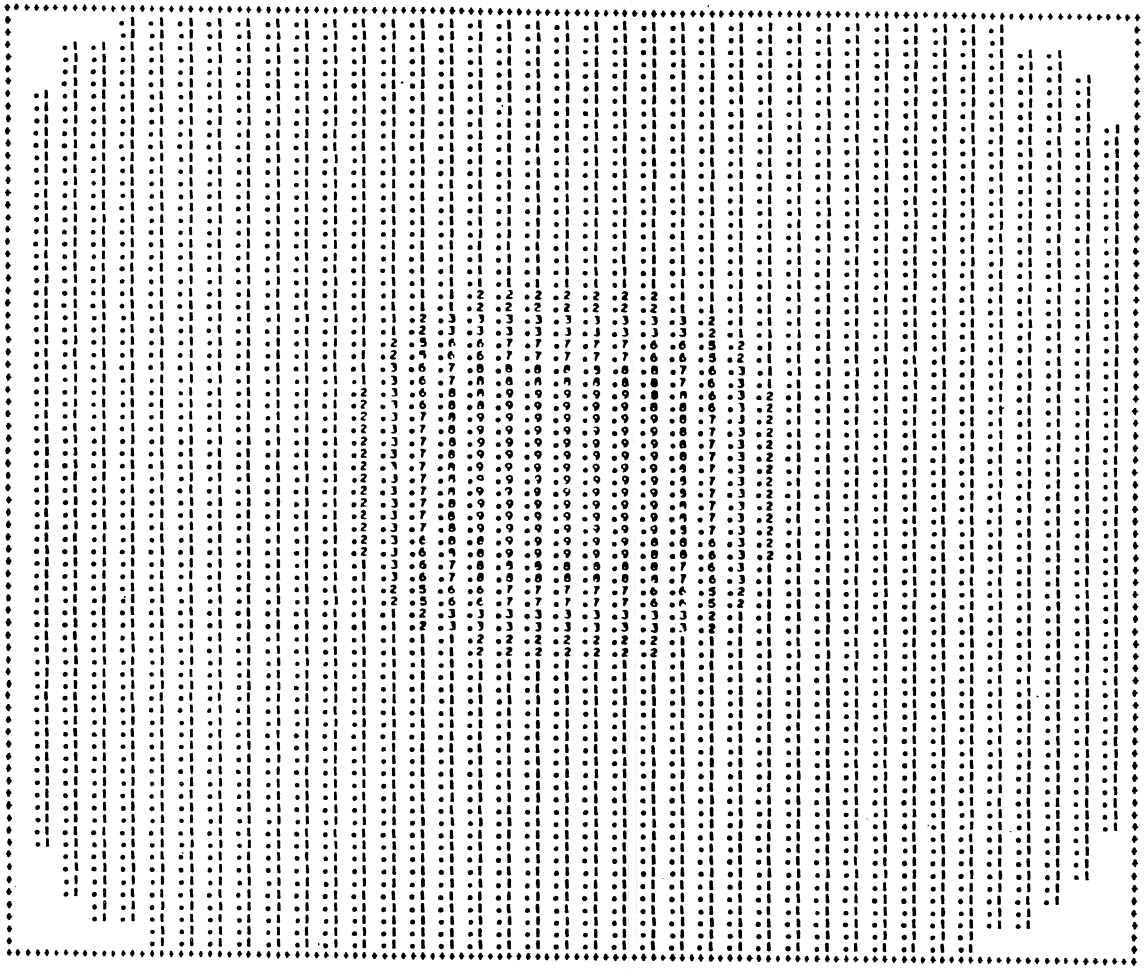

Figure 5.8b - Map of saltwater mound. a = 0.05 m, T = 2.0 days, maximal ordinate = 0.88 m.

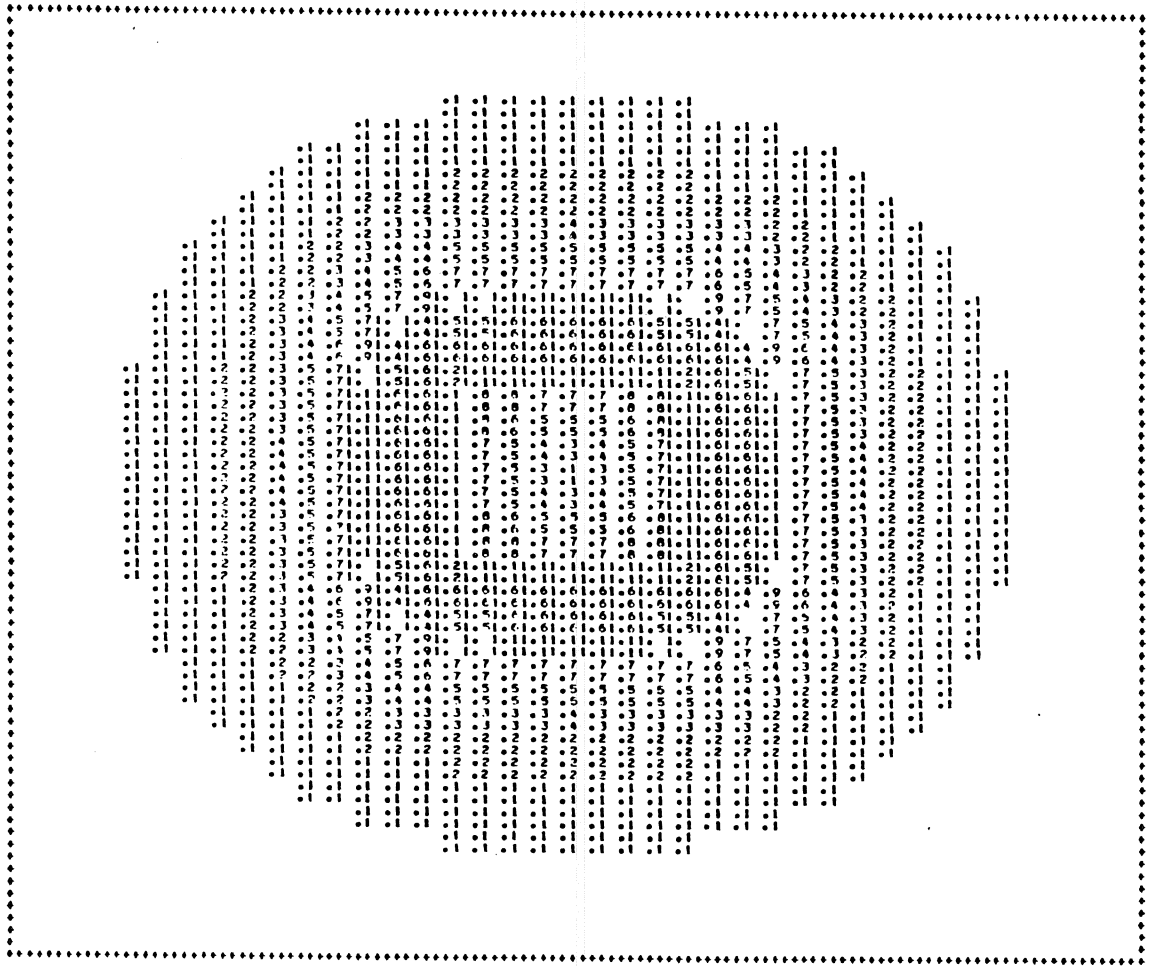

Figure 5.8c - Map of transition zone. a = 0.05 m, T = 2.0 days, maximal ordinate = 1.58 m.

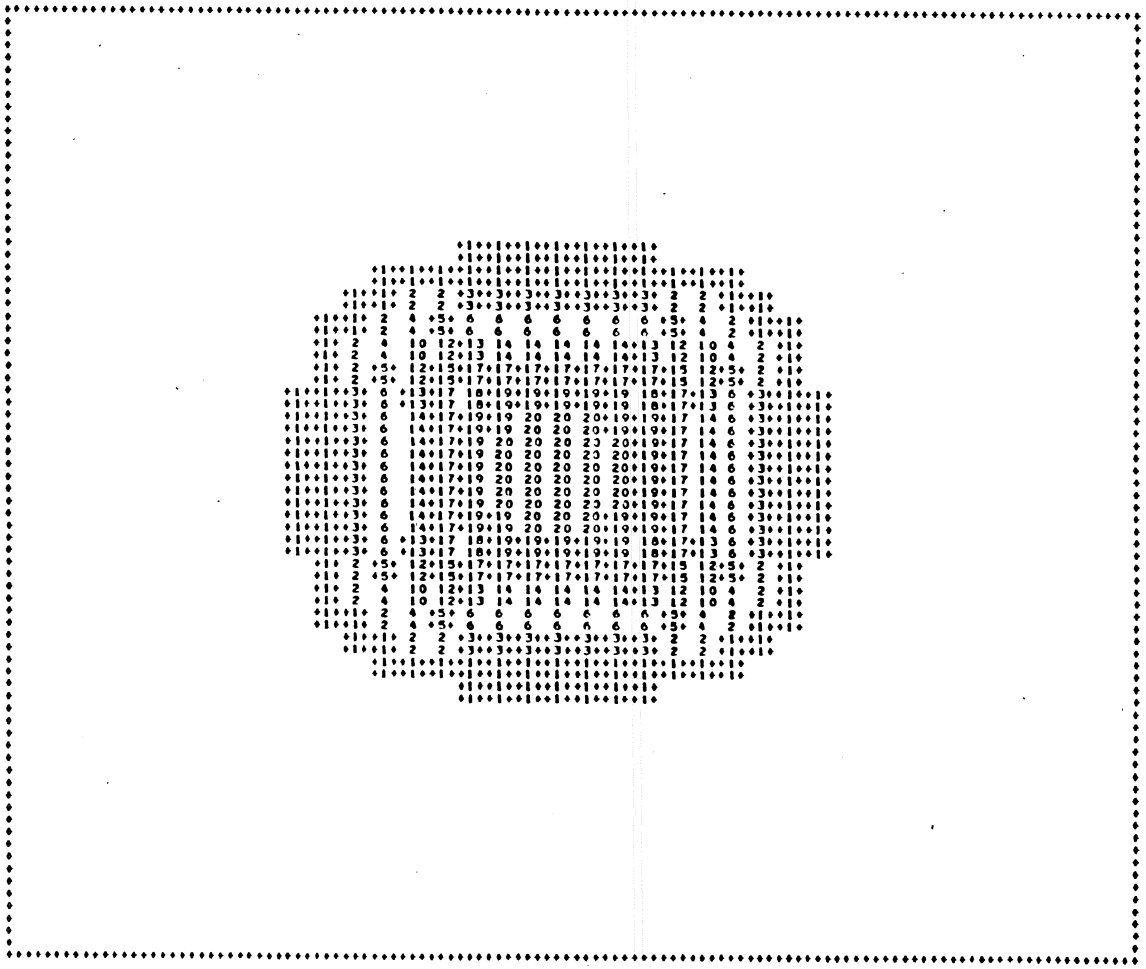

Figure 5.9a - Map of drawdowns. a = 0.05 m, T = 6.0 days, maximal ordinate = 20.08 m.

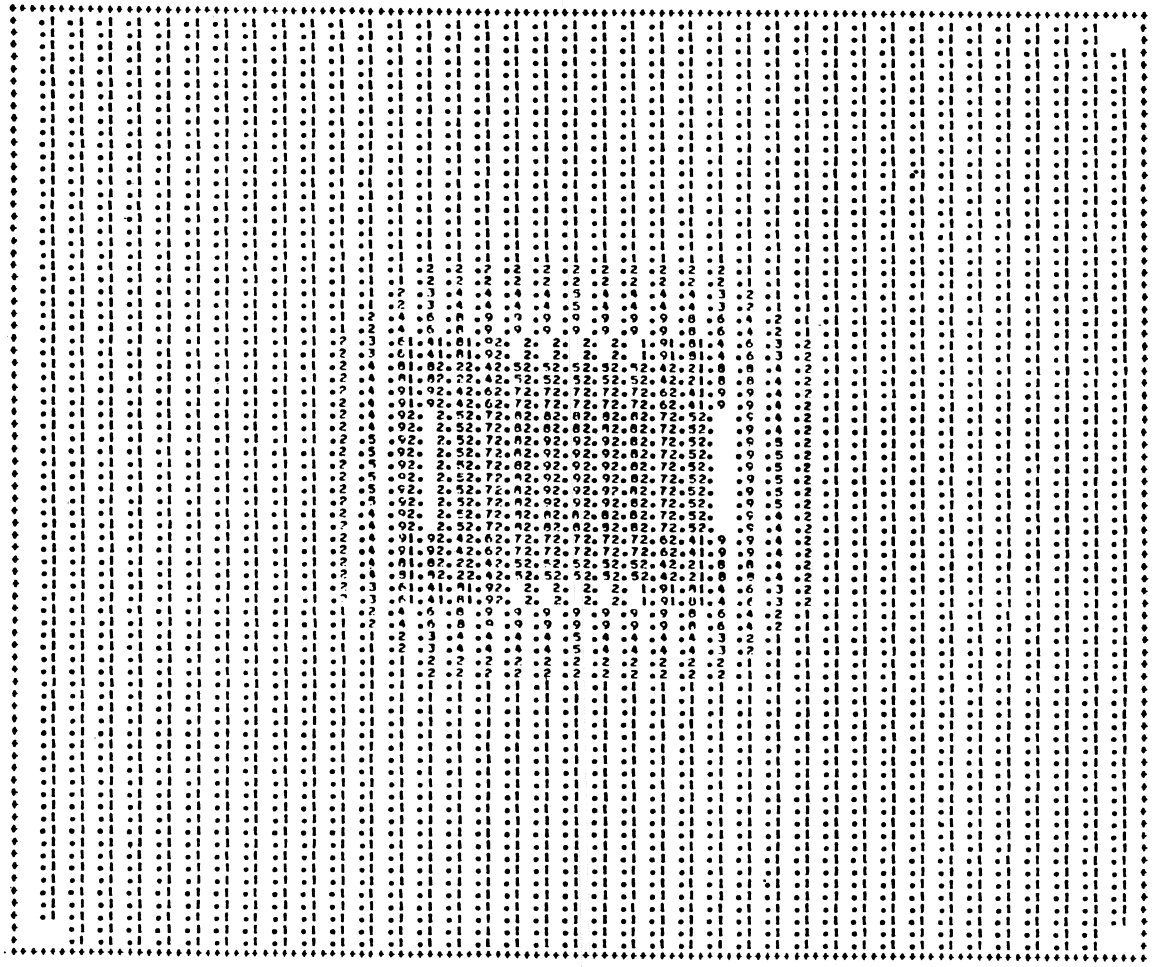

Figure 5.9b - Map of saltwater mound. a = 0.05 m, T = 6.0 days, maximal ordinate = 2.83 m.

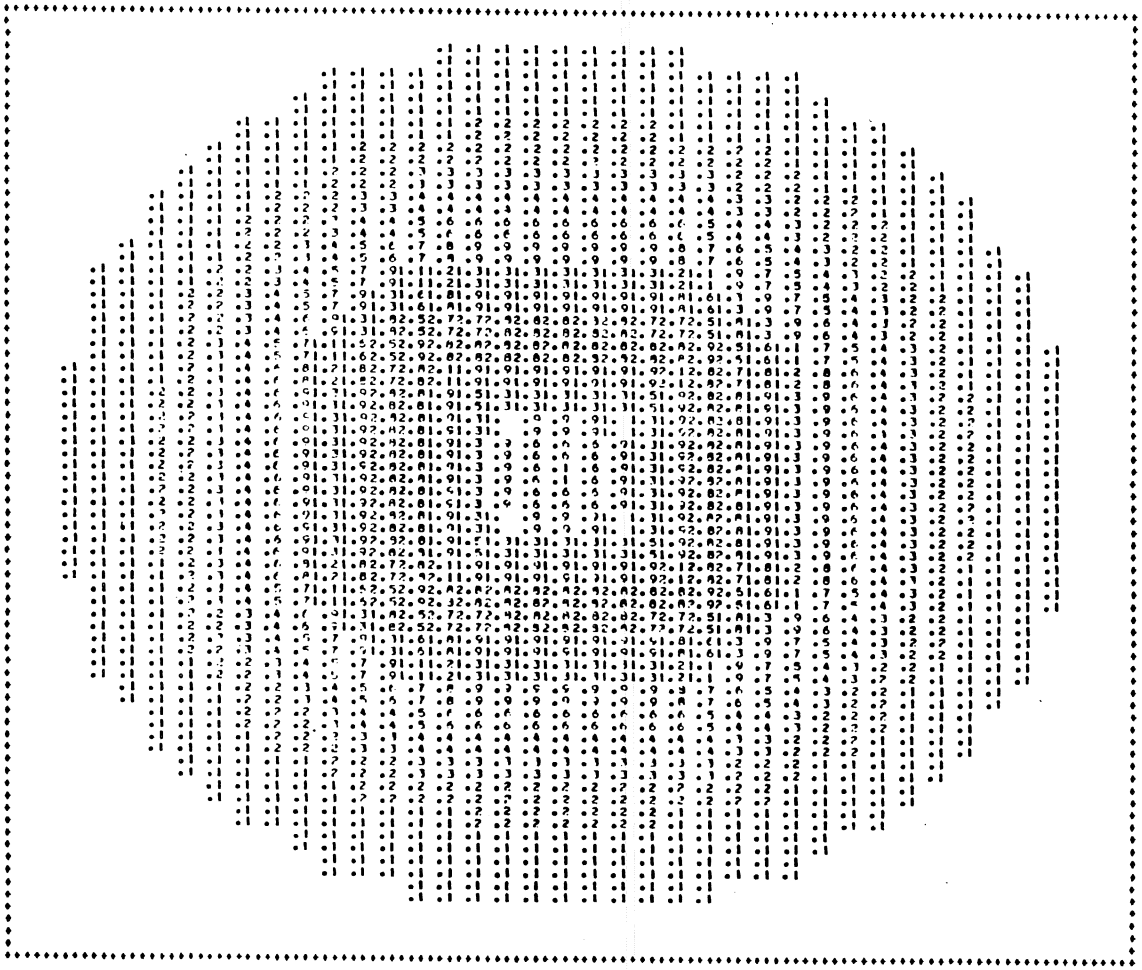

Figure 5.9c - Map of transition zone. a = 0.05 m, T = 6.0 days, maximal ordinate = 2.84 m.

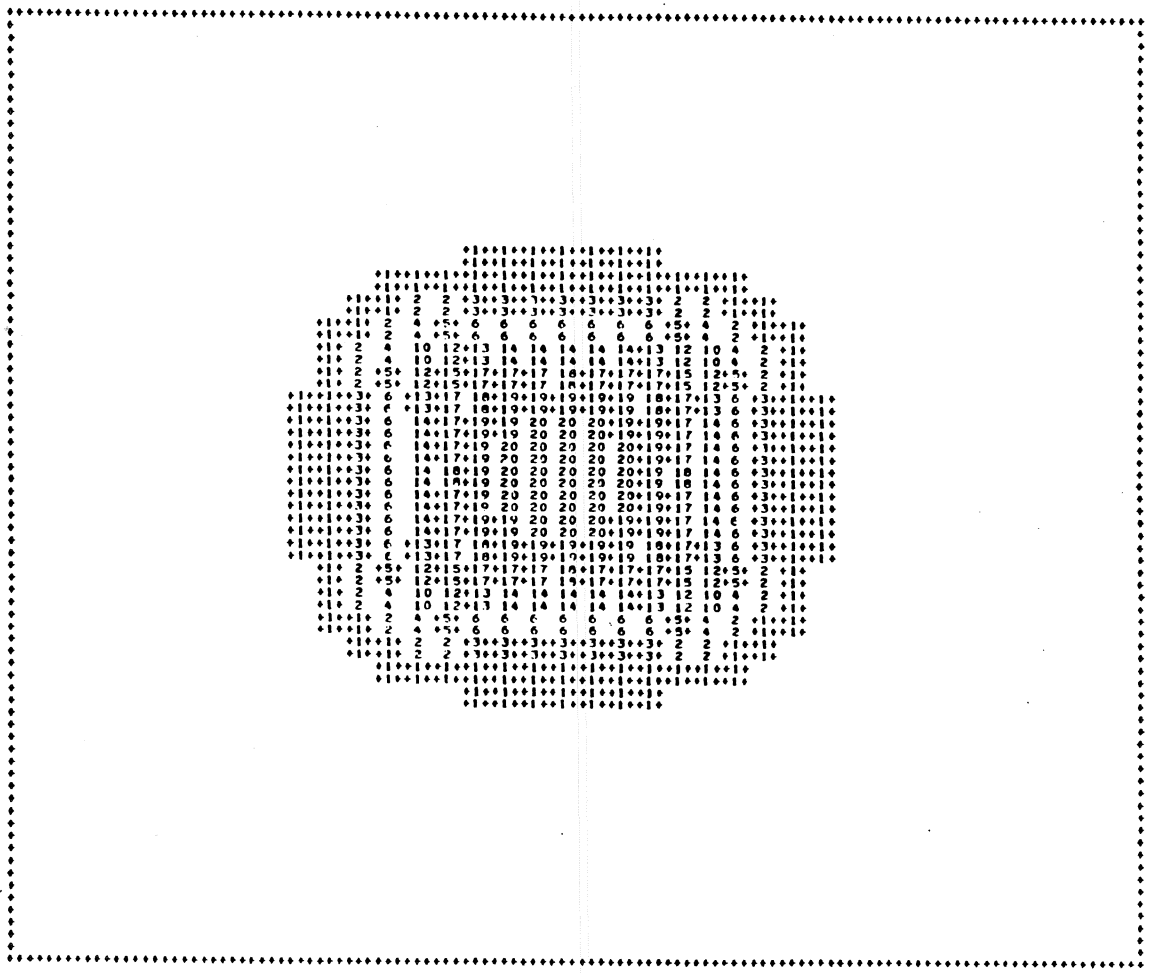

Figure 5.10a - Map of drawdowns. a = 0.05 m, T = 10.0 days, maximal ordinate = 20.17 m.

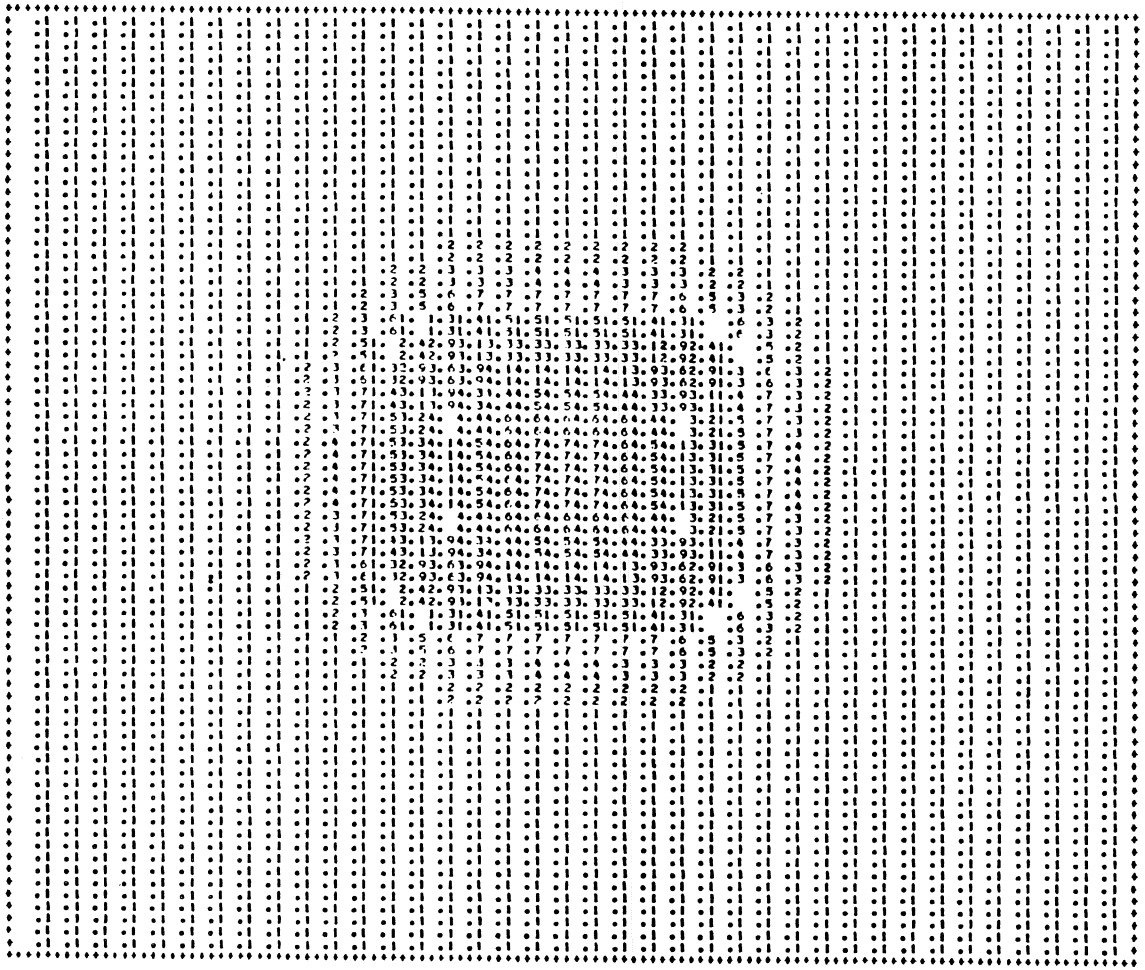

Figure 5.10b - Map of saltwater mound. a = 0.05 m, T = 10.0 days, maximal ordinate = 4.69 m.

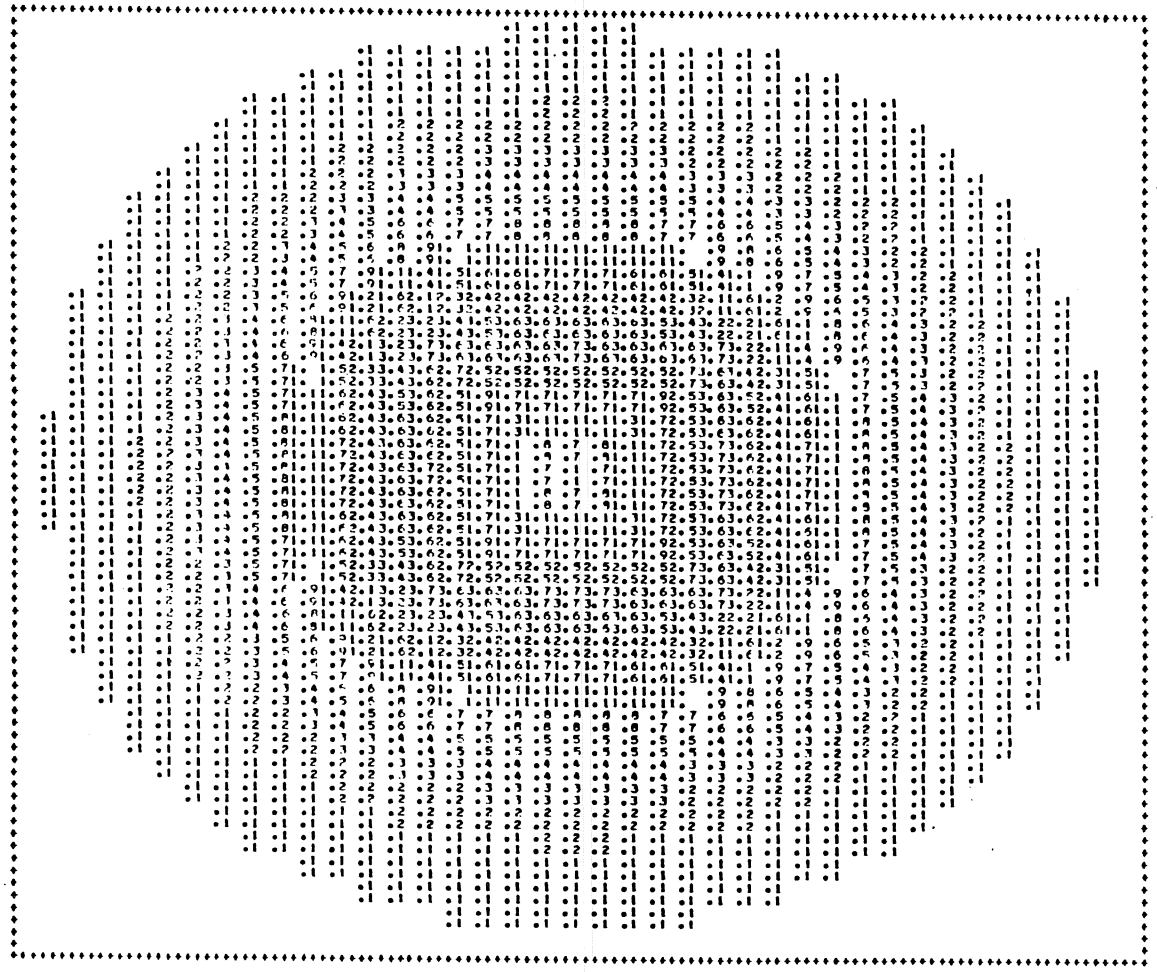

Figure 5.10c - Map of transition zone. a = 0.05 m, T = 10.0 days, maximal ordinate = 3.67 m.

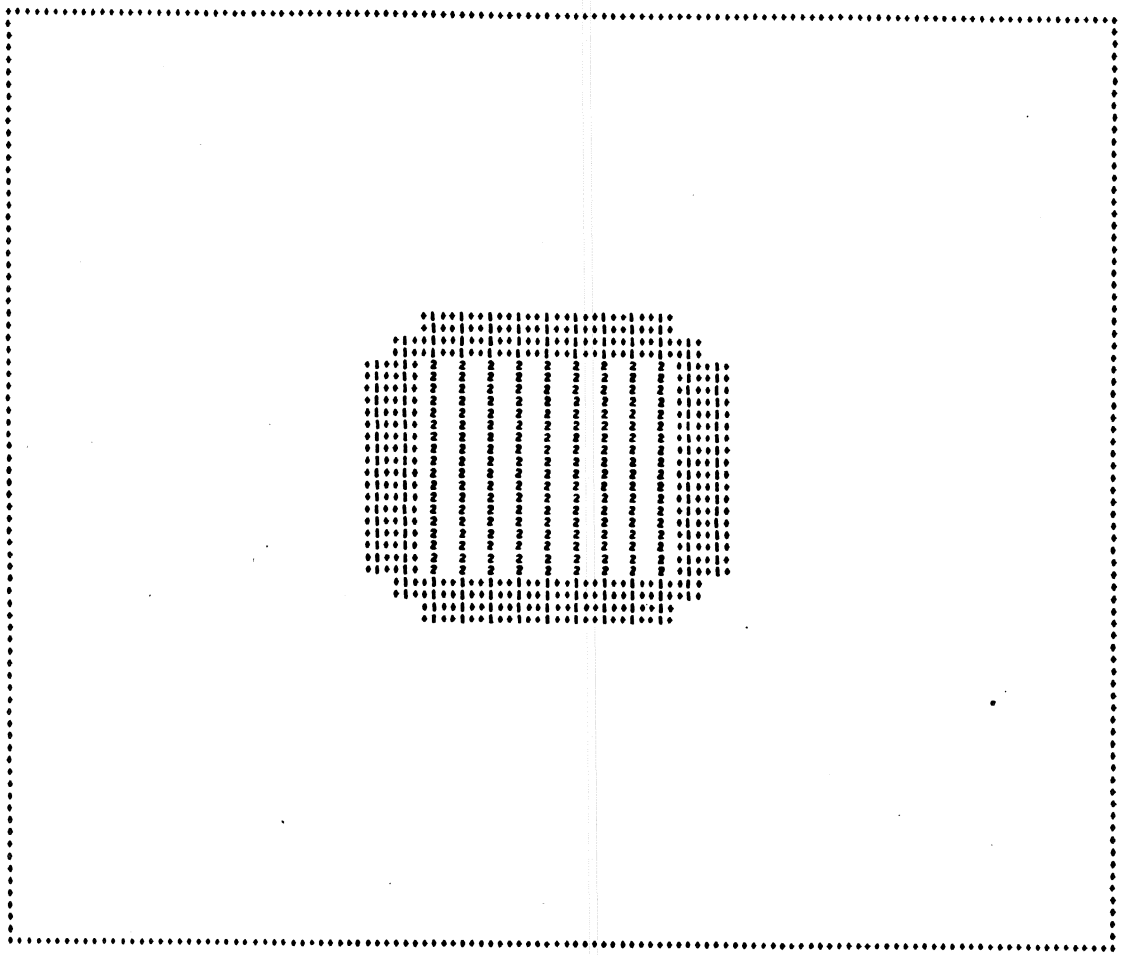

Figure 5.11a - Map of drawdowns. N = 0.01 m/day, T = 2.0 days, maximal ordinate = 2.00 m.

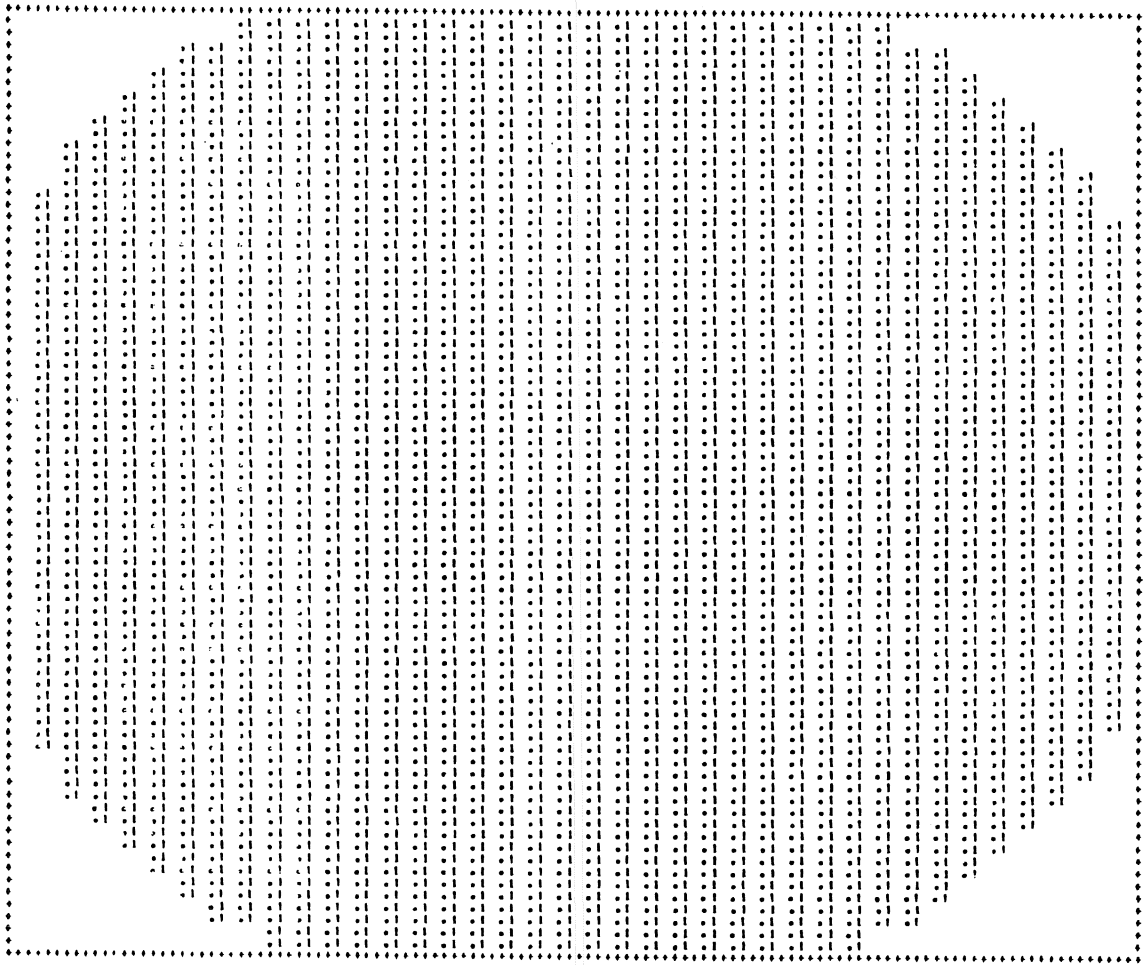

Figure 5.11b - Map of saltwater mound. N = 0.01 m/day, T = 2.0 days, maximal ordinate = 0.09 m.

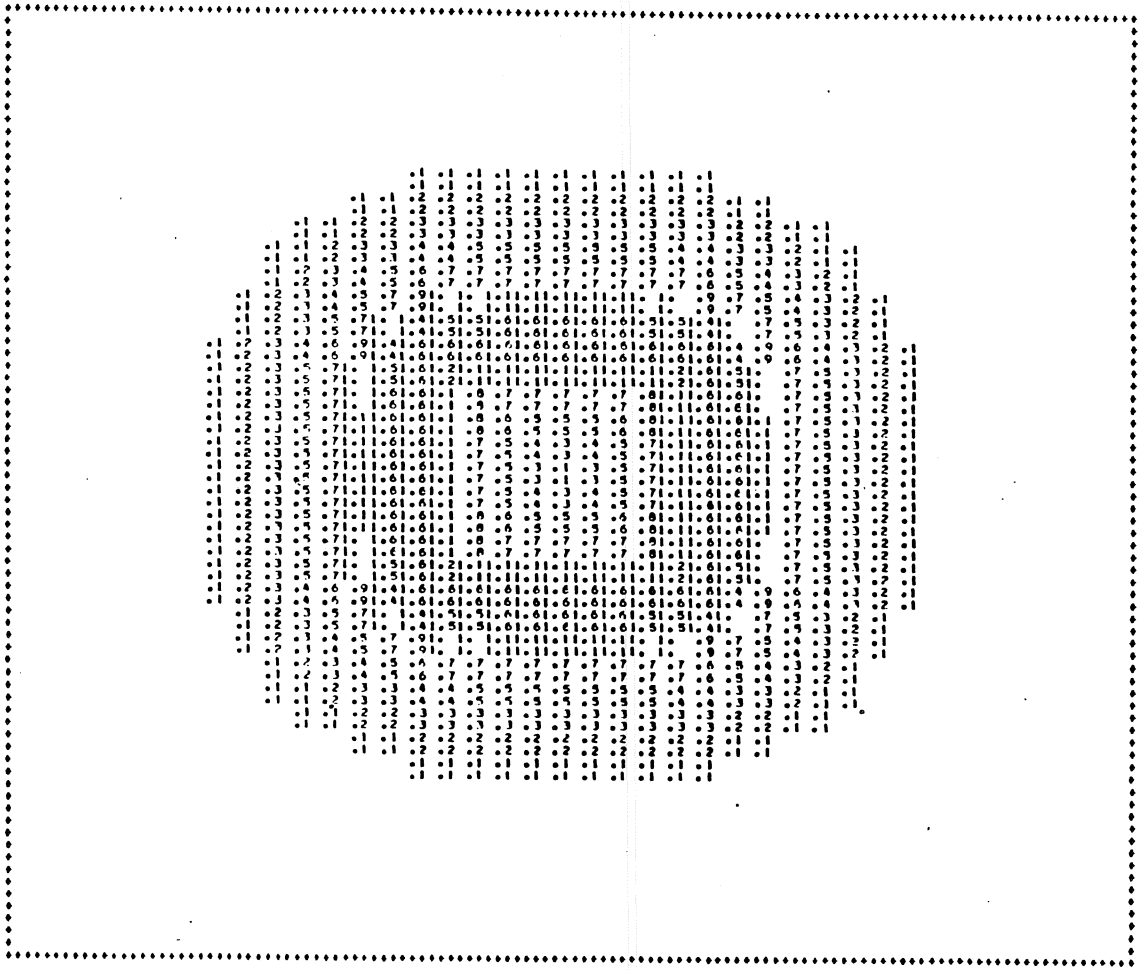

Figure 5.11c - Map of transition zone. N = 0.01 m/day, T = 2.0 day, maximal ordinate = 1.50 m.

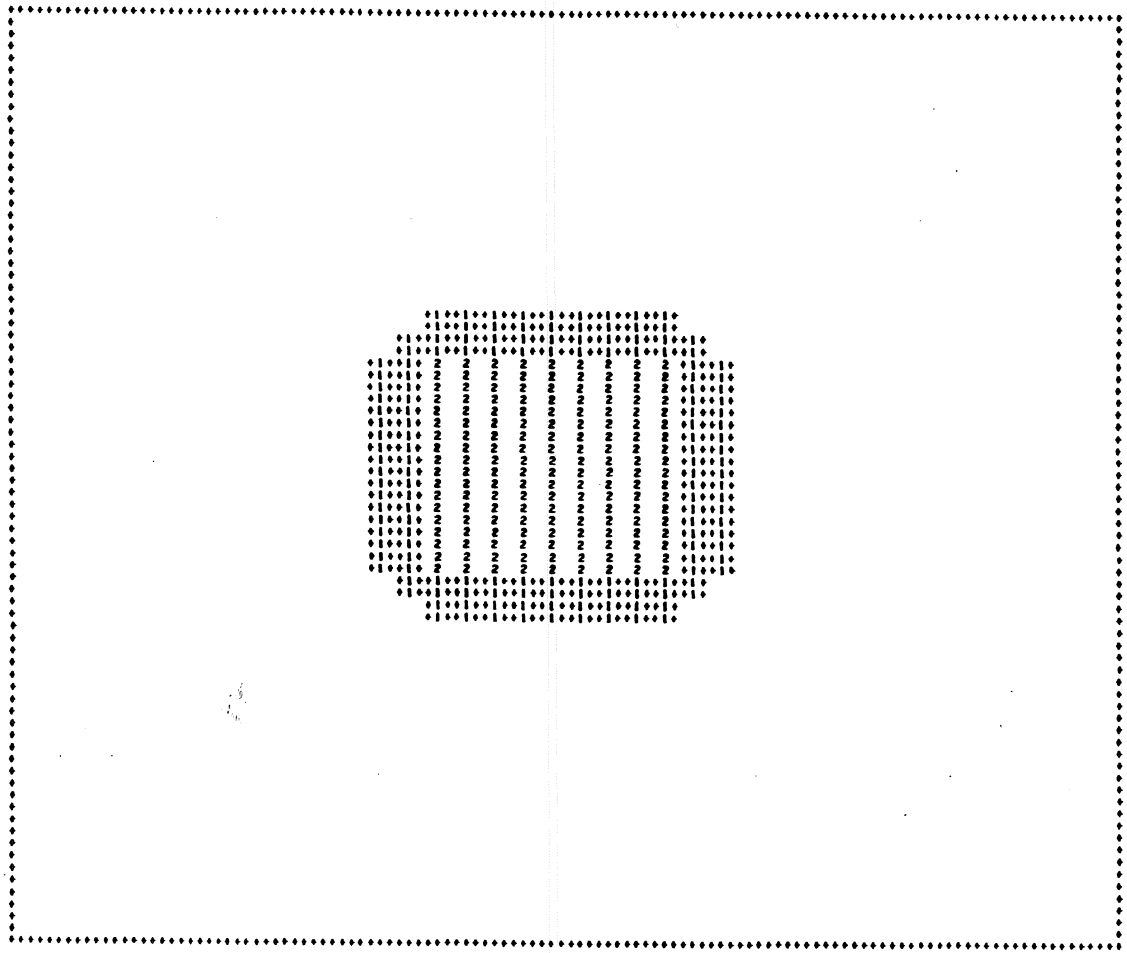

Figure 5.12a - Map of drawdowns. N = 0.01 m/day, T = 6.0 days, maximal ordinate = 2.01 m.

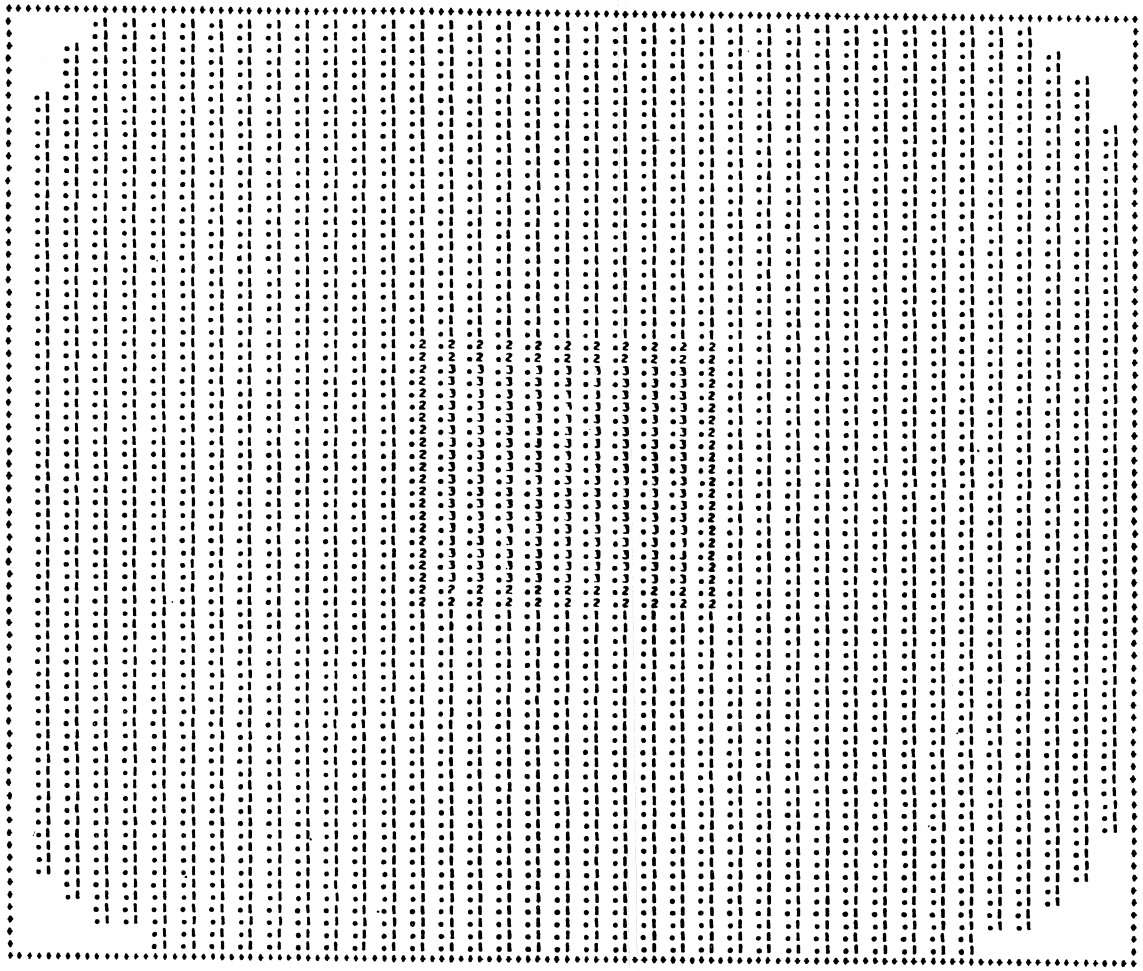

Figure 5.12b - Map of saltwater mound. N = 0.01 m/day, T = 6.0 days, maximal ordinate = 0.28 m.

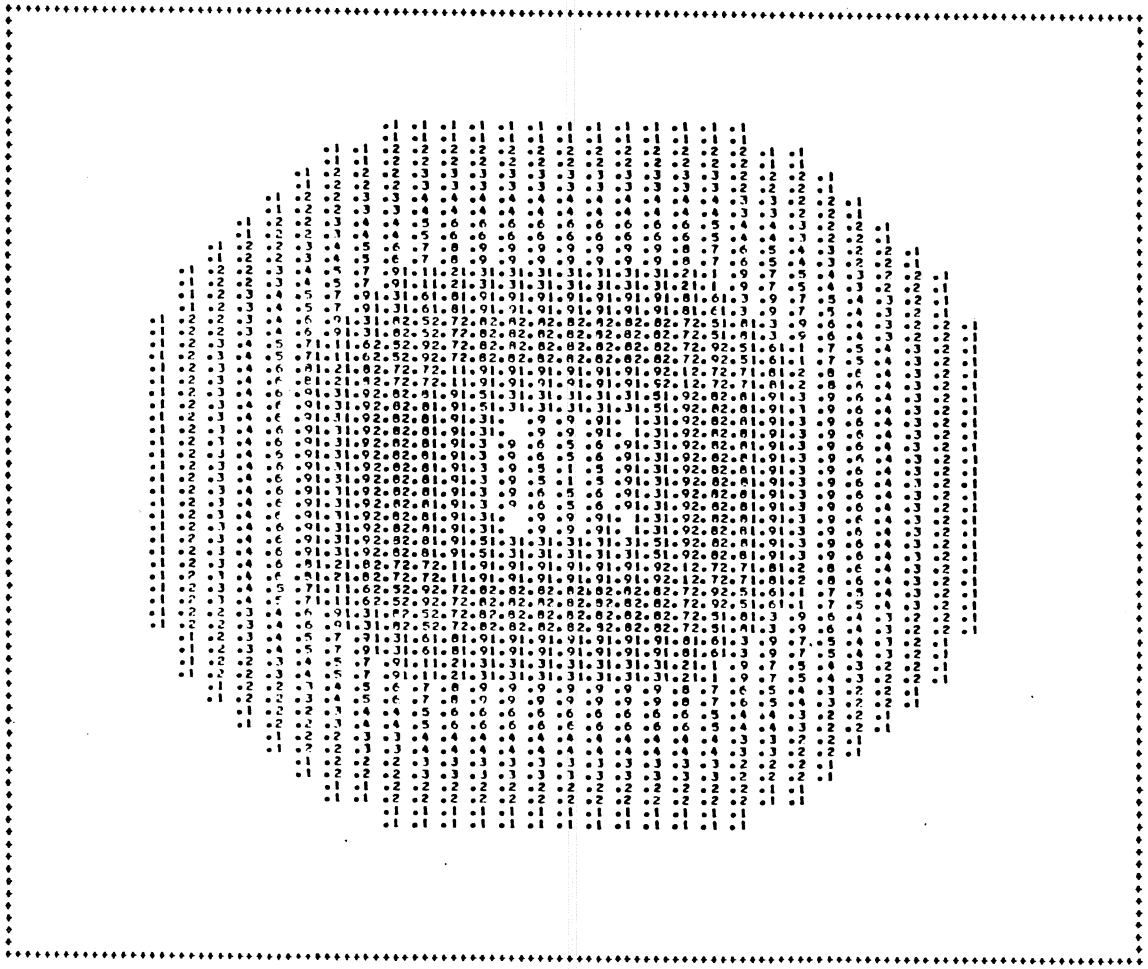

Figure 5.12c - Map of transition zone. N = 0.01 m/day, T = 6.0 days, maximal ordinate = 2.82 m.

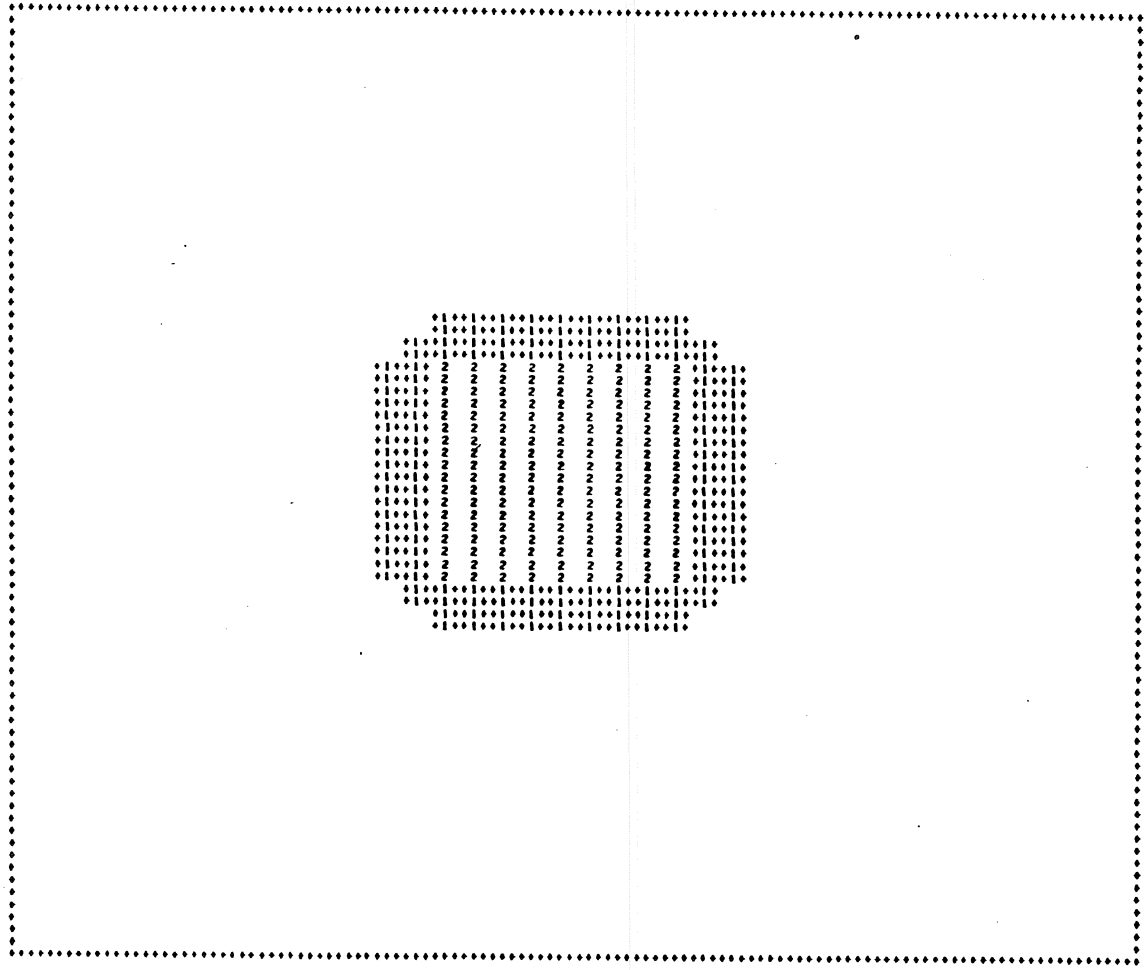

Figure 5.13a - Map of drawdowns. N = 0.01 m/day, T = 10.0 days, maximal ordinate = 2.02 m.

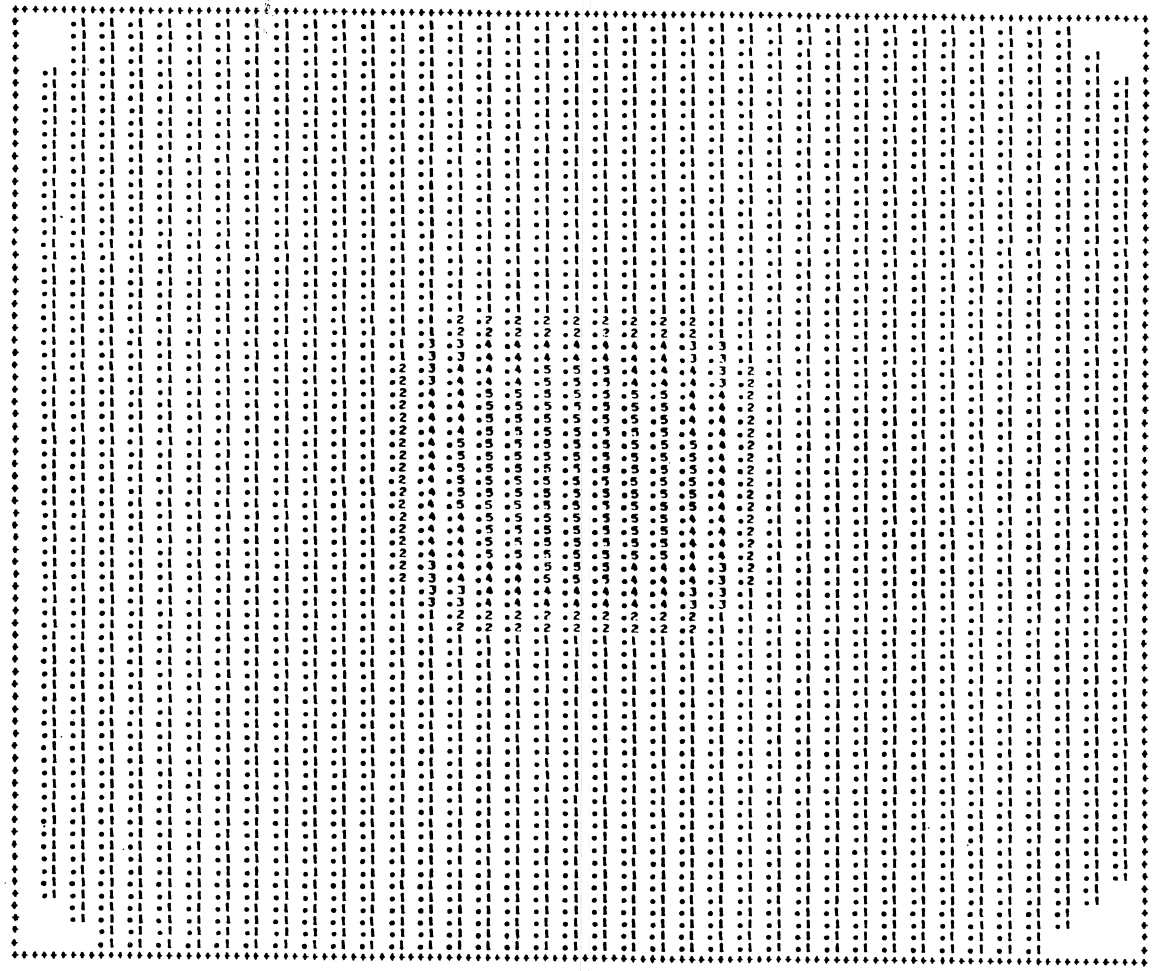

Figure 5.13b - Map of saltwater mound. N = 0.01 m/day, T = 10.0 days, maximal ordinate = 0.47 m.

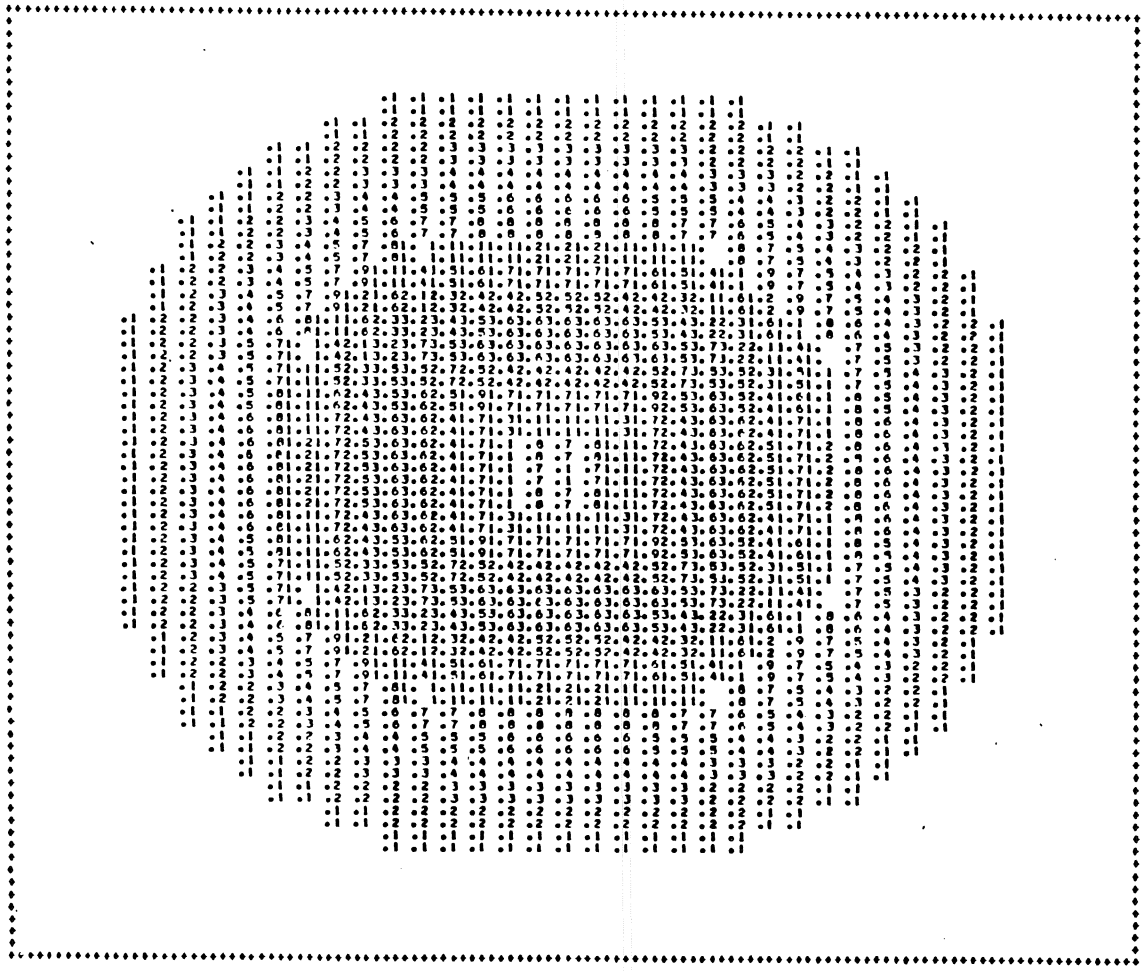

Figure 5.13c - Map of transition zone. N = 0.01 m/day, T = 10.0 days, maximal ordinate = 3.63 m.

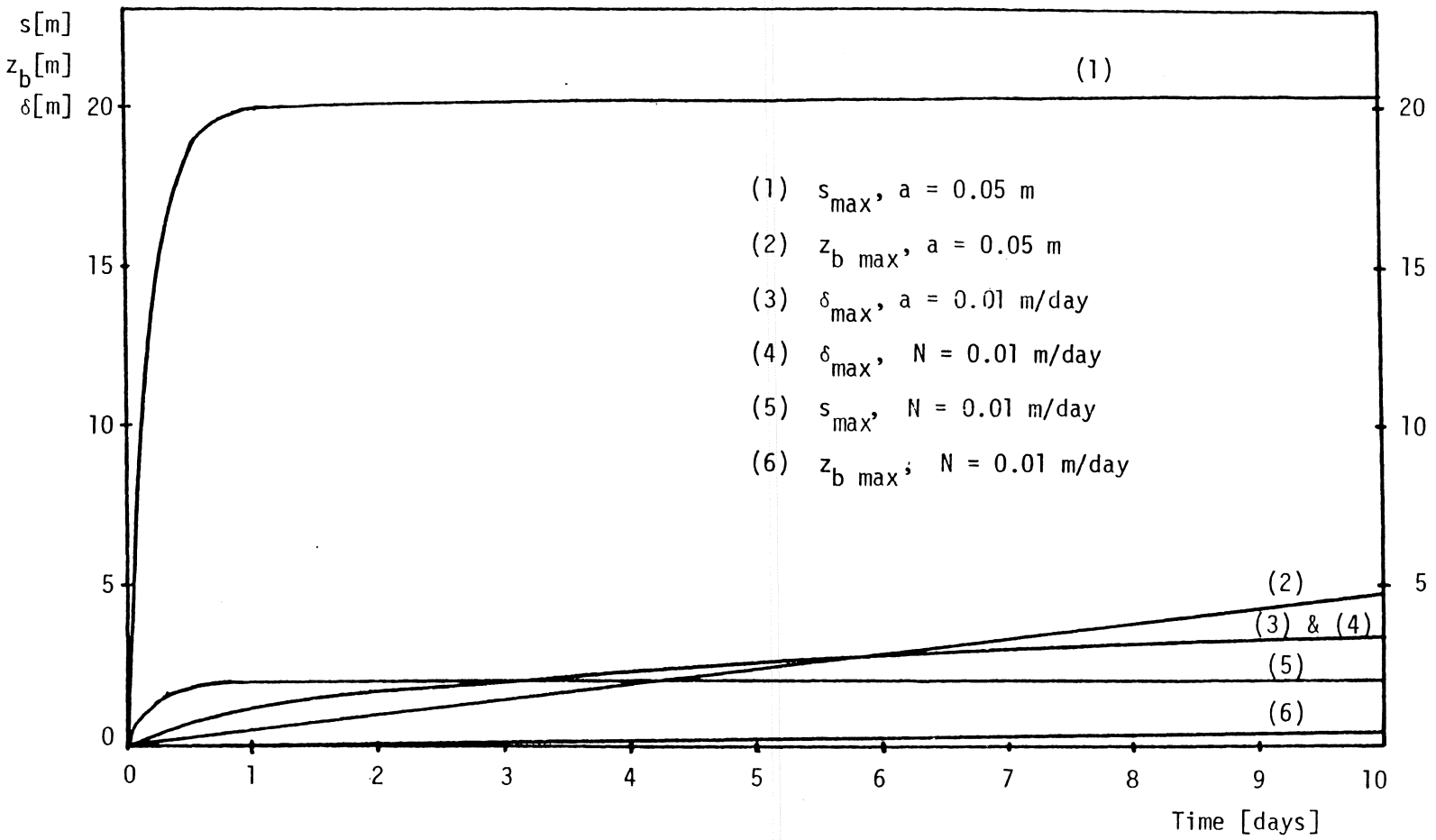

Figure 5.14 - Rate of growth of the maximal values of the drawdown, the height of the saltwater mound, and the thickness of the transition zone for experiment numbers 2 and 3.

5.5 Discussion and Conclusions

By virtue of the results presented in the previous section, the numerical model developed in this study is considered to be highly stable and convergent. The numerical results are coherent with both the physical phenomena associated with the mineralization process and the expected behavior of the governing equations.

The preliminary simulation is designed to determine the stability and convergence characteristics of the numerical model and to yield exploratory results. The numerical scheme converges rapidly and yields three-dimensional results similar to Rubin's [1932] two-dimensional results.

For the preliminary simulation, Figure 5.6 illustrates a rapid stabilization of the drawdown in the early stages of the simulation period. This phenomenon is quite typical for an aquifer of the type under consideration in this study. Horizontal flow in the freshwater zone and vertical leakage from the semiconfining formation is associated with the establishment of the drawdown within the aquifer.

According to equation (4.18) and (4.19), the system approaches steady state conditions with respect to the growth of the saltwater mound where

$$\frac{s}{\xi} = (z_b + \delta \int_0^1 L d\eta) \tag{5.7}$$

Given the parameter values in Table 5.1 and a drawdown of 20 m (Figure 5.5a), steady state conditions are reached when the right hand side of equation (5.7) is on the order of 800 m. Assuming this to be true, the aquifer would become completely mineralized before steady

state conditions are reached. However, this would rarely be the case in actual field applications since a well will most likely be abandoned when the chloride content of the well water reaches an intolerable level. Nevertheless, the transient simulation provided by the model can serve as a powerful tool when establishing safe yields for well users.

When pumpage begins it can be assumed that

$$z_b K_1 << B_1 K \qquad (z_b + \delta \int_0^1 L d\eta) << \frac{S}{\xi}$$

Therefore, in the initial stages of pumpage

$$\frac{\partial z_b}{\partial t} \simeq \frac{K_1 s}{n B_1 (1 + \xi)} \tag{5.8}$$

Equations (4.18) and (5.8) imply that when pumpage begins and the drawdown is small the leakage from the underlying saline formation is not significant. An increase in the drawdown is associated with an increase in the rate of leakage. As the drawdown subsequently stabilizes, the combination of the growth of both the saltwater mound and the transition zone contribute to a decrease in the rate of leakage. Although this is predicted by equation (4.19), the rate of leakage is found to be almost constant (Figure 5.6) for the simulation period. This would imply that for the simulation period the approximation given by equation (5.8) is valid. The use of equation (5.8) instead of equation (4.19) during the execution of the model would save computer time and memory.

The development of the transition zone is described by equation (4.22). The rate of growth of the thickness of the transition zone stems from the relative contributions made by both convective and

dispersive terms. The magnitude of these terms are determined by the horizontal specific discharge in the freshwater zone. Since longitudinal dispersion is neglected in the analysis, it seems reasonable to consider values of the effective dispersivity, a, which are larger than the predicted transverse dispersivity.

The true profiles of the specific discharge and the solute concentration within the transition zone are approximated by second order polynomial functions following Rubin [1982b]. Although other functions could be chosen, for example higher order polynomials or sine and cosine functions, a second order polynomial is considered sufficiently accurate for simulation purposes. The impact of the use of various approximating functions upon the similar profiles is not explored in this study, but it is anticipated that the results would not differ significantly.

In order to determine the relative contribution of the convective and dispersive terms in equation (4.22) toward the development of the transition zone, the preliminary simulation was executed without the convective terms. This operation reduces equation (4.22) to the form

$$(\frac{n}{2}\int_0^1 L d\eta)\ \frac{\partial\ \delta^2}{\delta t} = -\ a\ K\ [(\frac{\partial s}{\partial x})^2 + (\frac{\partial s}{\partial y})^2]^{1/2}\ L'(0) \qquad (5.9)$$

In comparing the results it is found that the development of both the drawdown and the saltwater mound were identical to that predicted with convective terms included. Figure 5.6 illustrates the results with regard to the rate of growth of the maximal value of the thickness of the transition zone. The results indicate that the convective terms in equation (4.22) make only minor contributions to the development of the transition zone for the simulation period. This can be deduced

from equation (4.22) in that for the initial stages of pumpage both the squared thickness of the transition zone and its gradient are small. The use of equation (5.9) as an approximation to equation (4.22) in the execution of the model leads to a reduction in computer time and memory of about 18 percent and a more conservative estimate of the thickness of the transition zone when applying the model for recommended safe well yields.

As simulation times are increased, the convective terms in equation (4.22) will increase in magnitude until steady state conditions are reached. Steady state conditions with respect to the transition zone are reached where

$$[\delta^2 (\frac{\partial u}{\partial x} + \frac{\partial v}{\partial y}) + \frac{1}{2} (U \frac{\partial \delta^2}{\partial x} + V \frac{\partial \delta^2}{\partial y})] \int_0^1 FL d\eta$$

$$= - a K [(\frac{\partial s}{\partial x})^2 + (\frac{\partial s}{\partial y})^2]^{1/2} L'(0) \qquad (5.10)$$

For the simulation period the development of the transition zone is attributed primarily to the dispersive term in equation (5.9). Here the rate of growth of the transition zone with respect to the horizontal coordinates is proportional to the dispersion coefficient and the horizontal specific discharge. Figure 5.6 demonstrates that while the rate of growth of the transition zone is initially very rapid, it declines in magnitude during the entire simulation period. This result is coherent with the physical phenomena in that during the initial stage of pumpage the salinity gradient within the transition zone is very large causing rapid growth of this zone. As the transition zone increases in thickness, the salinity gradient within the zone diminishes thereby reducing the rate of growth of the zone.

For the preliminary simulation both the saltwater mound and the transition zone propagate laterally in response to the pumpage. Once again this result is coherent with the physical phenomena. The maximum height of the saltwater mound is located at the center of the pumpage field. The maximum thickness of the transition zone is located where the gradient of the drawdown is the greatest. This can be deduced from equation (5.9) where the rate of growth of the transition zone is proportional to the gradient of the drawdown.

Referring to Figures 5.3c, 5.4c, and 5.5c, the thickness of the transition zone vanishes in the vicinity of the center of the pumpage field. This phenomenon is obtained because it is assumed that the coefficient of salinity dispersion is proportional to the horizontal flow in the freshwater zone. However, in the vicinity of the center of the pumpage field vertical flow and longitudinal dispersion in the vertical direction are significant. Therefore, the model seems to underestimate the growth of the transition zone in this region.

Experiment number 1 is designed to evaluate the accuracy of the convergence of the numerical model by altering the value of the time step (Table 5.2). A comparison of the results obtained in Figures 5.3a, 5.3b, and 5.3c and Figures 5.7a, 5.7b, and 5.7c demonstrates no significant differences between the respective ordinate values for an alteration in the time step. Therfore, it is found that the numerical model converges to the same values for two different time steps. While this in itself is not a guarantee of numerical accuracy, the results of experiment number 1 indicate that the numerical model converges to the true answer.

Experiment numbers 2, 3, and 4 were designed to observe the distribution of the drawdown, the saltwater mound, and the thickness of the transition zone within the flow field under a variety of parameter changes (Table 5.2). Experiment numbers 2 and 3 yield realistic results while the results from experiment number 4 are discarded. Although the numerical model converges for the parameter change in experiment number 4, the results are unrealistic. The decrease in the leakance value by an order of magnitude is associated with drawdown values in excess of 100 m. The system reacts more as a confined aquifer rather than a leaky aquifer.

Figure 5.14 illustrates some results with regard to experiment numbers 2 and 3. A reduction in the value of the dispersivity by an order of magnitude affects only the development of the transition zone. A similar reduction in the rate of pumpage affects the development of both the saltwater mound and the transition zone. These results are to be expected since the development of the saltwater mound depends primarily on the drawdown while the development of the transition zone depends on both the gradient of the drawdown and the dispersivity. It should be noted here that these results are valid only for the simulation period used in this study. As the simulation period is lengthened the terms in equations (4.19) and (4.22) containing the parameter, δ, play an increasing role in the development of the saltwater mound and the transition zone. At this point the approximation given in equations (5.8) and (5.10) are no longer valid.

A consequence of experiment numbers 2 and 3 is demonstrated by examining curves (3) and (4) from Figure 5.14. Here the rate of growth the maximal value of the thickness of the transition zone is almost identical

for both experiments. Although not immediately apparent, this result is explained by referring to equation (5.10) where the coefficient of salinity dispersion, D, is shown to be proportional to both the dispersivity and the horizontal specific discharge in the freshwater zone. Assuming the validity of equation (5.10) over the simulation period, an alteration in either the dispersivity or the specific discharge by an identical amount will produce the same effect with regard to the development of the transition zone.

The model is not calibrated in this study primarily due to a lack of suitable field data. Although the success of the model when applied to field applications remains to be seen, it is the feeling here that this model can be adapted to a variety of applications. The results should be sufficiently accurate for engineering purposes.

In conclusion, the numerical model is found to be highly stable and converges rapidly. The numerical results are coherent with both the physical phenomena and the expected behavior of the governing equations. Equations (5.8) and (5.10) are valid as approximations to equations (4.19) and (4.22), respectively, when used for a short simulation period. Their use leads to a decrease in the quantities of computer time and memory necessary for the execution of the model. The numerical accuracy of the model is indicated by altering the value of the time step.

5.6 Summary

The numerical model is formulated by the application of an ADI method and the appropriate linear finite difference representations of equations (4.18), (4.19), and (4.22). The ADI method was chosen as a

solution technique to the parabolic system because of its widespread application to groundwater studies.

The model is executed with the aid of a high speed digital computer. Numerical results are presented for a preliminary simulation and a series of experiments. The simulation period is 10 days.

The numerical model is found to be highly stable and it converges rapidly. The results are coherent with both the physical phenomena associated with the mineralization process and the expected behavior of the governing equations.

CHAPTER 6

CONCLUSIONS

(1) The problems associated with the mineralization phenomenon typical to northeastern Florida can be simulated by the model developed in this study.

(2) The majority of leakage occurs from underlying formations. Therefore, the aquifer appears to be a leaky confined aquifer subject to the mineralization process.

(3) It is possible to reduce the complexities of the basic model by the application of the Dupuit approximation in conjunction with the boundary layer theory to the flow field.

(4) Various numerical experiments indicate that the numerical scheme developed in this study is highly stable, convergent, and accurate.

(5) The numerical results generated by the model are coherent with the physical phenomena associated with the mineralization process as follows:

   (a) the drawdowns stabilize rapidly while the mineralization process continues throughout the entire simulation period;

   (b) the thickness of the transition zone is relatively large when compared to the thickness of the freshwater aquifer. This situation is commonly seen in the field where the chloride content of the well water increases gradually.

(6) Neglecting the convective terms in the equation describing the development of the transition zone leads to a substantial savings in computer time and memory.

(7) The rate of growth of the transition zone depends upon the rate of pumpage and the dispersivity. The rate of growth of the saltwater mound depends only on the rate of pumpage.

(8) The success of this model in the present study encourages further use of the basic approach. The model can be used for the improvement of groundwater use in the State of Florida.

APPENDIX A

THE DEVELOPMENT OF THE FINITE DIFFERENCE SCHEMES REPRESENTING EQUATION (4.22)

APPENDIX A

THE DEVELOPMENT OF THE FINITE DIFFERENCE SCHEMES REPRESENTING EQUATION (4.22)

Finite difference representations of hyperbolic systems generally arise from either an explicit or an implicit approach. In this Appendix explicit as well as implicit finite difference schemes are developed. However, this study utilizes only the implicit approach due to its superior stability characteristics.

Equation (4.22) is considered to be a hyperbolic equation as the dominant terms in this equation are

$$\left(\frac{n}{2}\int_0^1 L\,d\eta\right)\frac{\partial\delta^2}{\partial t} \qquad \left(\frac{U}{2}\frac{\partial\delta^2}{\partial x}+\frac{V}{2}\frac{\partial\delta^2}{\partial y}\right)\int_0^1 FL\,d\eta$$

Therefore, equation (4.22) may be reduced to the following hyperbolic form

$$\left(\frac{n}{2}\int_0^1 L\,d\eta\right)\frac{\partial\delta^2}{\partial t}+\left(\frac{U}{2}\frac{\partial\delta^2}{\partial x}+\frac{V}{2}\frac{\partial\delta^2}{\partial y}\right)\int_0^1 FL\,d\eta = DL'(0)$$

$$-\delta^2\left(\frac{\partial U}{\partial x}+\frac{\partial V}{\partial x}\right)\int_0^1 FL\,d\eta \qquad (A.1)$$

Equation (A.1) assumes that the convective term represented by the product, $\delta^2\left(\frac{\partial U}{\partial x}+\frac{\partial V}{\partial y}\right)$, in equation (4.22) is very small and that the right hand side of equation (4.22) is approximately constant.

An explicit finite difference expression for equation (A.1) involves a time difference for the term, $\frac{\partial\delta^2}{\partial t}$, and a backward difference

for the term, $(\frac{U}{2}\frac{\partial \delta^2}{\partial x} + \frac{V}{2}\frac{\partial \delta^2}{\partial y})$. The backward difference involves only the time level (m). For this situation, only the time dependent term produces unknown values at the time level (m+1). All constant and minor terms are formulated for the intermediate time level (m+1/2).

The approach used for the development of an implicit finite difference expression for equation (4.22) is identical to that used for the explicit expression except that the backward difference representation of the term, $(\frac{U}{2}\frac{\partial \delta^2}{\partial x} + \frac{V}{2}\frac{\partial \delta^2}{\partial y})$, involves the time level (m+1). Therefore, unknown values at time level (m+1) are generated from two different terms.

Following the explicit approach of Mitchell [1976], an explicit expression for the description of the development of the transition zone in the x direction is obtained from equation (4.22) as follows

$$(\frac{n}{2}\int_0^1 Ldn)\ \delta_{i,j}^{2(m+1)} = \delta_{i,j}^{2(m)}\ [\frac{n}{2}\int_0^1 Ldn - \frac{K_{i,j}\ \Delta t}{4(\Delta x)^2}\ (s_{i+1,j}^{(m+1/2)}$$

$$- s_{i-1,j}^{m+1/2)})\int_0^1 FLdn] + \delta_{i-1,j}^{2(m)}\ [\frac{K_{i,j}\ \Delta t}{4(\Delta x)^2}\ (s_{i+1,j}^{(m+1/2)} - s_{i-1,j}^{(m+1/2)})]\int_0^1 FLdn$$

$$- \delta_{i,j}^{2(m+1/2)}\ \{\frac{\Delta t}{(\Delta x)^2}\ [K_{i+1/2,j}\ (s_{i+1,j}^{(m+1/2)} - s_{i,j}^{(m+1/2)}) + K_{i-1/2,j}$$

$$(s_{i-1,j}^{(m+1/2)} - s_{i,j-1}^{(m+1/2)})] + \frac{\Delta t}{(\Delta y)^2}\ [K_{i,j+1/2}\ (s_{i,j+1}^{(m+1/2)} - s_{i,j}^{(m+1/2)}$$

$$+ K_{i,j-1}\ (s_{i,j-1}^{(m+1/2)} - s_{i,j}^{(m+1/2)})]\}\int_0^1 FLdn - \frac{K_{i,j}\ \Delta t}{8(\Delta y)^2}\ [(\delta_{i,j+1}^{2(m)}$$

$$- \delta^{2(m)}_{i,j+1}) \; (s^{(m+1/2)}_{i,j+1} - s^{(m+1/2)}_{i,j-1})] \int_0^1 Fld\eta = \frac{a \; K_{i,j} \; \Delta t}{2}$$

$$[(\frac{s^{(m+1/2)}_{i+1,j} - s^{(m+1/2)}_{i-1,j}}{\Delta x})^2 + (\frac{s^{(m+1/2)}_{i,j+1} - s^{(m+1/2)}_{i,j-1}}{\Delta y})^2]^{1/2} \; L'(0) \quad (A.2)$$

An explicit expression for the description of the development of the transition zone in the y direction is obtained from equation (4.22) as follows

$$(\frac{n}{2} \int_0^1 Ld\eta) \; \delta^{2(m+2)}_{i,j} = \delta^{2(m+1)}_{i,j} \; [\frac{n}{2} \int_0^1 Ld\eta - \frac{K_{i,j} \; \Delta t}{4(\Delta y)^2} \; (s^{(m+1 \; 1/2)}_{i,j+1}$$

$$- s^{(m+ \; 1 \; 1/2)}_{i,j-1}) \int_0^1 FLd\eta] + \delta^{2(m+1)}_{i,j-1} \; [\frac{K_{i,j} \; \Delta t}{4(\Delta y)^2} \; (s^{(m+1 \; 1/2)}_{i,j+1}$$

$$- s^{(m+1 \; 1/2)}_{i,j-1})] \int_0^1 FLd\eta - \delta^{2(m+1 \; 1/2)}_{i,j} \; \{\frac{\Delta t}{(\Delta y)^2} \; [K_{i,j+1/2} \; (s^{(m+1 \; 1/2)}_{i,j+1}$$

$$- s^{(m+1 \; 1/2)}_{i,j}) + K_{i,j-1/2} \; (s^{(m+1 \; 1/2)}_{i,j-1} - s^{(m+1 \; 1/2)}_{i,j})] + \frac{\Delta t}{(\Delta x)^2}$$

$$[K_{i+1/2,j} \; (s^{(m+1 \; 1/2)}_{i+1,j} - s^{(m+1 \; 1/2)}_{i,j}) + K_{i-1/2,j} \; (s^{(m+1 \; 1/2)}_{i-1,j}$$

$$- s^{(m+1 \; 1/2)}_{i,j})]\} \int_0^1 FLd\eta - \frac{K_{i,j} \; \Delta t}{8(\Delta x)^2} \; [(\delta^{2(m+1)}_{i+1,j} - \delta^{2(m+1)}_{i+1,j})]$$

$$(s^{(m+1 \; 1/2)}_{i+1,j} - s^{(m+1 \; 1/2)}_{i+1,j})] \int_0^1 FLd\eta = \frac{a \; K_{i,j} \; \Delta t}{2}$$

$$\left[\left(\frac{s_{i+1,j}^{(m+1\ 1/2)} - s_{i-1,j}^{(m+1\ 1/2)}}{\Delta x}\right)^2 + \left(\frac{s_{i,j+1}^{(m+1\ 1/2)} - s_{i,j-1}^{(m+1\ 1/2)}}{\Delta y}\right)^2\right]^{1/2}$$

$$L'(0) \qquad (A.3)$$

Following the implicit approach of Mitchell [1976] yields implicit expressions for the description of the development of the transition zone in the x and y directions given by equations (5.2) and (5.4), respectively.

APPENDIX B

COMPUTER PROGRAM

```
      $JOB
    1      DIMENSION S(50,50),SN(50,50),SE(50,50),Z(50,50),ZN(50,50)
           *  ,ZE(50,50),DZ(50,50),XN(50,50),XNT(50,50),BI(50,50)
           *  ,A(50),B(50),C(50),D(50),X(50)
           *  ,DL(50,50),DLN(50,50),DLE(50,50),D2(50,50),DN2(50,50)
           *  ,DE2(50,50)
      C     ------------------------------------------------------
      C           TWO DIMENSIONAL SIMULATION
      C     ------------------------------------------------------
      C            AQUIFER DETAILS
      C            ===============
      C     XK=AQUIFER'S HYDRAULIC CONDUCTIVITY
      C     XK1=HYDRAULIC CONDUCTIVITY OF SEMICONFINING FORMATION
      C     BO=AQUIFER'S THICKNESS    B1=THICKNESS OF SEMICONFING FORMATION
      C     PN=EFFECTIVE POROSITY     ST=STORAGE COEFFICIENT
      C     A1=DISPERSIVITY           XKSI=PARAMETER OF DENSITY RATIO
      C     N=NUMBER OF X NODAL POINTS   M= NUMBER OF Y NODAL POINTS
      C     NM=NUMBER OF GRID POINTS(=N*M)
      C     ------------------------------------------------------
      C      ID=TYPE OF PRINTING ID=0 MEANS DRAWING
      C     ------------------------------------------------------
    2       ID=0
    3       XK=40.
    4       XK1=0.1
    5       BO=50.
    6       B1=20.
    7       PN=0.2
    8       ST=0.001
    9       A1=0.5
   10       XKSI=0.025
   11       N=40
   12       M=40
   13       NM=N*M
   14       DB=0.
   15       IP=1
   16       PRINT 10,XK,XK1,BO,B1,PN,ST,A1,XKSI,N,M,NM
   17    10 FORMAT(1H1,///,5X,'=========================================='/
           *              ,5X,'GROWTH OF SALTWATER MOUND IN A LEAKY AQUIFER'/
           *              ,5X,'     TWO DIMENSIONAL ANALYSIS'
           *             /,5X,'==========================================',
           *  //5X,'AQUIFER DETAILS'/5X, '---------------'//,5X,'XK=',F4.0,
           *  5X,'XK1=',F4.1,5X,'BO=',F4.0,5X,'B1=',F4.0/,
           *  5X,'PN=',F4.2,5X,'ST=',F6.4,5X,'A1=',F6.4/,5X,'XKSI=',F5.3/,
           *  5X,'NODAL AND GRID POINTS  N=',I2,5X,'M=',I2,5X,'NM=',I4/)
```

```
C     ------------------------------------------------------------
C              CHARACTERISTICS OF THE TRANSITION ZONE
C              --------------------------------------
C     ALF=INTEGRAL OF F*DI(ETA)     BET=INTEGRAL OF L*DI(ETA)
C     AB=INTEGRAL OF F*L*DI(ETA)    AL=L'(0)
C     ------------------------------------------------------------
      ALF=2./3
      BET=1./3
      AB=2./15
      AL=-2.
      AL1=AL*A1
      PNL=PN*BET*0.5
      PRINT 20,ALF,BET,AB,AL
   20 FORMAT(//,5X,'CHARACTERISTICS OF THE TRANSITION ZONE'/
     *          ,5X,'----------------------------------------'/
     *
     *     5X,'ALF=',F6.4,5X,'BET=',F6.4,5X,'AB=',F6.4,5X,'AL=',
     *    F6.3,
     *    5X)
C     ------------------------------------------------------------
C                    PARAMETERS
C                    ==========
C     S(I,J),SN(I,J),SE(I,J)=INIT.,FI.,AVE DRAWDOWN
C     Z(I,J),ZN(I,J),ZE(I,J)=INIT.,FI.,AVE THICK. OF SALTWATER MOUND
C     DL(I),DLN(I),DLE(I)=INIT.,FI.,AVE.THICKNESS OF TRANS.ZONE
C     D2(I),DN2(I),DE2(I)=INIT.,FI.,AVE.SQUARE THICK. OF TRANS ZONE
C     BI(I,J)=AVERAGE THICKNESS OF THE FRESHWATER ZONE
C     DZ(I,J)=AVERAGE RATE OF GROWTH OF SALTWATER MOUND
C     XN(I,J)=RATE OF PUMGAGE PER UNIT AREA
C     ------------------------------------------------------------
      DO 50 I=1,N
      DO 40 J=1,M
      S(I,J)=0.
      SN(I,J)=0.
      SE(I,J)=0.
      Z(I,J)=0.
      ZN(I,J)=0.
      ZE(I,J)=0.
      DZ(I,J)=0.
      BI(I,J)=BO
```

```
36          XN(I,J)=0.
37          DL(I,J)=0.
38          DLN(I,J)=0.
39          DLE(I,J)=0.
40          D2(I,J)=0.
41          DN2(I,J)=0.
42          DE2(I,J)=0.
43       40 CONTINUE
44       50 CONTINUE
      C     ------------------------------------------------------------
      C     PUMPAGE DISTRIBUTION
      C     ------------------------------------------------------------
45          PRINT 60
46       60 FORMAT(5X,'PUMPAGE DISTRIBUTION',/5X,'====================')
47          DO 80 I=15,25
48          DO 70 J=15,25
49          XN(I,J)=0.1
50       70 CONTINUE
51       80 CONTINUE
52          IF(ID.EQ.1) GOTO 88
53          PRINT 82
54       82 FORMAT(///,10X,'MAP OF PUMPAGE'//)
55          CALL DRAW1(XN,IP,DB)
56          GOTO 132
57       88 DO 130 I=20,30
58          DO 120 K=1,2
59          J=20+(K-1)*6
60          J1=J+1
61          J2=J+2
62          J3=J+3
63          J4=J+4
64          J5=J+5
65          IF(K.EQ.2) GOTO 100
66          PRINT 90,I,J,XN(I,J),I,J1,XN(I,J1),I,J2,XN(I,J2),I,J3,XN(I,J3),
           * I,J4,XN(I,J4),I,J5,XN(I,J5)
67       90 FORMAT(3X,'XN(',I2,',',I2,')=',F4.2,3X,'XN(',I2,',',I2,')=',F4.2
           *  ,3X,'XN(',I2,',',I2,')=',F4.2,3X,'XN(',I2,',',I2,')=',F4.2,
           *   3X,'XN(',I2,',',I2,')=',F4.2,3X,'XN(',I2,',',I2,')=',
           *  F4.2)
68          GOTO 120
69       100 PRINT 110,I,J,XN(I,J),I,J1,XN(I,J1),I,J2,XN(I,J2),I,J3,XN(I,J3)
           * ,I,J4,XN(I,J4)
70       110 FORMAT(3X,'XN(',I2,',',I2,')=',F4.2,3X,'XN(',I2,',',I2,')=',F4.2,
           * 3X,'XN(',I2,',',I2,')=',F4.2,3X,'XN(',I2,',',I2,')=',F4.2,
           *   3X,'XN(',I2,',',I2,')=',F4.2)
71       120 CONTINUE
72       130 CONTINUE
```

```
      C     ------------------------------------------------------------
      C     GRID INTERVALS
      C     ------------------------------------------------------------
   73   132 DX=500.
   74       PRINT 140,DX
   75   140 FORMAT(/ 3X,'GRID INTERVALS DY=DX=',F4.0,' METERS')
   76       N1=N-1
   77       N2=N-2
   78       N3=N-3
   79       M1=M-1
   80       M2=M-2
   81       M3=M-3
   82       A(1)=0.
      C     ------------------------------------------------------------
      C     INITIAL TIME STEP=DT1
      C     ------------------------------------------------------------
   83       DT1=0.2
   84       PRINT 150,DT1
   85   150 FORMAT(//,5X,'TIME STEP DT=',F5.3,' DAYS',/5X,
     *  '====================')
   86       T=0.
   87       PRINT 160,T
   88   160 FORMAT(//5X,'T=',F8.3,' DAYS'/,5X,'==================')
   89       PRINT 170
   90   170 FORMAT(// 5X,'ALL PARAMETERS VANISH'/,5X,'----------------------')
   91       DT=DT1
   92       DX2=DX*DX
   93   180 CONTINUE
   94       XKK=XK*XK1/(PN*(1.+XKSI))
   95       BK=B1*XK
   96       DO 200 I=1,N
   97       DO 190 J=1,M
   98       XNT(I,J)=XN(I,J)*DT
   99   190 CONTINUE
  100   200 CONTINUE
  101       IX=1
  102   210 T=T+DT
```

```
103         IF(T.GT.2.) GOTO 660
      C     ------------------------------------------------------------
      C     STARTING ITERATION PROCEDURE
      C     ------------------------------------------------------------
104         R=DT/DX2
105         XKT=XK*R
106       220 IT=-1
107       222 IT=IT+1
108         BK=B1*XK
109         IF(IX.EQ.2) GOTO 590
      C     ------------------------------------------------------------
      C     IMPLICIT SCHEME IN THE X DIRECTION
      C     ------------------------------------------------------------
110         SBIG=0.
111         DO 280 J=2,M1
112         DO 230 I1=2,N2
113         I=I1+1
114         A(I1)=.5*XKT*(BI(I-1,J)+BI(I,J)+(DLE(I-1,J)+DLE(I,J))*ALF)
115       230 CONTINUE
116         DO 240 I1=1,N2
117         I=I1+1
118         B(I1)=ST+XKT*0.5*(BI(I+1,J)+2.*BI(I,J)+BI(I-1,J)
          *  +(DLE(I+1,J)+2.*DLE(I,J)+DLE(I-1,J))*ALF)
119         D(I1)=ST*S(I,J)-PN*DT*DZ(I,J)+XNT(I,J)+XKT*0.5*((BI(I,J+1)+
          *  BI(I,J)+(DLE(I,J+1)+DLE(I,J))*ALF)*(S(I,J+1)-S(I,J))+(BI(I,J)
          *  +BI(I,J-1)+(DLE(I,J)+DLE(I,J-1))*ALF)*(S(I,J-1)-S(I,J)))
120       240 CONTINUE
121         DO 250 I1=1,N3
122         I=I1+1
123         C(I1)=0.5*XKT*(BI(I,J)+BI(I+1,J)+(DLE(I+1,J)+DLE(I,J))*ALF)
124       250 CONTINUE
125         CALL THOMAS(A,B,C,D,X,N2)
126         DO 260 I=2,N1
127         I1=I-1
128         SN1=X(I1)
129         SB=ABS(SN1-SN(I,J))
130         IF(SB.GT.SBIG) SBIG=SB
131         IF(SN1.LT.0.) SN1=0.
132         SN(I,J)=SN1
133       260 CONTINUE
134         DO 270 I=2,N1
135         SE(I,J)=(S(I,J)+SN(I,J))*0.5
136       270 CONTINUE
137       280 CONTINUE
```

```
138           DO 284 J=2,M1
139           DO 283 I=2,N1
140           IF(Z(1,J).LT.0.0001) GOTO 283
141           DEN=PNL+.25*XKT*AB*(SE(I+1,J)-SE(I-1,J))
142           DN2(I,J)=(D2(I,J)*PNL-XKT*AB*(DE2(I,J)*(SE(I+1,J)+SE(I-1,J)-
             *  2.*SE(I,J))-.25*DN2(I-1,J)*(SE(I+1,J)-SE(I-1,J))+D2(I,J)*
             *  (SE(I,J+1)+SE(I,J-1)-2.*SE(I,J))+.25*(SE(I,J+1)-SE(I,J-1))*
             *  (D2(I,J+1)-D2(I,J-1)))-.5*DX*AL1*XKT*SQRT((SE(I+1,J)-
             *  SE(I-1,J))**2+(SE(I,J+1)-SE(I,J-1))**2))/DEN
143           IF(DN2(I,J).LT.0.) DN2(I,J)=0.
144       283 CONTINUE
145       284 CONTINUE
      C     ------------------------------------------------------------
      C     CALCULATION APPLIED TO X AND Y DIRECTIONS
      C     ------------------------------------------------------------
146       285 DBIG=0.
147           DBI2=0.
148           DO 288 I=2,N1
149           DO 287 J=2,M1
150           DLN(I,J)=SQRT(DN2(I,J))
151           DLE(I,J)=.5*(DLN(I,J)+DL(I,J))
152           DE2(I,J)=.5*(D2(I,J)+DN2(I,J))
153           DB1=ABS(DLN(I,J)-DL(I,J))
154           DB2=ABS(DN2(I,J)-D2(I,J))
155           IF(DB1.GT.DBIG) DBIG=DB1
156           IF(DB2.GT.DBI2) DBI2=DB2
157       287 CONTINUE
158       288 CONTINUE
159           ZBIG=0.
160           DO 300 J=2,M1
161           DO 290 I=2,N1
162           DZ(I,J)=XKK/(BK+ZE(I,J)*XK1)*(SE(I,J)-XKSI*(ZE(I,J)
             *  +BET*DLE(I,J)))
163           ZN(I,J)=Z(I,J)+DT*DZ(I,J)
164           IF(ZN(I,J).LT.0.) ZN(I,J)=0.
165           IF(SN(I,J).EQ.0.) ZN(I,J)=0.
166           ZE(I,J)=0.5*(ZN(I,J)+Z(I,J))
167           BI(I,J)=BO-ZE(I,J)-DLE(I,J)
168           ZB=ABS(ZN(I,J)-Z(I,J))
169           IF(ZB.GT.ZBIG) ZBIG=ZB
```

```
170      290 CONTINUE
171      300 CONTINUE
172          IF(IT/10.NE.0.1*IT) GOTO 312
173          PRINT 310,IT,SBIG,ZBIG,DBIG,DBI2
174      310 FORMAT(//3X,'IT=',I3,3X,'SBIG=',E8.2,3X,'ZBIG=',E8.2,
            *  3X,'DBIG=',E8.2,3X,'DBI2=',E8.2)
175      312 IF(IT.EQ.0) GOTO 222
176          IF(IT.GT.50) GOTO 340
177          IF(SBIG.GT.0.001) GOTO 222
178          IF(IX-2) 320,330,330
179      320 IX=2
180          GOTO 380
181      330 IX=1
182          GOTO 380
183      340 T=T-DT
184          DT=0.5*DT
185      350 DO 370 J=2,M1
186          DO 360 I=2,N1
187          SE(I,J)=S(I,J)
188          DLE(I,J)=DL(I,J)
189          DE2(I,J)=D2(I,J)
190          ZE(I,J)=Z(I,J)
191          BI(I,J)=BO-Z(I,J)-DL(I,J)
192          DZ(I,J)=XKK/(BK+ZE(I,J)*XK1)*(SE(I,J)-XKSI*(ZE(I,J)
            *  +BET*DLE(I,J)))
193      360 CONTINUE
194      370 CONTINUE
195          GOTO 210
196      380 DS=0.
197          DO 400 J=2,M1
198          DO 390 I=2,N1
199          DSS=ABS(SN(I,J)-S(I,J))
200          IF(DSS.GT.DS) DS=DSS
201      390 CONTINUE
202      400 CONTINUE
203          IF(DS.LT.0.00001) GOTO 660
204          DB=0.
205          DO 420 J=2,M1
206          DO 410 I=2,N1
207          S(I,J)=SN(I,J)
208          Z(I,J)=ZN(I,J)
209          DL(I,J)=DLN(I,J)
210          IF(DL(I,J).GT.DB) DB=DL(I,J)
211          D2(I,J)=DN2(I,J)
212      410 CONTINUE
213      420 CONTINUE
```

```
C     ------------------------------------------------------------
C     TRUNCATION OF THE EDGES
C     ------------------------------------------------------------
      K=N/2
      DO 480 J=2,M1
      DO 430 I=2,K
      IF(SN(I,J).EQ.0.) GOTO 430
      SL=(SN(I+2,J)-SN(I+ 1,J))*DX
      SM=SN(I+1,J)-SL
      IF(SM.LT.0.) GOTO 440
      IF(SN(I,J).LT.SM) GOTO 450
      SN(I,J)=SM
      S(I,J)=SM
      GOTO 450
  430 CONTINUE
  440 SN(I,J)=0.
      S(I,J)=0.
  450 DO 460 I=K,N1
      IF(SN(I,J).GT.0.) GOTO 460
      SL=(SN(I-3,J)-SN(I-2,J))*DX
      SM=SN(I-2,J)-SL
      IF(SN(I-1,J).LT.SM) GOTO 490
      IF(SM.LT.0.) GOTO 470
      SN(I-1,J)=SM
      S(I-1,J)=SM
      GOTO 490
  460 CONTINUE
  470 SN(I-1,J)=0.
      S(I-1,J)=0.
      GOTO 490
  480 CONTINUE
  490 K=M/2
      DO 550 I=2,N1
      DO 500 J=2,K
      IF(SN(I,J).EQ.0.) GOTO 500
      SL=(SN(I,J+2)-SN(I,J+1))*DX
      SM=SN(I,J+1)-SL
      IF(SM.LT.0.) GOTO 510
```

```
249           IF(SN(I,J).LT.SM) GOTO 520
250           SN(I,J)=SM
251           S(I,J)=SM
252           GOTO 520
253       500 CONTINUE
254       510 SN(I,J)=0.
255           S(I,J)=0.
256       520 DO 530 J=K,M1
257           IF(SN(I,J).GT.0.) GOTO 530
258           SL=(SN(I,J-3)-SN(I,J-2))*DX
259           SM=SN(I,J-2)-SL
260           IF(SN(I,J-1).LT.SM) GOTO 560
261           IF(SM.LT.0.) GOTO 540
262           SN(I,J-1)=SM
263           S(I,J-1)=SM
264           GOTO 560
265       530 CONTINUE
266       540 SN(I,J-1)=0.
267           S(I,J-1)=0.
268           GOTO 560
269       550 CONTINUE
270       560 CONTINUE
          C   ------------------------------------------------------------
          C   PRINTING RESULTS
          C   ------------------------------------------------------------
271       561 FORMAT(5X,'ALL ORDINATES ARE SMALLER THAN 0.05 METER'//)
272           PRINT 160,T
273           IF(ID.EQ.1) GOTO 568
274           PRINT 562
275       562 FORMAT(///,10X,'MAP OF DRAWDOWNS'//)
276           CALL DRAW(S,IP,DB)
277           PRINT 564
278       564 FORMAT(///,10X,'MAP OF SALTWATER MOUND'//)
279           IF(Z(20,20).GE.5.0) CALL DRAW(Z,IP,DB)
280           IF(Z(20,20).LT.5.0.AND.Z(20,20).GT.0.05) CALL DRAW1(Z,IP,DB)
281           IF(Z(20,20).LT.0.05) PRINT 561
282           PRINT 565
283           IP=2
284       565 FORMAT(///10X,'MAP OF TRANSITION ZONE'///)
285           IF(DB.GE.5.) CALL DRAW(DL,IP,DB)
286           IF(DB.LT.5.0.AND.DB.GT.0.05) CALL DRAW1(DL,IP,DB)
287           IF(DB.LT.0.05) PRINT 561
288           IP=1
289       567 GOTO 586
290       568 PRINT 570
291       570 FORMAT(/2X,'NODE',5X,'S',11X,'Z',8X,'NODE',5X,'S',11X,'Z',8X,
              *  'NODE',5X,'S',11X,'Z',8X,'NODE',5X,'S',11X,'Z'/)
```

```
292           DO 584 I=1,N
293           DO 582 K=1,10
294           J=(K-1)*4+1
295           J1=J+1
296           J2=J+2
297           J3=J+3
298           PRINT 580,I,J,S(I,J),Z(I,J),I,J1,S(I,J1),Z(I,J1)
             * ,I,J2,S(I,J2),Z(I,J2),I,J3,S(I,J3),Z(I,J3)
299       580 FORMAT(4(I3,I3,2E12.4))
300       582 CONTINUE
301       584 CONTINUE
302       586 DT=D11
303           GOTO 350
      C    ------------------------------------------------------------------
      C    IMPLICIT SCHEME IN THE Y DIRECTION
      C    ------------------------------------------------------------------
304       590 SBIG=0.
305           DO 650 I=2,N1
306           DO 600 J1=2,M2
307           J=J1+1
308           A(J1)=.5*XKT*(BI(I,J-1)+BI(I,J)+(DLE(I,J-1)+DLE(I,J))*ALF)
309       600 CONTINUE
310           DO 610 J1=1,M2
311           J=J1+1
312           B(J1)=ST+XKT*0.5*(BI(I,J+1)+2.*BI(I,J)+BI(I,J-1)+
             *   (DLE(I,J+1)+2.*DLE(I,J)+DLE(I,J-1))*ALF)
313           D(J1)=ST*S(I,J)-PN*DT*DZ(I,J)+XNT(I,J)+XKT*0.5*((BI(I+1,J)+
             *   BI(I,J)+(DLE(I+1,J)+DLE(I,J))*ALF)*(S(I+1,J)-S(I,J))+
             *   (BI(I,J)+BI(I-1,J)+(DLE(I,J)+DLE(I-1,J))*ALF)*
             *   (S(I-1,J)-S(I,J)))
314       610 CONTINUE
315           DO 620 J1=1,M3
316           J=J1+1
317           C(J1)=0.5*XKT*(BI(I,J)+BI(I,J+1)+(DLE(I,J+1)+DLE(I,J))*ALF)
318       620 CONTINUE
319           CALL THOMAS(A,B,C,D,X,M2)
320           DO 630 J=2,M1
```

```
321           J1=J-1
322           SN1=X(J1)
323           SB=ABS(SN1-SN(I,J))
324           IF(SB.GT.SBIG) SBIG=SB
325           IF(SN1.LT.0.) SN1=0.
326           SN(I,J)=SN1
327       630 CONTINUE
328           DO 640 J=2,M1
329           SE(I,J)=0.5*(S(I,J)+SN(I,J))
330       640 CONTINUE
331       650 CONTINUE
332           DO 655 I=2,N1
333           DO 654 J=2,M1
334           IF(Z(I,J).LT.0.0001) GOTO 654
335           DEN=PNL+.25*XKT*AB*(SE(I,J+1)-SE(I,J-1))
336           DN2(I,J)=(D2(I,J)*PNL-XKT*AB*(DE2(I,J)*(SE(I,J+1)+SE(I,J-1)-
             *  2.*SE(I,J))-.25*DN2(I,J-1)*(SE(I,J+1)-SE(I,J-1))+D2(I,J)*
             *  (SE(I+1,J)+SE(I-1,J)-2.*SE(I,J))+.25*(SE(I+1,J)-SE(I-1,J))*
             *  (D2(I+1,J)-D2(I-1,J)))-.5*DX*AL1*XKT*SQRT((SE(I+1,J)-
             *  SE(I-1,J))**2+(SE(I,J+1)-SE(I,J-1))**2))/DEN
337           IF(DN2(I,J).LT.0.) DN2(I,J)=0.
338       654 CONTINUE
339       655 CONTINUE
340           GOTO 285
341       660 CONTINUE
342           STOP
343           END
      C       ------------------------------------------------------------
      C       SUBROUTINE THOMAS SOLVES A SYSTEM OF LINEAR EQUATIONS
      C          REPRESENTED BY A TRIDIAGONAL MATTRIX
      C       ------------------------------------------------------------

344           SUBROUTINE THOMAS(A,B,C,D,X,N)
345           DIMENSION A(N),B(N),C(N),D(N),X(N),ALFA(70),SI(70)
346           ALFA(1)=B(1)
347           SI(1)=D(1)
348           DO 20 I=2,N
349           E=A(I)/ALFA(I-1)
350           ALFA(I)=B(I)-E*C(I-1)
351           SI(I)=D(I)+E*SI(I-1)
352       20  CONTINUE
353           X(N)=SI(N)/ALFA(N)
354           N1=N-1
355           DO 30 I=1,N1
356           J=N-I
357           X(J)=(SI(J)+C(J)*X(J+1))/ALFA(J)
358       30  CONTINUE
359           RETURN
360           END
```

```
C     ------------------------------------------------------------
C     SUBROUTINE DRAW MAPS VARIABLES BY APPLYING THE TYPEWRITER
C     ------------------------------------------------------------

361         SUBROUTINE DRAW(W,IP,DB)
362         CHARACTER *3 AA,BB,CC
363         DIMENSION W(50,50),BB(50),AA(50),CC(50)
364         DATA CC/'   ',' +1+',' 2 ',' +3+',' 4 ',' +5+',' 6 ',' +7+',' 8 ',
           *  ' +9+',' 10',' +11',' 12',' +13',' 14',' +15',' 16',' +17',' 18',
           *  ' +19',' 20',' +21',' 22',' +23',' 24',' +25',' 26',' +27',' 28',
           *  ' +29',' 30',' +31',' 32',' +33',' 34',' +35',' 36',' +37',' 38',
           *  ' +39',' 40',' +41',' 42',' +43',' 44',' +45',' 46',' +47',' 48',
           *  ' 50'/
365         BB(1)=' ++'
366         BB(40)='++ '
367         DO 10 I=2,39
368         BB(I)='+++'
369      10 CONTINUE
370         PRINT 20,(BB(I),I=1,40)
371      20 FORMAT(40A3)
372         BB(1)=' + '
373         BB(40)=' + '
374         DO 60 J=2,39
375         DO 40 I=2,39
376         DO 30 K=1,50
377         X1=K-1.5
378         X2=X1+1
379         IF(W(I,J).LT.X2.AND.W(I,J).GE.X1) BB(I)=CC(K)
380      30 CONTINUE
381      40 CONTINUE
382         PRINT 20,(BB(I),I=1,40)
383         PRINT 20,(BB(I),I=1,40)
384      60 CONTINUE
385         BB(1)=' ++'
386         BB(40)='++ '
```

```
      DO 70 I=2,39
      BB(I)='+++'
   70 CONTINUE
      PRINT 20,(BB(I),I=1,40)
      IF(IP.EQ.2) GOTO 75
      PRINT 80,W(20,20)
      RETURN
   75 PRINT 80,DB
   80 FORMAT(//5X,'MAXIMAL ORDINATE=',F8.3,' METER'//)
      RETURN
      END
C     ------------------------------------------------------------
C     SUBROUTINE DRAW1 MAPS PUMPAGE BY APPLYING THE TYPEWRITER
C     ------------------------------------------------------------

      SUBROUTINE DRAW1(W,IP,DB)
      CHARACTER *3 AA,BB
      DIMENSION W(50,50),BB(50),AA(50)
      DATA AA/'   ',' .1',' .2',' .3',' .4',' .5',' .6',' .7',' .8',
     *  ' .9','1. ','1.1','1.2','1.3','1.4','1.5','1.6','1.7','1.8',
     *  '1.9','2. ','2.1','2.2','2.3','2.4','2.5','2.6','2.7','2.8',
     *  '2.9','3. ','3.1','3.2','3.3','3.4','3.5','3.6','3.7','3.8',
     *  '3.9','4. ','4.1','4.2','4.3','4.4','4.5','4.6','4.7','4.8',
     *  '4.9'/
      BB(1)=' ++'
      BB(40)='++ '
      DO 10 I=2,39
      BB(I)='+++'
   10 CONTINUE
      PRINT 20,(BB(I),I=1,40)
   20 FORMAT(40A3)
      BB(1)=' + '
      BB(40)=' + '
      DO 60 J=2,39
      DO 40 I=2,39
      DO 30 K=1,50
      X=.1*K-0.05
      X1=X-0.15
      IF(W(I,J).LT.X.AND.W(I,J).GE.X1) BB(I)=AA(K)
   30 CONTINUE
   40 CONTINUE
      PRINT 20,(BB(I),I=1,40)
      PRINT 20,(BB(I),I=1,40)
   60 CONTINUE
      BB(1)=' ++'
      BB(40)='++ '
      DO 70 I=2,39
      BB(I)='+++'
   70 CONTINUE
      PRINT 20,(BB(I),I=1,40)
      IF(IP.EQ.2) GOTO 75
      PRINT 80,W(20,20)
      RETURN
   75 PRINT 80,DB
   80 FORMAT(//5X,'MAXIMAL ORDINATE=',F8.3,' METER'//)
      RETURN
      END

$ENTRY
```

REFERENCES

Arthur, M.G., Fingering and coning of water and gas in homogeneous oil sand, Trans. Am. Inst. Mining Met. Engrs., 155, 184-201, 1944.

Bear, J., and G. Dagan, Moving interface in coastal aquifers, J. Hydraul. Div., Amer. Soc. Civil Eng., 90 (HY4), 193-216, 1964.

Benedict, B.A., Modeling of toxic spills into waterways, Hazard Assessment of Chemicals, Current Developments, Vol. 1, Ed. by J. Saxena and F. Fisher, Academic Press, New York, 251-301, 1981.

Bentley, C., Aquifer test analysis of the Floridan Aquifer in Flagler, Putnam, and St. Johns Counties, Florida, U.S. Geol. Survey Water Resources Investigation Series, WRI 77 (36), 1977.

Bermes, B.J., G.W. Leve, and G.R. Tarver, Geology and groundwater resources of Flagler, Putnam, and St. Johns Counties, Florida, Fla. Geol. Survey Rept. Inv. No. 32, 1963.

Chen, C.S., The regional lithostratigraphic analysis of Paleocene and Eocene rocks of Florida, Fla. Bur. of Geol. Bulletin 45, 1965.

Dagan, G., Pertubation solutions of the dispersion equation in porous media, Water Resources Res.,7 (1), 135-142, 1971.

Eldor, M., and G. Dagan, Solutions to hydrodynamic dispersion in porous media, Water Resources Res.,8 (5), 1316-1331, 1972.

Gelhar, L.W., and M.A. Collins, General analysis of longitudinal dispersion in nonuniform flow, Water Resources Res.,7 (6), 1511-1521, 1971.

Ghyben, B.W., and J. Drabbe, Nota in verband met de voorgenomen putboring nabij Amsterdam, Tijdscrift von het Koninklujk Institut von Ingeniurs, The Hague, Netherlands, 8-22, 1888.

Hantush, M.S., Unsteady movement of freshwater in thick unconfined saline aquifers, Bulletin of the I.A.S.H.,13 (2), 40-48, 1968.

Haubold, R.G., Approximation for steady interface beneath a well pumping freshwater overlying saltwater, Groundwater,13 (3), 254-259, 1975.

Herzberg, B., Die Wasserversorgung einiger Nordscebader, Jour. Gasbeleuchtung und Wasserversorgung, 44, 815-819, 842-844, 1901.

Hunt, B., Dispersion calculation in nonuniform seepage, J. Hydrol., 36, 261-277, 1978.

Johnson, R.A., Geology of the Oklawaha Basin, St. Johns River Water Management District, Tech. Rept. No. 1, 1979.

Mitchell, A.R., Computational Methods in Partial Differential Equations, John Wiley and Sons Ltd., London, 50-81, 1976.

Munch, D.A., B.J. Ripy, and R.A. Johnson, Saline contamination of a limestone aquifer by connate intrusion in agricultural areas of St. Johns, Putnam, and Flagler Counties, Northeast Florida, St. Johns River Water Mgmt. Dist. Florida, 2 (1), 1979.

Muskat, M., and R.D. Wychoff, An approximate theory of water-coning in oil production, Trans. Am. Inst. Mining Met. Engrs., 114, 144-163, 1935.

Ozisik, M.N., Heat Conduction, John Wiley and Sons, New York, Chapter 9, 1980.

Peaceman, D.W., and H.H. Rachford, The numerical solution of parabolic and elliptic differential equations, J. Soc. Indust. App. Math., 3, 28-41, 1955.

Pinder, G.F. and H.H. Cooper, A numerical technique for calculating the transient position of the saltwater front, Water Resources Res. 6 (3), 875-882, 1970.

Prakash, A., Groundwater contamination due to vanishing and finite-size continuous sources, Journal of the Hydraulics Division, American Society of Civil Engineers, 108, No. HY4, 572-590, April, 1982.

Rubin, H., On the application of the boundary layer approximation for the simulation of density stratified flows in aquifers, to be published in Advances in Water Resources, 1982.

Rubin, H., and B.A. Christensen, Simulation of stratified flow in the Floridan Aquifer, ASCE Irrigation and Drainage Div. Specialty Conference, Orlando, FL, July 21-23, 1982.

Rubin, H., and G.F. Pinder, Approximate analysis of upconing, Advances in Water Resources, 1, 97-101, 1977.

Sagar, B., Dispersion in three dimensions: approximate analytic solutions, Journal of the Hydraulics Division, American Society of Civil Engineers, 108, No. HY1, 47-62, January, 1982.

Segol, G., G.F. Pinder, and W.G. Gray, A Galerkin finite element technique for calculating the transient position of the saltwater front, Water Resources Res., 11 (2), 343-347, 1975.

Shamir, U., and G. Dagan, Motion of the seawater interface in coastal aquifers: a numerical solution, Water Resources Res. 7, (3), 644-657, 1971.

Wilson, J.L., and P.J. Miller, Two-dimensional plume in uniform groundwater flow, Journal of the Hydraulics Division, American Society of Civil Engineers, 108, No. HY4, 503-514, April, 1982.